DEPOSITION AND DIFFERENTIATION OF WINDWARD AND LEEWARD SLOPES IN A SILURIAN REEF COMPLEX: PIPE CREEK JR. QUARRY, GRANT COUNTY, INDIANA

By

JAMES WYNTON KARSTEN

Bachelor of Science in Geology

Calvin College

Grand Rapids, Michigan

2015

Submitted to the Faculty of the
Graduate College of the
Oklahoma State University
in partial fulfillment of
the requirements for
the Degree of
MASTER OF SCIENCE
May, 2020

DEPOSITION AND DIFFERENTIATION OF WINDWARD AND LEEWARD SLOPES IN A SILURIAN REEF COMPLEX: PIPE CREEK JR. QUARRY, GRANT COUNTY, INDIANA

Thesis Approved:

Dr. G. Michael Grammer

Thesis Adviser

Dr. Jack Pashin

Dr. James Puckette

ACKNOWLEDGEMENTS

I would like to my mentor and advisor, Dr. Mike Grammer. Without his expertise, guidance, encouragement, and professionalism, none of this would have been possible. I am very glad I have been able to work with him these past 4 years, and I am certain that I will be well prepared to go out into the world and search for the "so what" in every situation.

I would like to thank all the members of the "Carbonate Clan" past and present for their example and friendship. Specifically, I would like to thank Elizabeth Elium, CJ Appleseth, Yulun Wang, Ibk Bode, Maria Reistroffer, Julie Cains, and Alejandra Santiago Torres for their friendship, encouragement, and feedback on countless presentations and posters over the years. My time at Oklahoma State would not have been nearly as enjoyable without them, and I know that I have improved as a scientist and as a person because I have worked with them.

I would like to thank the other two members of my thesis committee, Drs. Jack Pashin and Jim Puckette. They have always been there whenever I have had a question in classes and concerning my thesis. I thank them for their consummate expertise and willingness to share that expertise.

I also would like to thank IMI, Inc. for giving us access to the quarry as well as Jon Havens for his willingness to lead us around the quarry and answer any of our questions. I also want to thank Dennis Prezbindowski for his support and encouragement throughout this whole process, as well as for turning us on to the quarry as a possible site for this thesis work.

Lastly, I would like to thank my family for their support and encouragement. Specifically, I want to thank my wife for being willing to move to Oklahoma in the first place, and then to support me in every way throughout this entire journey. I know I would not have been able to make it through without her. I could not imagine doing this without her, and I am a better person just because I am with her.

Name: JAMES WYNTON KARSTEN

Date of Degree: MAY, 2020

Title of Study: DEPOSITION AND DIFFERENTIATION OF WINDWARD AND LEEWARD SLOPES IN A SILURIAN REEF COMPLEX: PIPE CREEK JR. QUARRY, GRANT COUNTY, INDIANA

Major Field: GEOLOGY

Abstract: Silurian reefs are significant hydrocarbon reservoirs in the Michigan Basin, having produced over 490 MMBO and 2.9 TCF of gas. Primary production from the reefs is typically averages 20-25% due to the complex internal heterogeneity of the reservoir. To date, a majority of the exploration and development of these reservoirs has been directed towards the cores of the reefs, rather than the associated reef slope deposits. Reef slope deposits exposed in the Pipe Creek Jr. reef quarry complex of Indiana exhibit many similarities to several other productive slope reservoirs reported from the rock record (e.g. Tengiz and Karachaganak in the Caspian region). As such, an understanding of the depositional processes and the resulting geometry of potential reservoirs and seals in these Silurian reef slopes may provide valuable insight into the formation and evolution of similar slope deposits.

This study is focused on the upper slope (forereef) deposits of the Pipe Creek Jr. reef complex and includes an analysis of the facies distribution, bed geometry, faunal distribution, and reservoir characterization of the reef slope deposits, coupled with the development of a drone-based, georeferenced outcrop model. The main objectives of the study include determining how the slope beds were deposited and whether a windward/leeward orientation for the reef system can be determined by examining the slope beds. The Pipe Creek Jr. Reef has been previously studied with a focus on faunal assemblages, dolomitization of the reef, and the general depositional facies of the reef core. The reef complex has a minimum thickness of 48m, and the original height of the reef has been speculated as being anywhere from 35 to 200 meters. The exposed reef flank (forereef) facies consist of a mixture of coarse skeletal grainstone-packstone, skeletal mudstone-wackestone, and argillaceous silty dolomite mudstone. Similar to other forereef deposits, lenticular bedding consisting of skeletal packstone and grainstone deposited by grainflow make up the majority of the 40-45° depositional slopes. A proposed S to SE dominant wind direction was determined through analysis of slope declivity, facies composition, percent facies coverage, syndepositional marine cement, faunal diversity, and faunal density. This wind direction is corroborated by other studies of Silurian reefs in the Michigan basin, as well as by paleoclimactic modeling of the Wabash Platform.

TABLE OF CONTENTS

Chapter Page

LIST OF TABLES

Table Page

LIST OF FIGURES

Figure Page

Figure Page

CHAPTER I

Introduction

Summary of the Problem:

Silurian reefs are important reservoirs for oil and gas in the Michigan Basin, having produced over 490 MMBO and 2.9 TCF of gas. Typically, the oil recovery from these reefs averages only about 20-25% of the original oil in place (Grammer et al., 2009). This is due to complex vertical and lateral heterogeneity of the depositional architecture. This heterogeneity is true for both the reef core facies and the reef slope facies, which for the purposes of this study includes the dipping beds which flank the inferred reef core. The reef slope facies of these Silurian reefs are understudied, at least in the Michigan Basin. Despite this knowledge gap, the depositional processes and resulting bed geometry, along with sediment composition, texture, fabric, and porosity types are similar in many ways to other marginal slope reservoirs around the world (e.g. Tengiz Buildup in Kazakhstan).The similarity of the Silurian-aged reef slopes in the Michigan Basin to producing slope reservoirs in other parts of the world indicates the possibility for reef slope deposits of Silurian-age in the U.S. Northern Midwest and Southern Ontario to be conduits or reservoirs for hydrocarbons.

Several studies have proposed different models to explain the deposition and diagenesis of the slope beds exposed in the Pipe Creek Jr. quarry (e.g. Shaver, 1977; Lehmann and Simo, 1989; DeVaney et al., 1986; Shaver and Sunderman, 1989, etc.). Some workers have interpreted the reef slope beds having been shed off of pinnacle reefs where the core of the reef reached heights of 88m and 100-200m (Suchomel, 1975; Lehmann, 1978). Others interpreted the reef complex as a flat-topped, isolated carbonate platform with much more modest height (Simo and Lehmann, 2000). DeVaney et al. (1986) posited the sloping beds were deposited as clinothems dipping at much low angles on a carbonate shelf with slope declivity later enhanced via differential compaction of carbonate mud. In this model, there was no true reef core, but simply a series of low angle clinothems on a carbonate shelf. It should be noted that during all previous studies of the Pipe Creek Jr. complex, only the eastern section of the quarry was exposed, making it impossible to see the complete structure of the reef slope beds and the azimuthal dip directions of the sloping beds in all sections of the quarry. Continued quarrying has now made these other dimensions of the complex available for study.

Lehmann and Simo (1989) and Simo and Lehmann (2000) supported the interpretation that the Pipe Creek complex was an isolated carbonate platform and that the slope beds were likely at or close to the depositional slope angle, with early marine cement playing a role in stabilizing these slope beds. They also supported the idea that the reef system had a true reef core based on observed talus blocks composed of reefal material and an observed change from reef associated fauna at the tops of slope beds to inter-reef fauna at the bottom of slope beds. This study examines the validity of these claims and presents additional evidence through analysis of samples, thin sections, and core, as well as observations of bedding geometry and style in order to show similarities to other carbonate slopes and isolated carbonate platform systems which also contain high-angle slope beds.

In addition, this study also examined the potential reservoir quality of the reef slope facies and attempted to determine a windward/leeward orientation for the reef complex. This determination was made by looking at several different lines of evidence and characteristics, which included elevated faunal abundance and diversity on the windward side, a higher percentage of early marine cement on the windward side, steeper slopes on the windward side, and less mud on the windward side. This determination is important not only for assessing the paleowind direction, but also has important reservoir implications, with the overall grainier, coarser, and poorly sorted nature of windward forereef slope deposits typically offering a better reservoir target (Wold and Grammer, 2018; Trout et al., 2018).

Fundamental Questions and Hypotheses:

The fundamental questions for this study are as follows:

1. What are the dominant depositional processes associated with forereef slope deposits exposed in the quarry, and how might these processes exert control on reservoir quality and architecture?
2. What are the main lithofacies in the quarry and how are they distributed?
3. Can a windward/leeward orientation for the reef complex be determined through analysis of facies composition, texture, fabric, and distribution, and how might this control reservoir potential?

The first hypothesis is the exposed reef slope facies display similar bed geometry, facies types and depositional and diagenetic processes to other forereef slope and reef systems, and therefore might show similar distribution of facies and cementation, which, together with porosity and permeability, govern reservoir quality. The second hypothesis is that defining a windward/leeward orientation of the reef system, determined through analysis of facies composition and distribution, will be a key to understanding the original structure and geometry of the reef system and the distribution of potential reservoir intervals within the reef slope facies.

Stratigraphy and Geologic Background:

The Pipe Creek Jr. Quarry is in North Central Indiana in Grant County (Figure 1). It is an active quarry which supplies aggregate for a variety of purposes from construction-grade to high calcium lime for use in animal feed. Analysis of aerial photos using Google Earth software shows approximately 4.8km of exposure within the quarry today, with walls ranging from 13 to

>30m in height. The quarry can be divided into Western, Eastern, and Southern sections, all with multiple walls showing various cross-sectional cuts of the slope facies (Figure 2). Most of the work for this project focused in the Western Section of the quarry, which provided the best 3D view of the slope beds; however, samples and images were taken from all sections of the quarry.

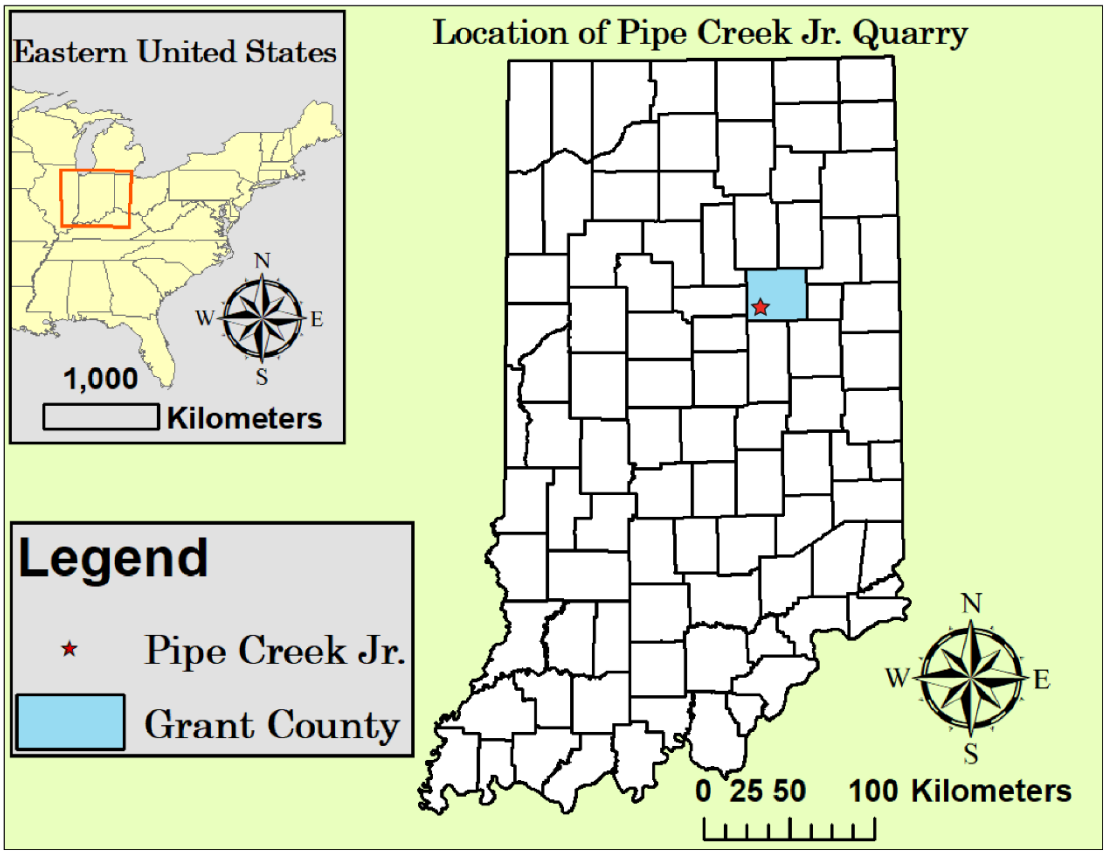

Figure 1: Map showing location of Pipe Creek Jr. Quarry in Grant County, Indiana. TIGER/Line shapefiles accessed through Data.gov.

The limestone and shale exposed in the Pipe Creek Jr. Quarry are part of the Wabash Formation which consists of two major subdivisions, the lower Missisinewa Shale member and the upper Liston Creek, Kokomo, and Kenneth Limestone members (Simo and Lehmann, 2000). The limestones exposed at Pipe Creek Jr. are part of the Mississinewa Shale member, while the upper members are not present. Generally, the Mississinewa shale member is an argillaceous, silty dolomite, but contains the skeletal-rich, reef-associated limestones which make up most of the exposures in Pipe Creek Jr. A stratigraphic column of Silurian and Devonian strata in Northern Indiana is shown in Figure 3. There is a major unconformity at the top of the Silurian section which is overlain by Middle Devonian strata. During this time, the core of the reef and the top of the reef slope facies were eroded, preserving only the reef slope facies that are exposed in the quarry today (Simo and Lehmann, 2000).

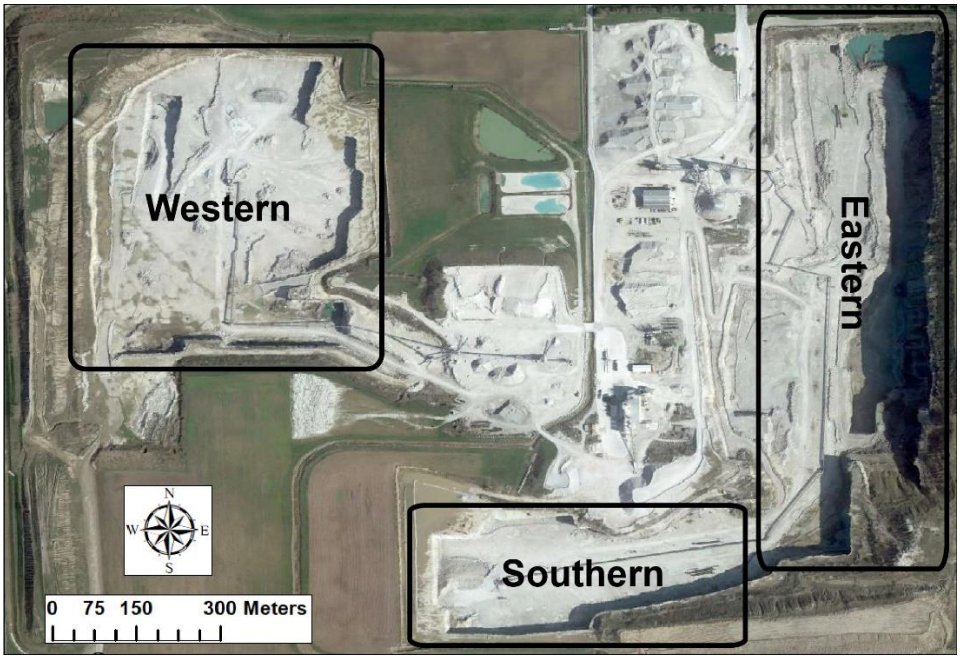

Figure 2: Satellite map showing the Western, Eastern, and Southern sections (outlined in black) of the Pipe Creek Jr. quarry. Satellite image from Google Earth.

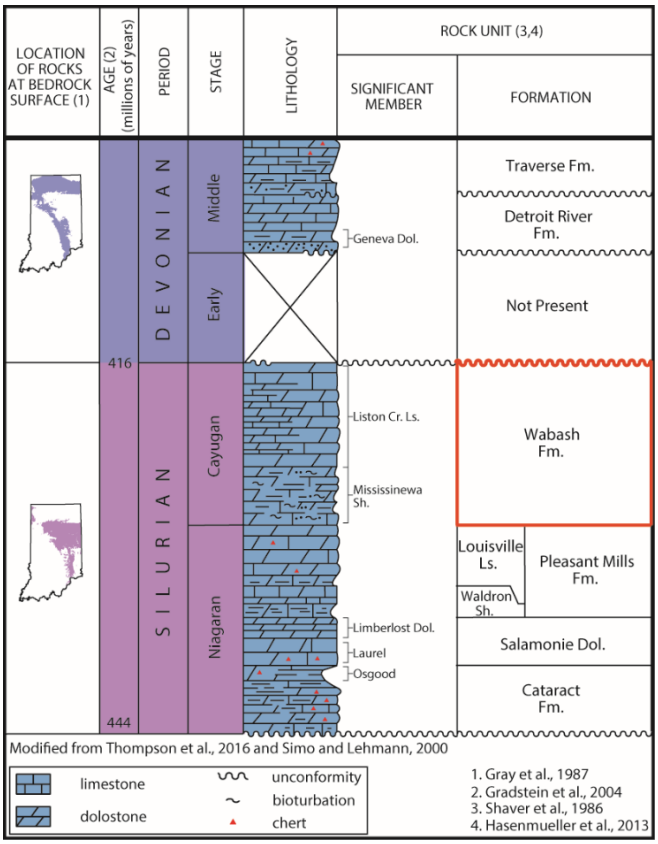

Figure 3: Silurian through Middle Devonian stratigraphy of Northern Indiana. The Pipe Creek Jr. complex is contained within the Wabash Formation (outlined in red). Note the unconformity at the top of the Silurian section (modified from Thompson et al., 2016 and Simo and Lehmann, 2000).

The Pipe Creek Jr. reef complex was deposited on the Wabash Platform during Late Silurian (Cayugan) time. At this time, the Wabash Platform was a normal marine carbonate platform located between the Michigan, Illinois, and Appalachian basins, with paleogeographic reconstructions placing the reef complex at about 15-20°S (Lehmann and Simo, 1989). Reconstructions have also shown that Laurentia was rotated approximately 45° counterclockwise from the North American continent today, and paleoclimactic modeling indicates the Wabash Platform was dominated by southeasterly trade winds (Spengler and Read, 2010). Analysis of the structure, facies and faunal distribution, and overall geometry of Ray Reef, a Wenlockian-age (Silurian) reef in the Michigan Basin, corroborates this potential paleowind direction as it suggests a possible paleowind direction from the S to SE (Wold and Grammer, 2018; Trout et al., 2018). Reconstructions of the regional paleo-oceanography and paleogeography can be seen in Figures 4A and 4B.

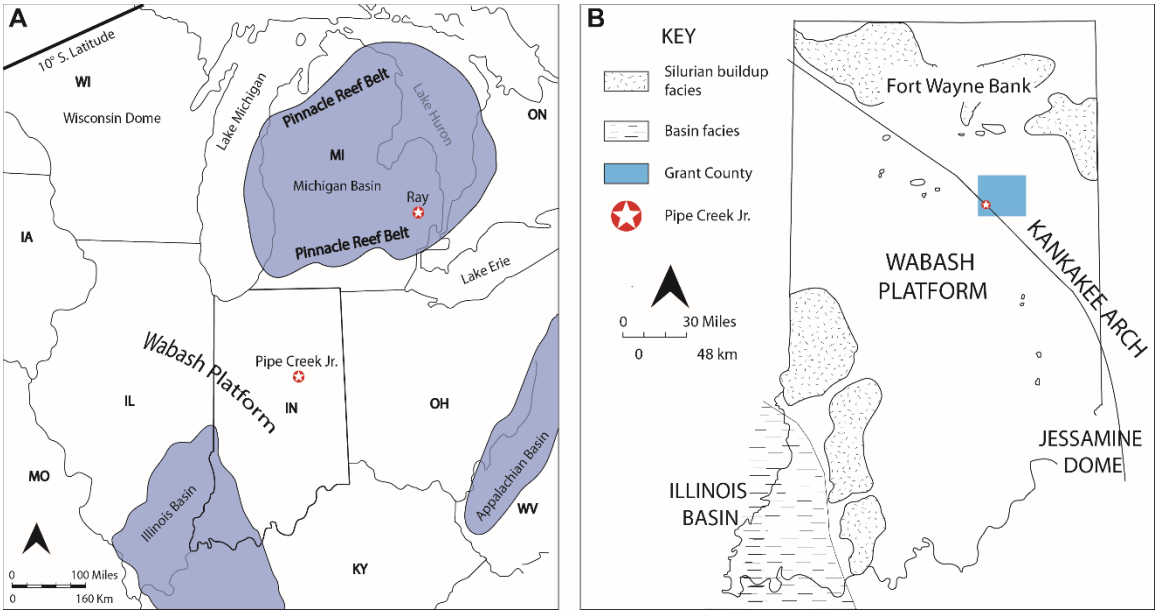

Figure 4: 4a) Silurian palaeoceanographic reconstruction showing the Pipe Creek complex on the Wabash Platform between the Michigan, Illinois, and Appalachian Basins as well as the location of Ray Reef in the southern reef trend of the Michigan Basin (Modified from Trout et al., 2018 and Santiago Torres, 2019). 4b) Paleogeographic reconstruction showing the Pipe Creek complex at approximately 20°S Latitude and its location relative to the Fort Wayne Bank in Northern Indiana (Modified from Spengler and Read, 2010 and Santiago Torres, 2019).

Several authors have shown that changes in sea level are important factors in the growth of Silurian reefs in the Michigan Basin (e.g., Wold and Grammer, 2018; Ritter and Grammer, 2018; Wold, 2008; Ritter, 2008). These authors showed that correlation of 3rd- and probable 4th-order shallowing upward packages provided information about the cyclic nature of their deposition and the resultant compartmentalization of reservoir intervals. The correlation of facies stacking patterns and time correlative exposure surfaces also provide information on the complex growth history of the Silurian reefs in the Michigan Basin (Wold and Grammer, 2018). Because the reef core has been truncated and is not exposed in the Pipe Creek Jr. complex and because direct sampling from the quarry walls is difficult due to limited access, it is difficult to work out the sequence stratigraphy of the slope beds in great detail. Despite this fact, it is useful to

understand the changes in relative sea level in the Late Silurian, which in turn may help to gain a better understanding how these changes affect the deposition and ultimate reservoir architecture of the reef slope facies. There are several published sea level curves for the Silurian in North America (e.g. Ross and Ross, 1996; Haq and Schutter, 2008; Spengler and Read, 2010; Johnson, 2010) that have been constructed utilizing different methodologies, including use of biostratigraphy, depositional sequences, sequence stratigraphy, and calibrating highstands with buried coastal topography. These curves represent both eustacy and local changes of relative sea level. The Spengler and Read (2010) curve likely represents the most accurate sea-level curve for this study, as it was developed using 12 cores from the Wabash Platform in Indiana and Ohio. This curve shows 11 3rd-order sequences in the Silurian (5 in the Ludlovian and Pridolian), showing that reef growth (and exposure) during this time was likely episodic (Figure 5).

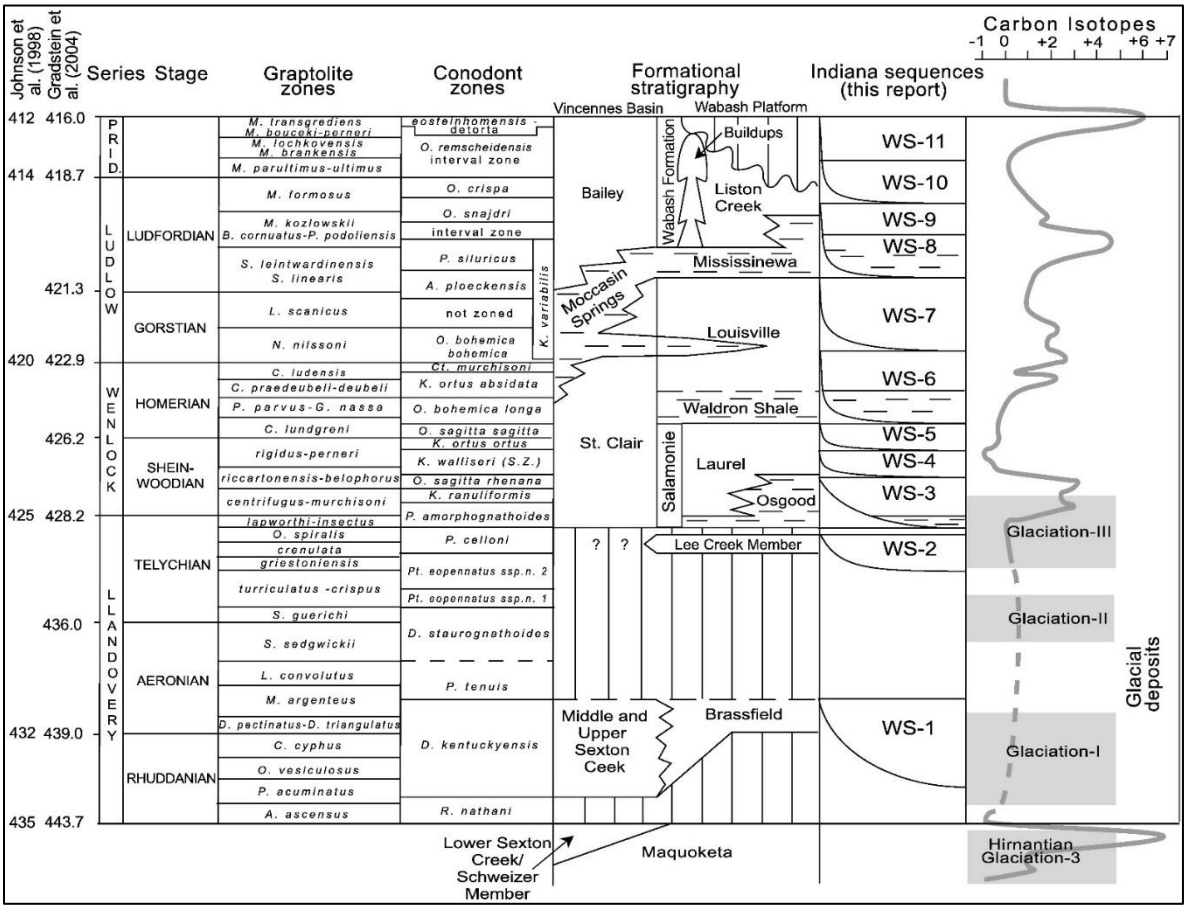

Figure 5: Biostratigraphy, formational stratigraphy, sea level curve, and carbon isotope curve for the Silurian in Northern Indiana, showing 11 3rd-order eustatic sea level cycles, 5 of which were in the Ludlovian and Pridolian (WS-7-WS-11) (after Spengler and Read, 2010).

Data and Methods:

Data:

Data for this study include 6 slabbed hand samples with corresponding thin sections, 11 thin sections from smaller samples, and 1 2-ft. (.61m) long section of H-gauge (4 in; 10 cm) core with 8 corresponding thin sections from the western section. From the southern section of the quarry, 3 slabbed hand samples with corresponding thin sections, 11 thin sections from smaller samples, and 1 2-ft. (.61m) section of H-gauge core with 9 corresponding thin sections. In the Eastern section, 8 slabbed hand samples (5 with thin sections, 3 without), and 7 thin sections from smaller samples were utilized. In addition to the rock data, approximately 2,900 images of the western quarry walls were taken using a DJI Inspire 1 Pro drone as well as approximately 1,800 images taken using a Gigapan Pro tripod.

Field Methods:

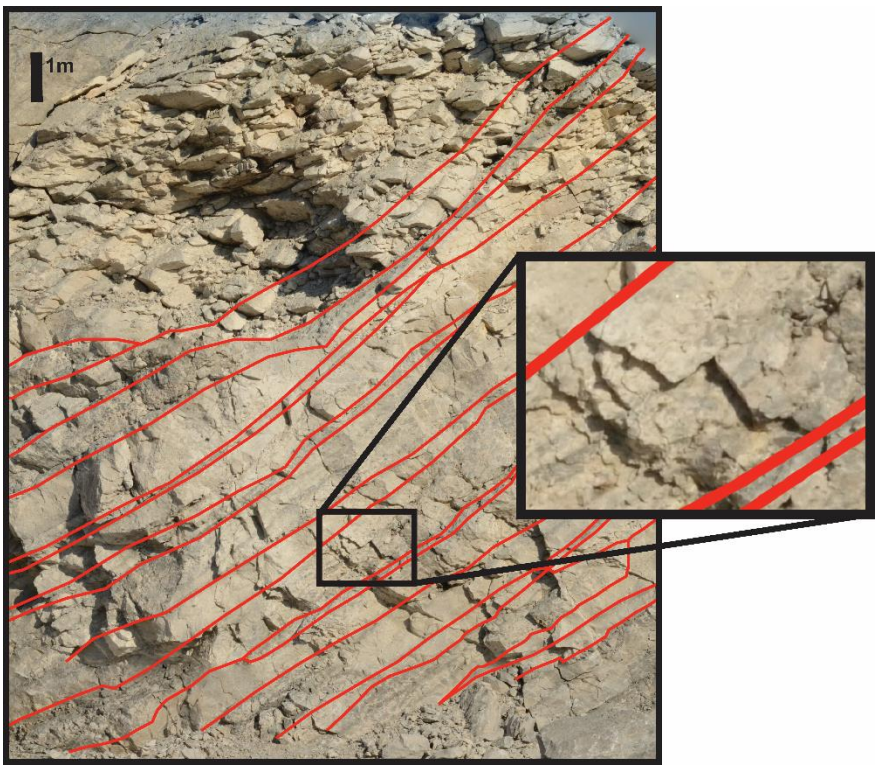

Figure 6: Image showing the resolution of GigaPixel images of quarry walls, which allowed observation of cm-scale features of the slope beds. Red lines represent bedding planes, and the scale bar is 1 m.

Traditional field methods including measuring sections and outcrop sampling were not possible because Pipe Creek Jr. is an active quarry and safety regulations required a minimum distance of 10 ft from any wall. Therefore, samples were collected from float on the quarry floor, with special care being taken to note from which section of the quarry each sample was taken. However, pseudo-measured sections were possible due to observations in GigaPixel images, which were stitched together using GigaPan software. The high resolution of these images

allowed for the identification of the facies observed in core and hand samples, and for identification and characterization of sedimentary structures, in some cases at the cm scale (Figure 6). This allowed for the distinction between beds and facies on some walls without actually sampling from the wall. Beds were traced and were identified as either wackestones-packstones (WS-PS), packstones-grainstones (PS-GS), or brachiopod beds (BR), and indistinguishable (ID) where distinction was not possible. On certain walls facies distinction was not possible (e.g. western wall of the western section) and some facies were able to be distinguished but the majority of the face was obscured by tailings piles (e.g. eastern wall of the western section). Because of these limitations, the southern wall of the western section was selected for intensive analysis.

The direct measurement of slope angle and dip direction also was not possible. Measurement of the apparent dip angle was possible using GigaPixel images. Approximate dip direction could be measured from the quarry floor using a compass in the eastern and southern sections of the quarry and using the digital outcrop model in the western section.

Drone Based Photogrammetry:

As stated before, approximately 2,900 images were taken with a DJI Inspire 1 Pro drone equipped with a ZenMuse X5 12-megapixel camera. Each of these images is geotagged using the onboard geographic positioning (GPS) unit. Aerial images were taken at elevations of approximately 80 and 40 m, while parallel and oblique images of the quarry walls were taken from a distance of ~3 m to capture small scale features and ~6-8 m to capture larger scale features and stratal geometry. All sky and vegetation were cut out of the images. These geotagged images were stitched together using Agisoft PhotoScan Professional software, in which a georeferenced, dense point cloud was created. This point cloud was then processed, and a digital outcrop model was created with overlying textured meshes to aid in interpretation. Images taken for the digital outcrop model were acquired with an overlap of no less than 60% in all directions, and images were captured from oblique and parallel angles to maintain the complex geometry and dip angles of the strata in each quarry wall. Once produced, the digital outcrop model, in conjunction with GigaPixel images, was used to measure apparent dip angles and azimuthal dip directions of the slope beds in the western section of the quarry.

Visual Estimation Analysis:

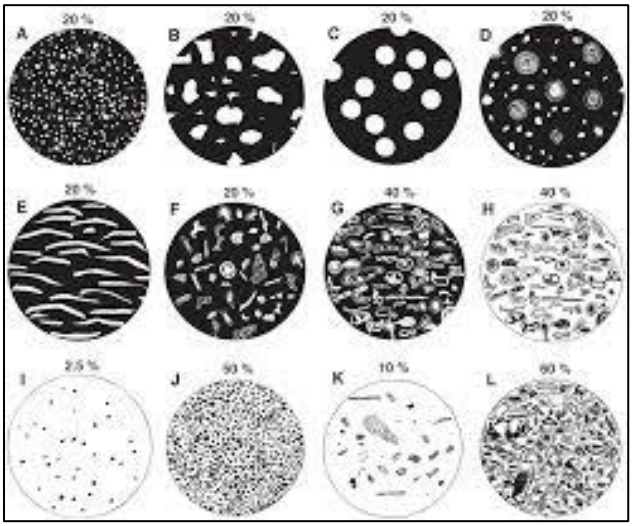

Figure 7: Visual Estimation charts used to estimate relative percent cover of grains and allochems, cement, mud, and porosity (after Baccelle and Bosellini, 1965).

The relative percentage of allochems, cement, mud/matrix, and porosity were estimated for each thin section, slabbed sample, and core and were organized according to which section of the quarry the sample came from. This was accomplished using visual estimation charts from Baccelle and Bosellini (1965) (Figure 7). These charts give a semi-quantitative estimate of each component. Detailed, bed-by-bed sampling was not possible, and the precision of the visual estimation charts better matched the precision of the sampling. If adequate core coverage or sample coverage straight from the quarry walls had been possible, more precise measurements would have been possible (e.g. point counting, digital image analysis, and whole core analysis). The relative percentages were then used to compare each section of the quarry to aid in the identification of windward and leeward parts of the reef system.

Analysis of Fauna, Cement, and Pore Types:

A high-level assessment of the faunal abundance and diversity, as well as the size and different morphotypes of various species, was made to compare the different sections of the quarry. For the purposes of this study, broad faunal categories were used, as a more sophisticated and detailed taxonomic classification and identification was not the focus of this study. For a much more detailed study of faunal assemblages and the Silurian fauna present in Pipe Creek, please refer to Lehmann and Simo (1989) and Suchomel (1975), respectively. The dominant allochem type for each thin section and some of the slabbed hand samples was identified using visual estimation charts, as well as other allochem types that could be recognized. Relative abundance of cement types, and the occurrence of different pore types in thin section and hand sample were also examined to aid in the determination of the windward and leeward parts of the reef system.

CHAPTER II

Results

Structure of Slope Beds:

General dip directions of the slope beds were measured with a compass in the Eastern and Southern sections of the quarry, and measured in the western section with the aid of the DOM. The inability to sample and measure straight from the walls made it infeasible to ascertain the exact dip direction and angle. Despite this limitation, a general reversal of dip direction is observable when moving from the western section to the eastern section. In addition, all the slopes appear to be sourced from the center of the quarry. The measured dip azimuths are illustrated in Figure 8.

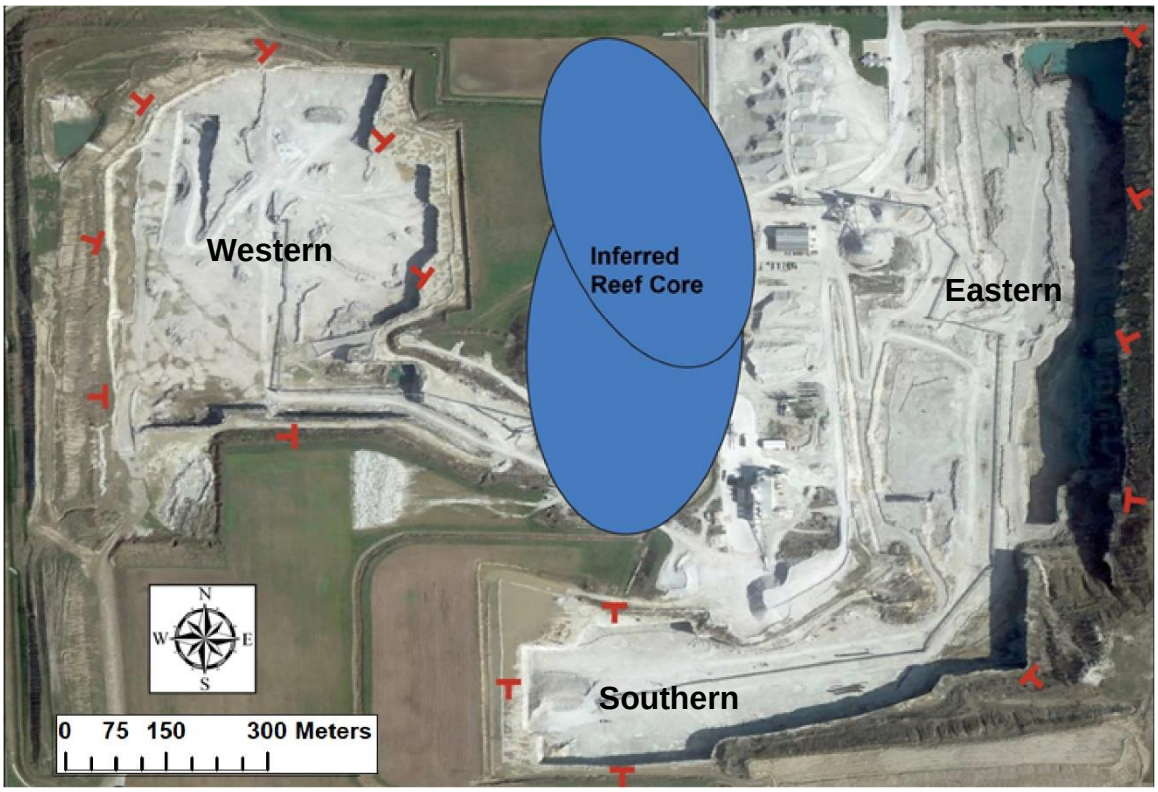

Figure 8: Apparent dip directions in the Pipe Creek, Jr. quarry. The beds seem to slope away from a common center where the inferred reef core lies. Satellite image from Google Earth.

Lithofacies:

There are many lithofacies within the quarry, including skeletal wackestone-packstone (WS-PS), skeletal packstone-grainstone (PS-GS), coral and stromatoporoid rudstone, silty dolomitic mudstone, algal/microbial mudstone, brachiopod wackestone-packstone (BR), and possible stromatactis mudstone. These lithofacies have been observed previously (Lehmann and Simo, 1989) and were observed in samples of float from the quarry floor, but the three main lithofacies which make up the exposure of the reef slopes are the wackestone to packstone (WS-PS), packstone to grainstone (PS-GS), and the brachiopod bed (BR) facies. These three facies were able to be identified in some of the quarry walls from GigaPixel imagery by observing variations of color, texture, and fabric. Accordingly, these 3 lithofacies are the main focus of this study.

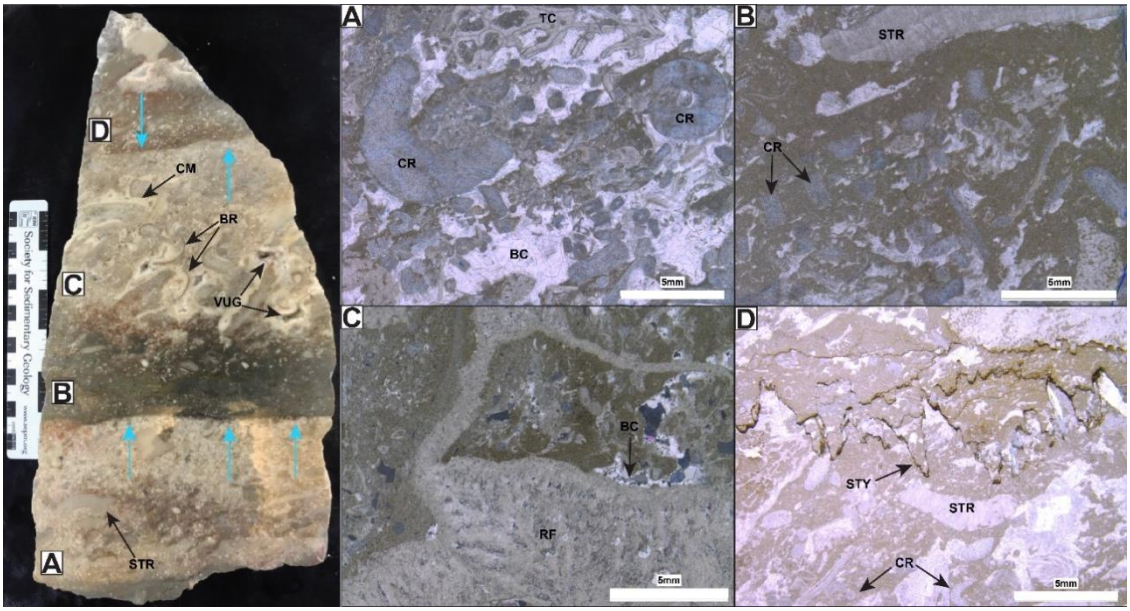

Figure 9: Slabbed sample and corresponding photomicrographs from the western section of the quarry showing the main lithofacies. Blue arrows indicate borings. STR=Stromatoporoid, VUG=Vuggy porosity, BR=Brachiopod, CM=Cement. Scale is in centimeters and inches, A) Skeletal packstone to grainstone containing crinoids (CR), tabulate corals (TC), and blocky calcite cement (BC). Scale = 5mm, plane polarized light (PPL), B) Skeletal wackestone (locally mud-rich packstone) containing dominantly crinoids (CR) with minor stromatoporoid fragments (STR). Scale = 5mm, PPL, C) Skeletal packstone-grainstone to rudstone containing both radiaxial fibrous cement (RF) and blocky calcite cement (BC). Scale= 5mm, cross polarized light (XPL), D) Mud-rich skeletal packstone containing crinoids and stromatoporoids (STR) as well as 3-5 mm amplitude sutured stylolites (STY). Scale = 5 mm, PPL

Figure 9 shows a slabbed sample and corresponding thin section photomicrographs from the western section of the quarry where the 3 main lithofacies are in mutual contact. Bed A is an example of the PS-GS. It is a poorly sorted, coarse grained, skeletal packstone-grainstone. The skeletal components in order of relative abundance are crinoids, tabulate corals, stromatoporoids, and brachiopods. The cement types in order of abundance are blocky calcite, fibrous calcite cements, and syntaxial overgrowth calcite cement. Bed A contains intraparticle, intercrystalline,

and vuggy porosity. According to visual estimation, bed A has an average composition of 58% allochems, 33% cement, 8% mud, and 1% porosity.

Bed B is in sharp contact with bed A, with borings into bed A visible along the contact. bed B is a poorly sorted, skeletal WS (local PS) with fewer large (> 3 mm) grains than bed A. 3-5 mm amplitude sutured seam stylolites have been observed in both hand sample and in thin section. Crinoid fragments make up the majority of the allochems in bed B. Blocky calcite cement was present as well as intraparticle porosity within the crinoid grains. Bed B had an average composition of 25% allochems, 10% cement, 64% mud, and 1% porosity.

Bed C has a gradational contact with bed B and displays a mottled texture with abundant cement surrounding the allochems and filling voids in some areas. Bed C is an example of a mud lean, packstone-grainstone to rudstone which is poorly sorted and contains abundant allochems larger than 3 mm. Bed C contains tabulate corals, brachiopods, stromatoporoids, and crinoids in order of relative abundance. The cement is largely fibrous, but blocky calcite cement also is present. Pore types include intraparticle, framework, and cm-scale vugs, many of which are visible in hand sample. Overall, bed C has an average composition of 45% allochems, 43% cement, 11% mud, and 1% porosity.

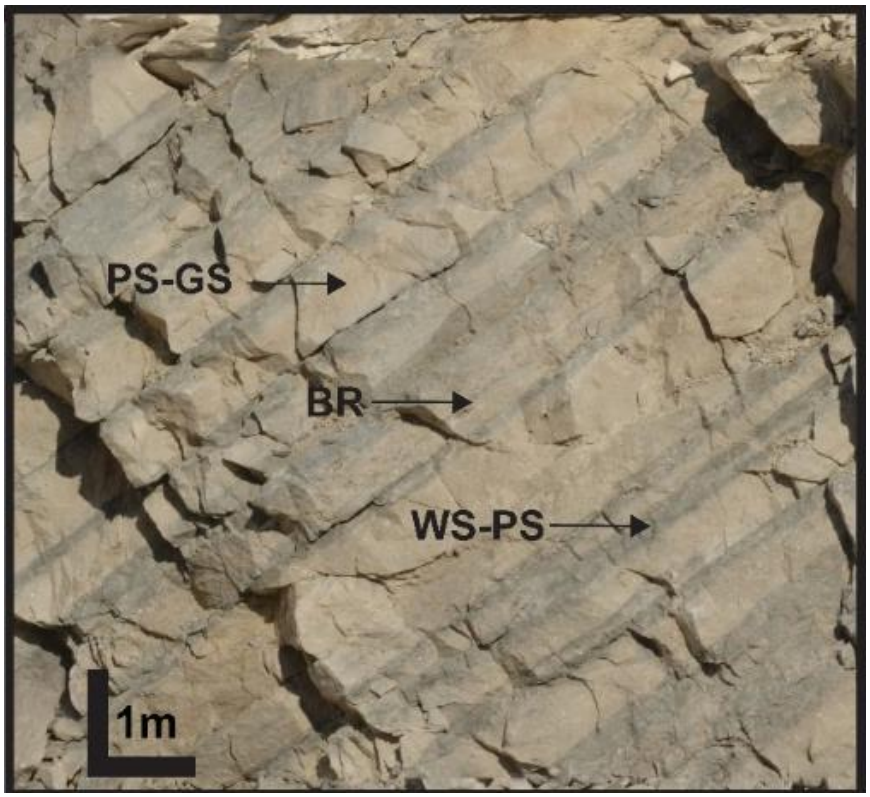

Figure 10: Stitched image of a section of the eastern wall in the Western section of the quarry which shows the 3 main facies in outcrop, namely the lighter-colored packstone-grainstone (PS-GS), the darker-colored, thinly bedded wackestone-packstone (WS-PS), and the brachiopod beds, (BR) which display a mottled texture

Bed D sharply overlies bed C, and also shows evidence of borings along the contact. Bed D is a poorly sorted, mud rich, skeletal packstone with few allochems larger than 3 mm. As observed in Bed B, the makeup of the allochems is dominated by crinoids but also includes stromatoporoids, tabulate corals, and rugose corals. Also like Bed B, sutured seam stylolites can be seen in hand sample and in thin section. The major cement types include a vug lining dolomitic cement and blocky calcite cement, and the major pore type is intraparticle inside crinoid grains.

Bed Geometry:

Figure 10 shows the distribution and characteristics of the main facies exposed in the quarry walls. The PS-GS are the lighter beds, the WS-PS are the darker beds, and the brachiopod beds display a mottled texture, often with mud-filled brachiopods and an abundance of white cement in a muddy matrix. This happens much in the same way as in stromatactis mudstone, with brachiopods providing shelter porosity which is then filled by syndepositional cement (Bathurst, 1980; McGovney, 1988). These beds are inclined at angles of up to 40°, but in other walls, specifically the southern wall of the western section, beds are inclined up to 45°. It should be noted that these angles are apparent dip. For example, while the beds in the southern wall of the western section have 40-45° dip, the beds in the western wall, which display a cut perpendicular to the southern wall, are essentially flat. Therefore, the southern wall shows true dip.

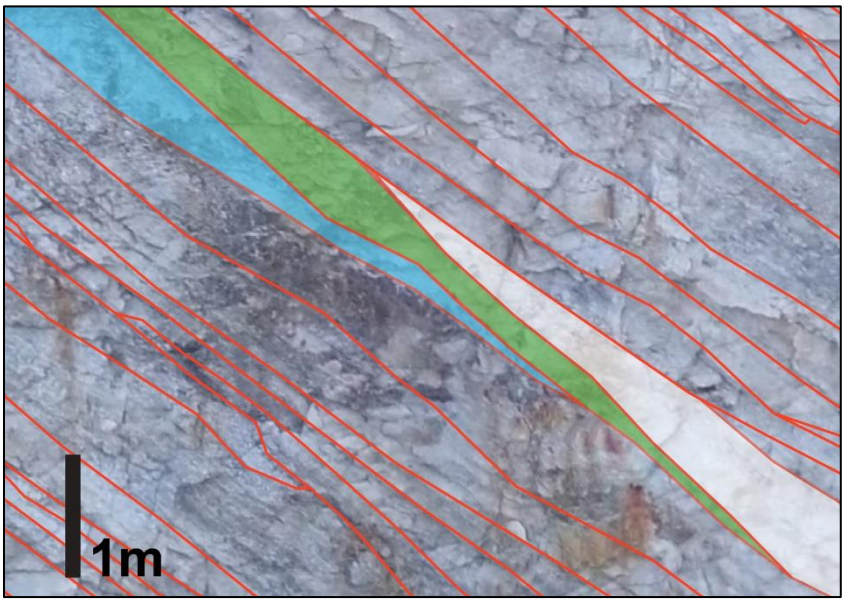

Figure 11: Stitched image showing a section of the southern wall in the western section of the quarry. Red lines represent bedding planes and the beds highlighted in blue, green, and white show the lenticular nature of the individual decimeter-scale beds.

These are decimeter to meter thick beds with distinct lenticular geometry. A bed tracing of the southern wall shows the lenticular nature of these beds, which are highlighted in blue, green, and white (Figure 11). Generally, the packstone to grainstone beds are more laterally extensive than the wackestone-packstone and the brachiopod beds. The PS-GS beds, which can exceed a meter in thickness, typically extend more than 10 to 20 m along dip. The WS-PS beds are generally less laterally extensive than the PS-GS (<3m to ~15m), while the brachiopod beds tend to be more thickly bedded (up to 1.4m), but don't extend as far (>15 m). These beds are also lenticular in strike view (Figure 12). While the lithofacies cannot be resolved in the western wall, the beds can still be traced as decimeter thick, lenticular beds with lateral extent of up to 15 m, showing that the slope beds are lenticular in both a dip and strike direction. Table 1 summarizes information pertaining to the average thickness and lateral extent of each facies.

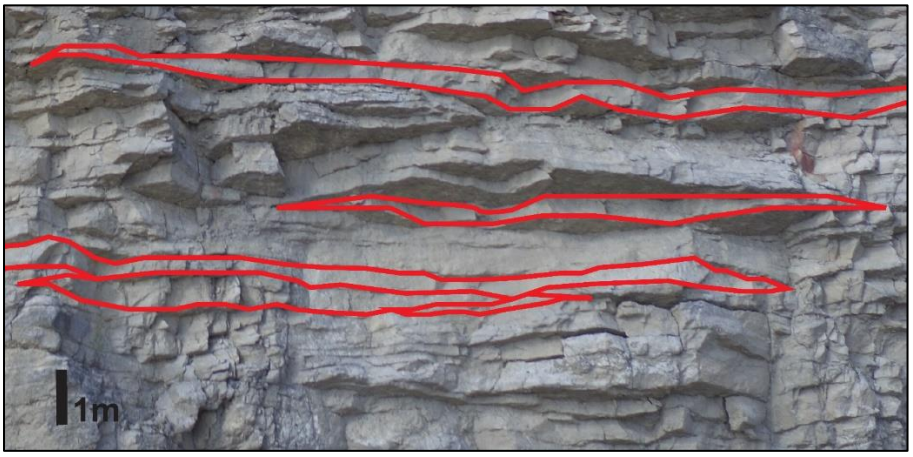

Figure 12: Stitched image showing a section of Western wall in the Western section of the quarry which shows the lenticular nature of the slope beds in an approximate strike view. The beds dip back away from the field of view.

Table 1: Average thickness, thickness range, and downslope extent or length of beds in the three main facies.

Bed Geometry Summary			
Facies Types	**PS-GS**	**WS-PS**	**BR**
Average Thickness (m)	0.37m	0.20m	0.51m
Thickness Range (m)	.05-1m	.05-.6m	.1-1.4m
Downslope Extent (m)	10-20m	<3-15m	5-15m

In the eastern section, where the exposures are older and more weathered, groupings of the decimeter thick, lenticular beds can be traced. These groupings are meter(s) thick, elongate lobes or lenses, one of which is highlighted in red in Figure 13. While these lobes pinch out quickly in the dip direction and most likely in the strike direction, synchronous lobes or lenses might extend further in a strike direction depending on the shape of the inferred reef core.

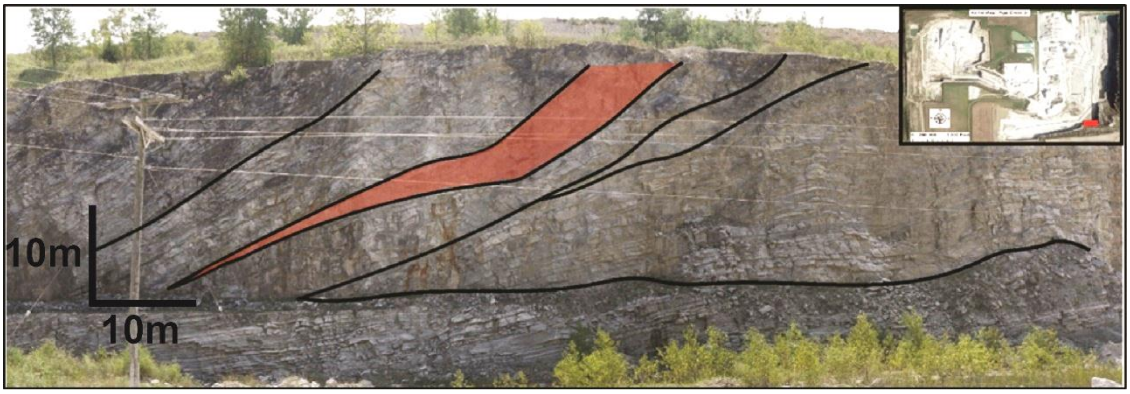

Figure 13: Stitched image of the SE corner of the eastern section of the quarry. Meter-scale lobes and lenses made up of subordinate lenticular beds have been traced, one of which is highlighted in red.

Drone Photogrammetry:

A textured mesh overlain onto the dense point cloud model compared to Gigapixel images of the quarry walls can be seen in Figure 14. The dip angles and azimuthal directions of the beds could be resolved from the digital outcrop model (DOM). On certain walls, the individual beds could be resolved and the facies could be identified from the DOM.

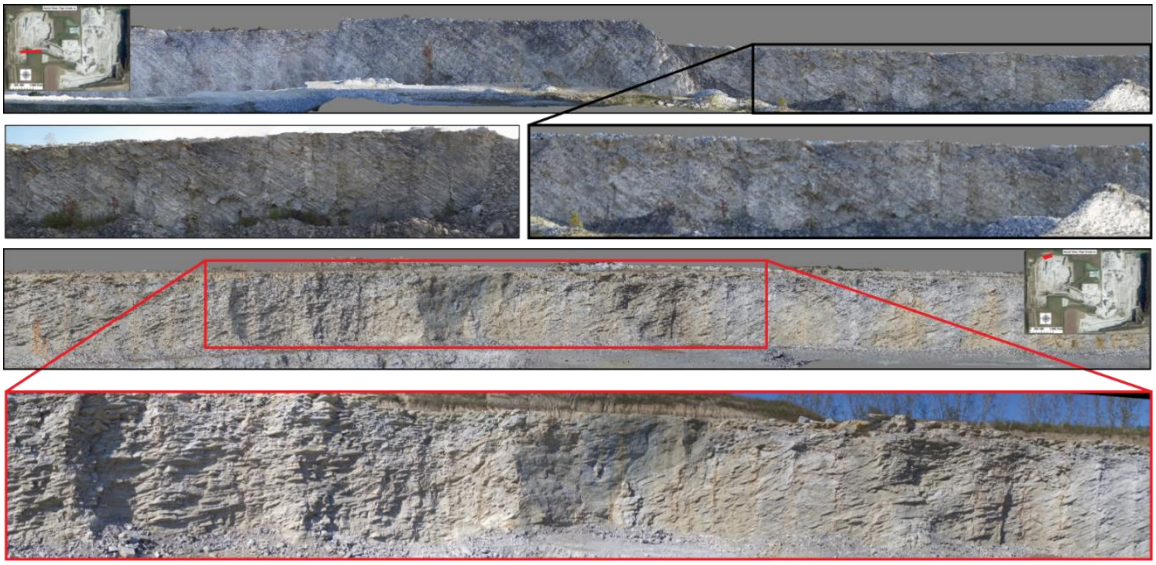

Figure 14: Comparison of DOM with GigaPixel images of the southern wall of the Western section (Top) and the northern wall of the Western section (Bottom). These images show that the geometry of the beds is preserved in the DOM and that even individual dm-scale beds can be resolved. The approximate dip directions were measured in the western section using the DOM.

Pseudo-Measured Sections:

Using the Gigapixel images of the quarry walls, 3 main facies could be picked out, namely the PS-GS, WS-PS, and the BR. Bed tracings were performed on all walls of the Western section to show the overall bed geometry (Figure 15). Figure 16 shows a 21 m section of the southern wall of the western section. The beds dip 40-45°. This high dip, along with the decimeter thick beds with abundant pinch outs, necessitates close spacing (~3 m) of the measured sections. On the southern wall, 24 measured sections were constructed from the high resolution GigaPan images. The measured sections and pseudo-wells which populated with facies logs can be seen overlain onto the southern wall in the western section (Figure 17). In general, the PS-GS beds are thicker (ranging from 5cm-1m) than the WS-PS beds which range from 5-60 cm in thickness. The BR are similar in thickness (ranging from 10 cm-140 cm) to the PS-GS but can be significantly less extensive laterally. In general, the PS-GS are most laterally extensive in the dip direction, and they are often truncated at the top, making it difficult to give a range of downslope length. Some of the beds are preserved in entirety and extend up to approximately 20 m along dip. The WS-PS is the least extensive laterally (< 3 m-~15m) and commonly fill lows between PS-GS beds.

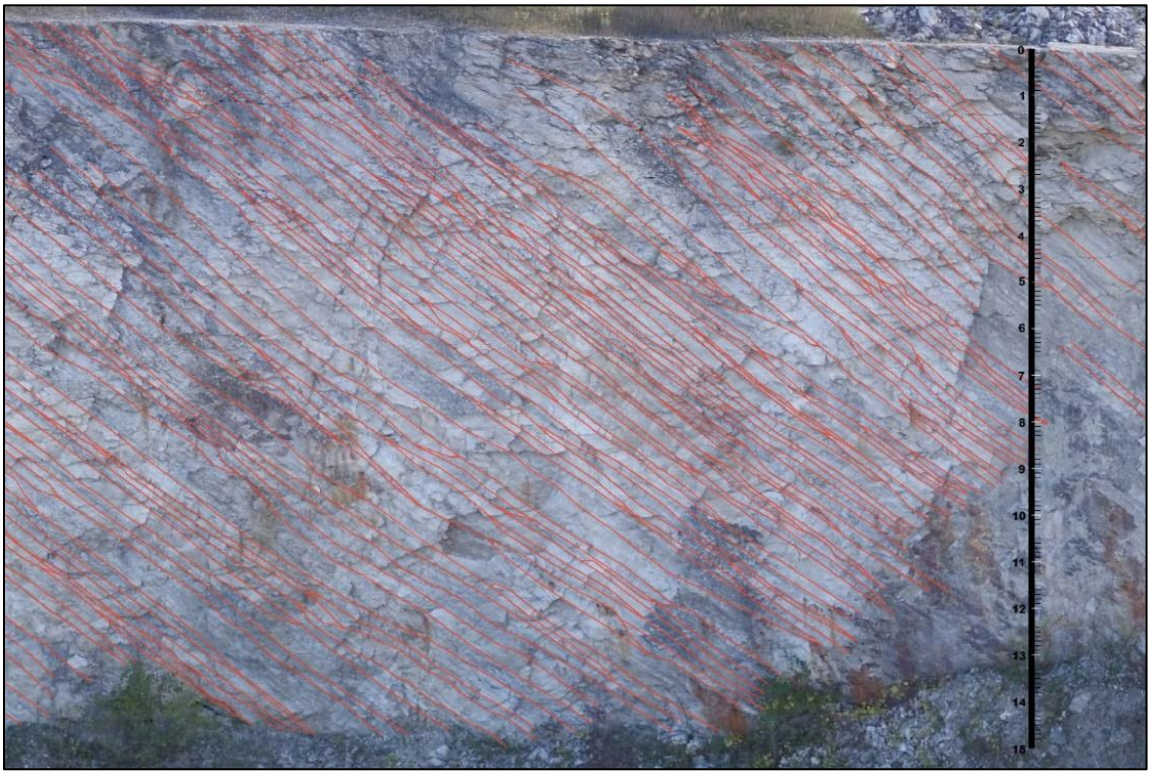

Figure 15: Bed tracings on a 21m section of the southern wall of the western section of the quarry. This was the first step in creating pseudo measured sections. In some sections of the wall, beds could not be traced or were indistinguishable. Note the ~40° apparent dip and the lenticular geometry of the beds. Scale bar is 15 m and is subdivided into meter and decimeter increments.

Figure 16: A 21 m section of the southern wall of the Western section showing bed tracings and the pseudowells at 3 m spacing. This was the second step in the process of creating pseudo measured sections. The meter-scale lateral (downslope) variability and the dm- to m-scale vertical variability of the slope beds can be observed in this image. Scale bar is 15 m and is subdivided into meter and decimeter increments.

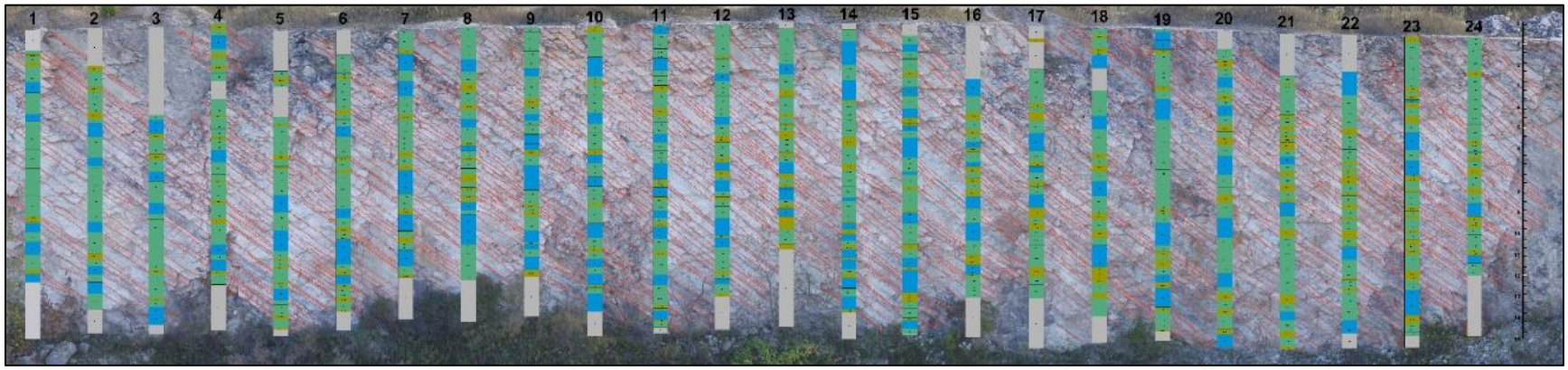

Figure 17: All 24 pseudowells from the southern wall of the Western section of the quarry showing the facies logs overlain on the bed tracings and pseudowells. Green is PS-GS, Brown is WS-PS, Blue is BR, and Grey is Indistinguishable. Each bed was placed into these 4 categories where it intersected the pseudowell. This allowed for calculation of the percent cover of each facies.

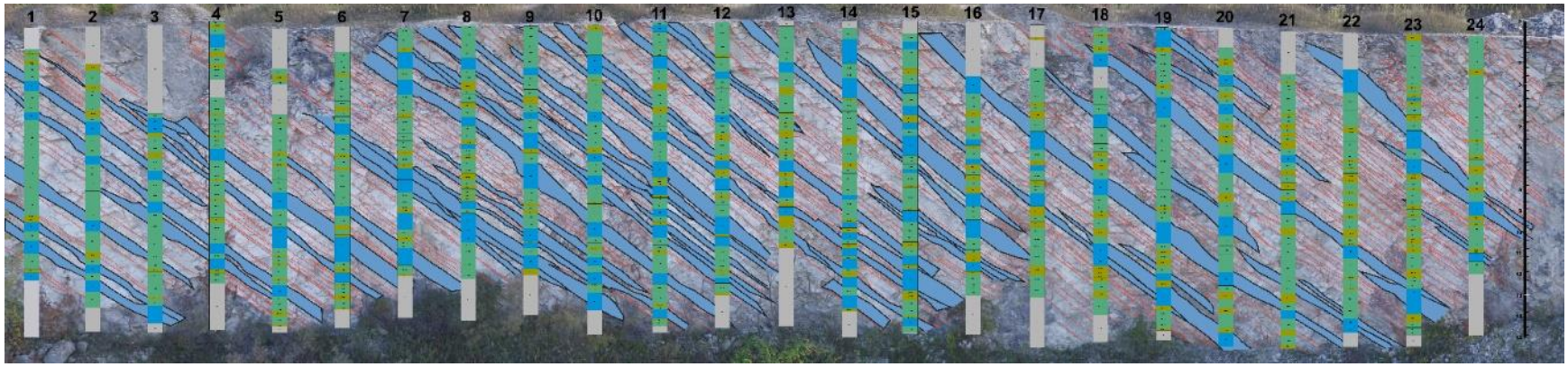

Figure 18: Brachiopod beds (or groups of brachiopod beds) occurring approximately every 2-3 m when measured perpendicular to bedding (brachiopod beds infilled with blue). In some instances, the BR facies graded into the PS-GS facies in the same bed. In those cases the entire bed was colored blue to maintain continuity. This possible cyclicity could be a potential avenue for developing a sequence stratigraphic framework in the future, but more detailed sampling would be necessary. Scale is 15 m long and is broken up into meter and decimeter increments.

The percent cover for each facies is shown in Table 2. The PS-GS makes up the majority (51%) of the strata in the 24 wells, with the WS-PS making up an average of 12%, BR making up 21%, and ID beds making up 16%. While the BR does not make up much of the volume of the slopes, the beds appear to be distributed in what may be a cyclical pattern (the beds may be deposited by storms or some other non-cyclical process) and have a spacing of about 2-3 m when measured perpendicular to bedding (Figure 18).

Table 2: Table displaying the total length and percent cover of each facies in the 24 pseudowells. The PS-GS makes up the majority of the slopes, followed by BR, ID, and WS-PS, respectively.

Well #	Total Length (m)	PS-GS (%)	WS-PS (%)	BR (%)	ID (%)
1	14.7	54	5	16	25
2	14.5	55	7	17	20
3	14.6	46	5	17	32
4	14.6	54	9	15	21
5	14.4	50	9	16	25
6	14.3	56	12	18	15
7	13.7	44	10	31	15
8	14	53	11	22	14
9	13.7	47	9	30	14
10	14.7	53	6	32	8
11	14.7	57	11	30	2
12	14.5	57	10	22	11
13	14.5	41	18	14	28
14	15	45	12	33	10
15	14.8	50	12	34	4
16	14.7	34	14	22	30
17	15.4	45	16	11	28
18	14.9	46	18	20	15
19	14.8	57	12	28	3
20	15.1	50	17	27	6
21	15	57	20	9	13
22	14.9	53	15	16	16
23	14.8	53	23	20	4
24	14.2	60	13	7	20
Total	**350.5**	**51**	**12**	**21**	**16**

Because of the high dip of the beds (up to 45°), there are rapid lateral changes in facies. Even with a well spacing of 3 m, approximately 2 m of the ~15 m of vertical exposure does not intersect the next well. Figure 19 shows the lateral heterogeneity of bedding. The blue triangle shows the coverage of beds which intersect measured section A, while the green triangle shows the beds which intersect measured section B, assuming that all beds traverse the wells and maintain constant dip. Accordingly, two wells 21m apart and drilled to the same depth could potentially intersect entirely different foreset strata. However, these assumptions do not represent the slope beds very well, as some of the WS-PS beds form lenses that are not intersected by any pseudo wells. Indeed, very few of the more extensive PS-GS beds actually span the full 21 m. Therefore, there is potential for completely new groups of foreset strata at even closer well spacing.

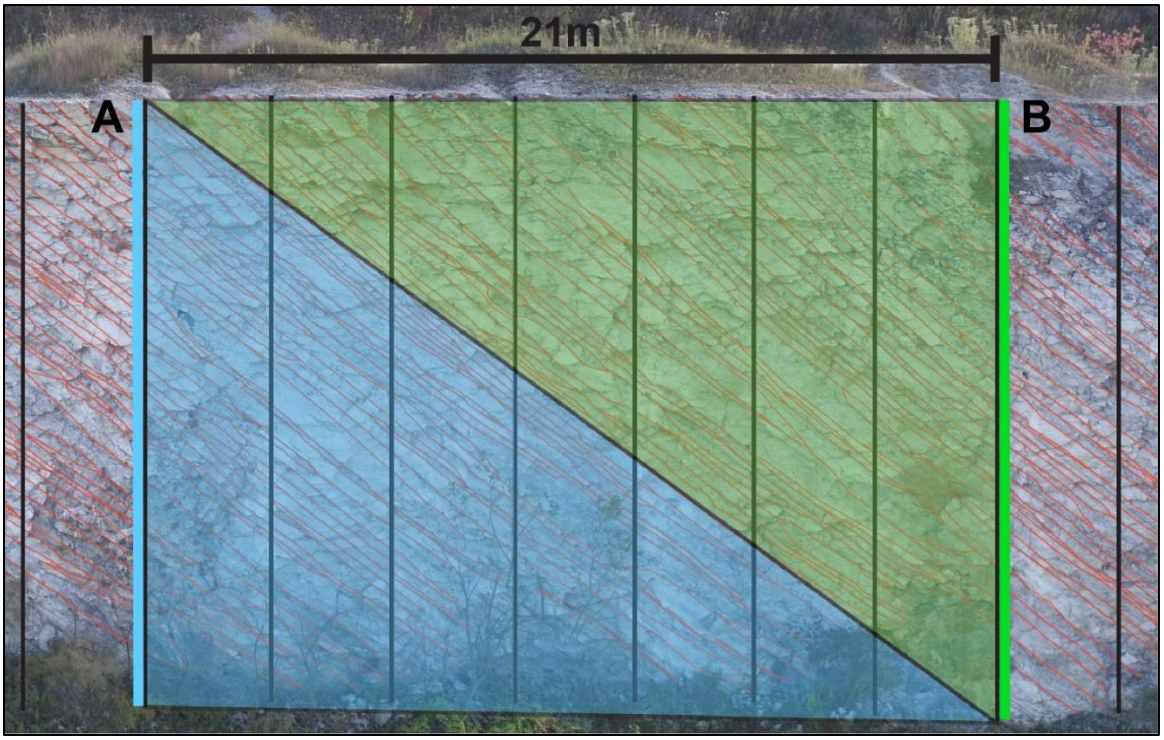

Figure 19: Photograph of the southern wall of the western section showing that two wells drilled 21m apart could potentially intersect different foreset strata. The blue triangle represents the beds intersecting the far left well (A) and the green triangle represents the beds intersecting the far right well (B).

Bed tracings of some walls in the eastern quarry were also constructed (Figure 20). The beds of the SE corner of the eastern section of the quarry have apparent dip varying from 2° at the bottom of the wall to approximately 35° at the top. This change in dip may record the aggradation of the reef core as the declivity of carbonate slopes shedding off of platforms have been shown to increase with the height of the platform (Schlager and Camber, 1986). The same lenticular, decimeter scale beds can be observed in the eastern section (inset picture); however, the beds are more laterally extensive than in the western section of the quarry, with some beds extending for

approximately 60 m before pinching out downdip or being truncated updip, suggesting the possibility of further extension.

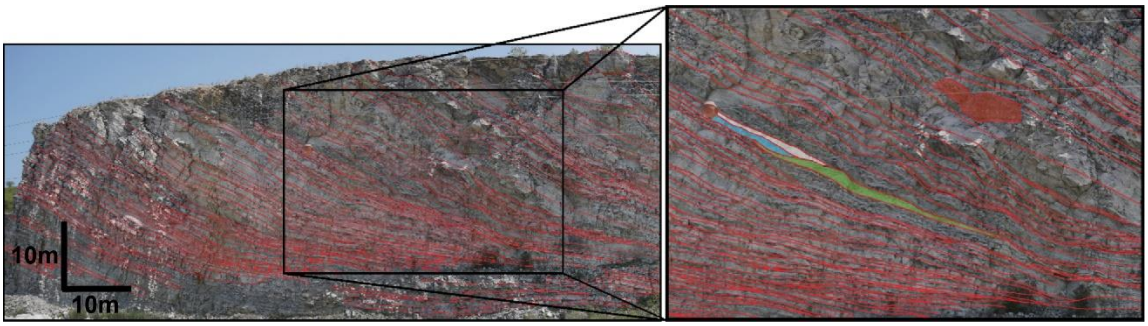

Figure 20: Bed tracings at the SE corner of the eastern section of the quarry, with apparent dip ranging from 2° at the bottom to 35° at the top, likely recording the aggradational growth of the reef core. The inset picture shows the lenticular geometry with the beds infilled in blue, white and green as well as a talus block from the inferred reef crest infilled with red.

Analysis of Faunal Abundance and Diversity

There are various types of fauna, but the most abundant include stromatoporoids (laminar, domal (low and high), and rare columnar morphotypes), crinoids, brachiopods, tabulate and rugose corals, bryozoa, gastropods, and rare trilobites. Overall, crinoids were the most abundant allochem type in the form of disaggregated columnals and ambulacra. However, some samples from the western section contained tabulate corals as the dominant allochem, along with large (dm scale) tabulate coral colonies in blocks from the Western section of the quarry (Figure 21), as well as beds and samples full of large (multiple cm in length) brachiopods (Figure 22). Amalgamated laminar to low domal stromatoporoids are present in samples from the western section of the quarry (Figure 23). Large, cm-scale high domal stromatoporoids were observed in the eastern section (Figure 24). Table 3 shows the percentage of samples containing each allochem as the dominant (highest percent cover) allochem, and Table 4 shows the percentage of samples containing each allochem.

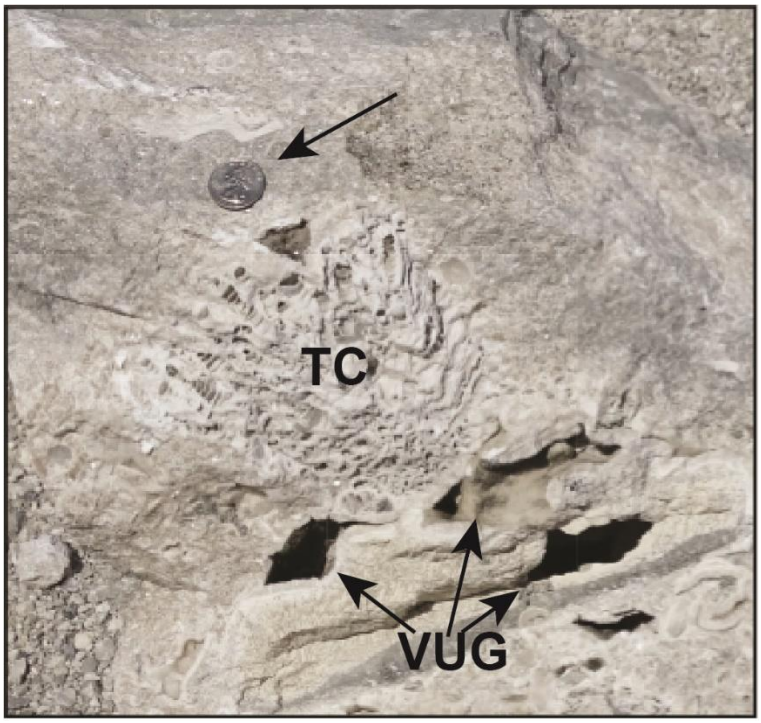

Figure 21: Float block in the Western section of the quarry with a tabulate coral colony (TC). Also present are vugs that are partially or completely infilled with cement. US Quarter for scale indicated by a black arrow.

Figure 22: Float block from a brachiopod bed in the western section of the quarry. The sample is composed mainly of large pentamerid brachiopods, likely *Kirkidium,* sp. Photo scale is in centimeters and inches.

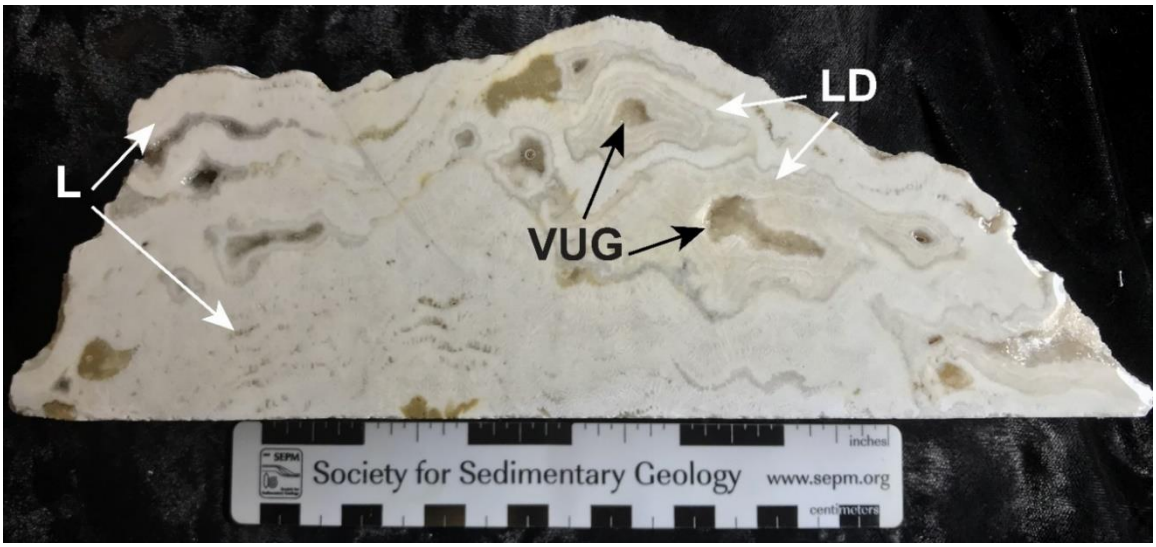

Figure 23: Laminar (L) to low domal (LD) stromatoporoid colonies from the western section of the quarry. Cm-scale vugs are present throughout the sample. Scale is in centimeters and inches.

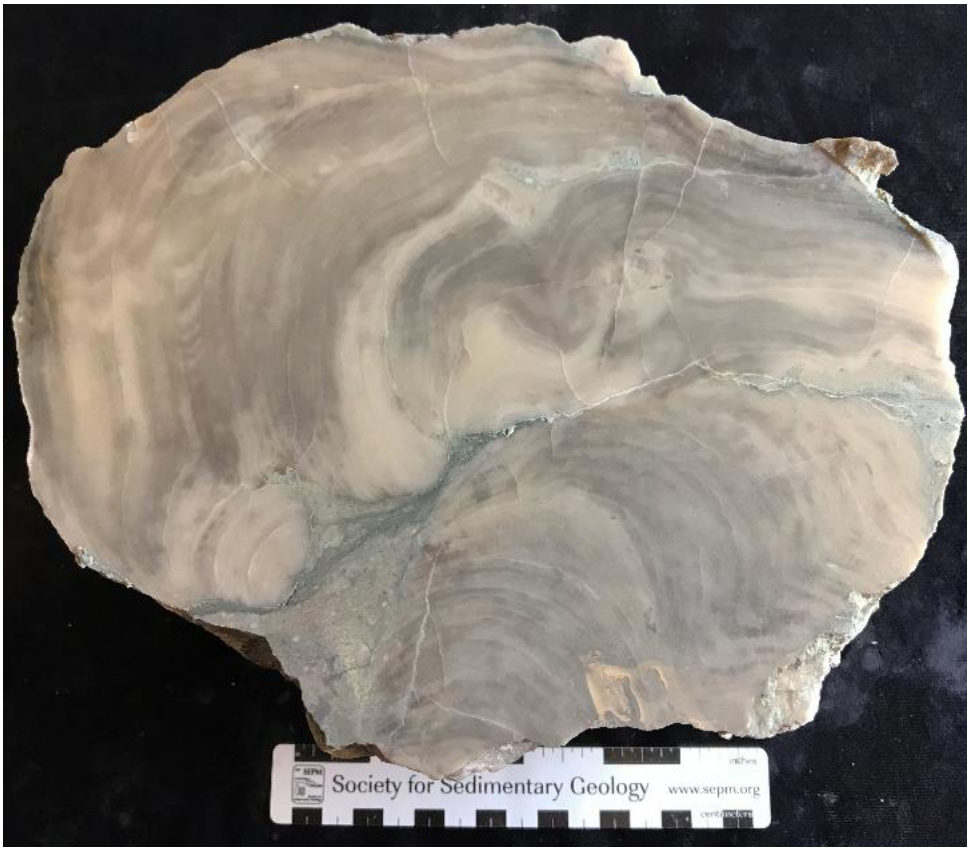

Figure 24: Cross sectional view of high domal stromatoporoids from the eastern section of the quarry. These types of stromatoporoids were observed only in the eastern section of the quarry. Scale is in centimeters and inches.

Table 3: Percentage of samples which had each allochem as its dominant constituent. The samples from the eastern section were the least diverse and are dominated by crinoidal debris. The western and southern sections are dominated by other types of allochems, most notably tabulate corals and stromatoporoids.

	Dominant Allochem Percentage		
	Western	**Eastern**	**Southern**
Crinoids	52%	100%	83%
Stromatoporoids	16%	0%	9%
Brachiopods	0%	0%	0%
Tabulate Corals	24%	0%	4%
Rugose Corals	4%	0%	4%
Trilobite	0%	0%	0%
Bryozoa	4%	0%	0%

Table 4: Percentage of samples which contained each allochem. The Eastern section samples are the least diverse with a low percentage of samples containing stromatoporoids, brachiopods, tabulate corals, and rugose corals.

	Allochem Occurrence Percentage		
	Western	**Eastern**	**Southern**
Crinoids	92%	100%	100%
Stromatoporoids	52%	9%	26%
Brachiopods	68%	18%	61%
Tabulate Corals	64%	36%	65%
Rugose Corals	20%	18%	52%
Trilobite	8%	9%	4%
Bryozoa	8%	9%	13%

Visual Estimation Results:

Table 5: Average percent cover of grains, mud, cement, and porosity for each section of the quarry. The Western and Southern sections had the highest percent cover of grains and cement, while the Eastern section had the highest percent cover of mud.

Visual Estimation Results					
Quarry Section	**No. of Samples**	**Average % Grains**	**Average % Cement**	**Average % Mud**	**Average % Porosity**
Western	25	38%	41%	19%	2%
Eastern	11	29%	30%	36%	5%
Southern	23	44%	40%	10%	6%

A summary of the details of the visual estimation results by quarry section is in Table 5. These values are averages of all samples analyzed, which were a mixture of hand samples and thin sections and they show that the western and southern sections had a higher percentage of grains and a lower percentage of mud than the eastern section. The average percentage of cement for all sections of the quarry, but this only accounts for the bulk percent coverage of cement and does not consider the different types of cement. The porosity percentage is also similar, but because many of the samples were thin sections, this measurement does not take into account the cm-scale vugs which were found mostly in the western and southern sections of the quarry.

Grain/Allochem Analysis:

The Western section contained an average of 38% grain cover. The lowest grain cover was 15% and several samples contained 60% grain cover. The samples from the eastern section of the quarry had an average of 29% grain coverage, with the lowest percentage being 5 and the highest being 65%. The southern section samples average 44% grain coverage, with a range of 5-60%.

Cement Types and Abundance:

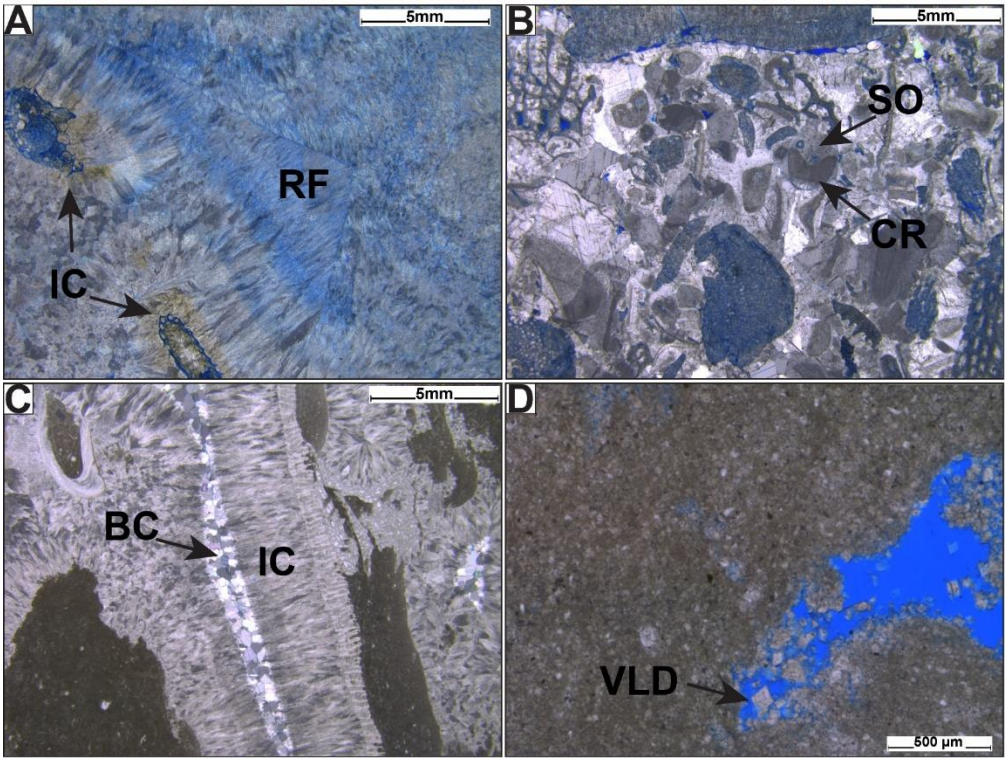

Figure 25: Thin section photomicrographs showing different types of cement. A) Radiaxial fibrous (RF) calcite cement and isopachous cement (IC) surrounding skeletal fragments (XPL, Scale=5mm), B) Syntaxial overgrowth (SO) cement surrounding crinoid (CR) fragments (PPL, Scale=5mm), C) Isopachous cement (IC) surrounding blocky calcite (BC) cement (XPL, Scale=5mm), and D) Vug lining dolomite (VLD) cement in the form of euhedral dolomite rhombs (PPL, Scale = 500µm).

Many types of calcite and dolomite cement are present in samples from the Pipe Creek Jr. complex. These include the following types of calcite cement: 1) radiaxial Fibrous, 2) isopachous, 3) syntaxial overgrowth, and 4) blocky. The only type of dolomite cement observed was a vug lining cement composed of euhedral rhombs (Figure 25).

The western section of the quarry contains the highest average percent cover of cement on among all samples with approximately 41%. The thin sections from the western quarry have seemingly no cement (<1%) to more than 60% cement. All types of cement are in the samples from the Western section, but the dominant type is typically isopachous or radiaxial fibrous cement. Also present within the western section of the quarry are large (cm-scale) void-filling botryoids of radiaxial fibrous cement (Figure 26).

Figure 26: Sample showing cm-scale, void filling botryoidal cement in hand sample (indicated by black arrows) from the western section of the quarry. Scale is in inches and centimeters.

The eastern section of the quarry contains an average of 30% cement, with all types of cement present. Blocky calcite and radiaxial fibrous cement are dominant. No void-filling botryoids were found in the eastern section.

The Southern section of the quarry contains an average of 40% cement, again with all types of cement present. One sample contains 92% radiaxial fibrous cement, while the lowest cement content is 5%. Syntaxial overgrowth and radiaxial fibrous cement are dominant in the southern quarry samples. Sample B1-01 contains void-filling botryoids of radiaxial fibrous cement.

Mud/Matrix Analysis:

The western section samples has an average of 19% mud, with a range of 0% to 70%. The eastern section has an average of 36% mud, with a range of 0% to 85%. The southern section has an average of 10%, with a range of 0% to 85%.

Porosity Estimation:

The Western section has an average of 2% porosity, with a range of 0% to 5%. This number is likely low, as there were many cm-scale vugs which were not observable in thin sections. The Eastern section has an average of 5% porosity, with a range of 0% to 15%. The Southern section samples have an average porosity of 6%, with a range of 0% to 25%. Once again, this is likely a low estimate because of the cm-scale vugs which were not observable in thin sections Many samples had very little pore space because much of the primary porosity has been occluded with cement of various types.

Grain and Allochem Size Comparison

Partial sections of the cores from the western (A) and southern (B) sections and a slabbed sample from the eastern section are shown in Figure 27. Allochems greater than 3mm in size are outlined and color filled. Table 6 shows the results for each sample. The western and southern sections of the quarry showed a greater percentage of allochems greater than 3 mm.

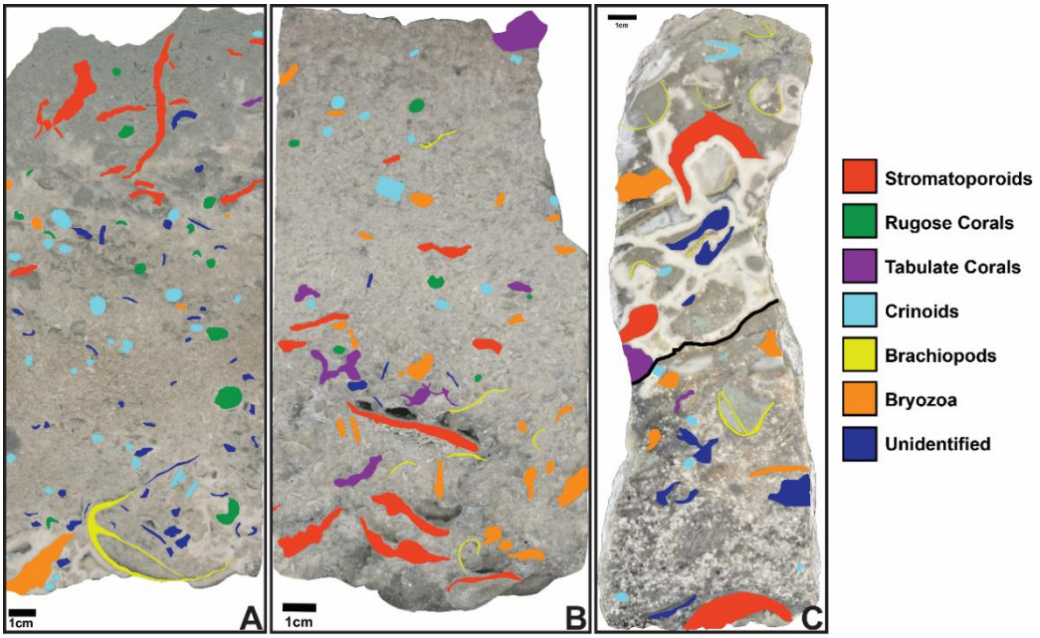

Figure 27: Sections of core from the western section (A) and southern section (B) along with a slabbed sample from the eastern section (C) which have had all allochems larger than 3 mm colorized to aid in estimation of macrofauna coverage. In this case, only the grainstone portions of each sample or core were compared. All scale bars are 1 cm.

Table 6: Table showing the visual estimation results for each of the samples from the different sections of the quarry. The Western and Southern sections had a higher percent of fauna greater than 3 mm.

Macrofauna Coverage (Greater than or equal to 3mm)					
Quarry Section	**% >3mm**	**% <3mm**	**% Cement**	**% Mud**	**% Porosity**
Western	25%	55%	10%	8%	2%
Eastern	15%	60%	5%	25%	0%
Southern	25%	55%	5%	2%	2%

CHAPTER III

Discussion

Deposition of the Pipe Creek Jr. Beds:

In order to better understand the depositional system in which the beds exposed at Pipe Creek Jr. were deposited, it is useful to look at analogs, both modern and ancient. This aids in determining the kinds of depositional and diagenetic processes which might have been active during the deposition of the Pipe Creek Jr. reef complex. It also aids in the determination of the origin of the high angle beds present in the Pipe Creek Jr. quarry.

A useful modern analog for these slope deposits are the Holocene slope beds in the Tongue of the Ocean (TOTO), an intraplatform basin in the Bahamas. Grammer et al. (1993a) divided the foreslope margins in the TOTO, Bahamas into four different zones, each with a distinct morphology: 1) platform edge, 2) the wall, 3) cemented slope, and 4) sediment slope. Of particular interest to this study is the cemented slope, which extended from the base of the wall at around (130-140 m) to depths greater than 365 m at slopes of 35-45°. This cemented slope consists of decimeter thick internal bedding arranged in elongated lenses of coarse or angular debris (Grammer, 1993a). These types of beds are interpreted to have been transported by hyperconcentrated density flows or grain flows along the slope surface because of the lenticular geometry and the coarse, poorly sorted nature of the sediments (Playton et al., 2010). A picture and line drawing from the Tongue of the Ocean shows the elongate lobes or lenses with decimeter thick lenticular beds (Figure 28). Observations of the geometry of the beds, sediment fabric, and types of cement indicate that some of these same processes may have been active during the deposition of the beds in the quarry.

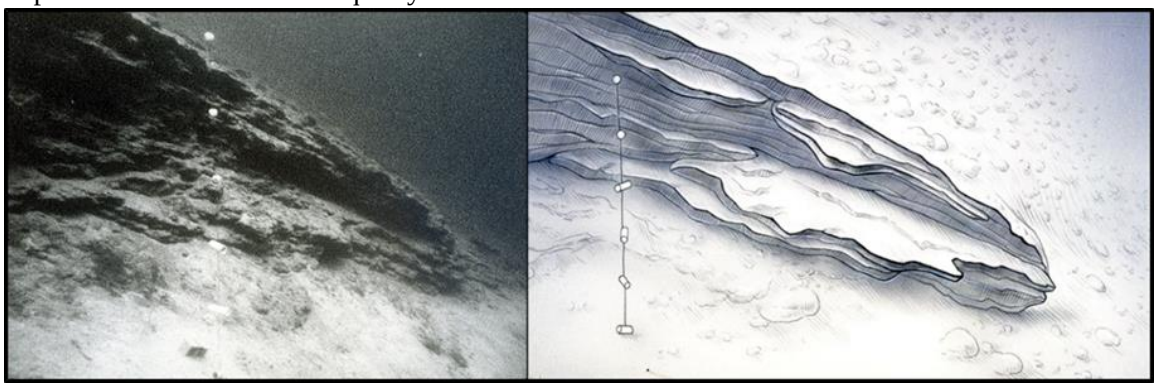

Figure 28: Image and corresponding line drawing of the upper cemented slope beds in the Tongue of the Ocean, which are made up of m-scale lobes of dm-scale lenticular beds of coarse grained, angular, skeletal grainstones. Scale is in 1m increments. Source: Grammer et al., 1993a.

DeVaney et al. (1986) proposed that the high angle (up to 45°) slopes present at Pipe Creek Jr. were above the angle of repose, which they defined as no greater than 35°. However, in a study of over 20 carbonate platform flanks, Kenter (1990) described how the sediment fabric plays a role in the angle of repose and he places the angle of repose for granular, non-cohesive material, like the packstone-grainstone found in the slopes of the TOTO and in Pipe Creek Jr., at 40°. Slopes approaching 45° are considered to be at the angle of yield, which is the upper limiting slope angle at which shearing takes place (Kenter, 1990). This information supports the claim that the slope angles displayed in the Pipe Creek Jr. quarry are depositional and have not been tilted or otherwise modified significantly. This information may also help to explain the arcuate, convex-up cracks running parallel to strike on the slopes in the TOTO. If the slopes are oversteepened and approach the angle of yield, incipient shearing or slumping may occur, causing these cracks to appear on the slope surface (Grammer et al., 1993a; Kenter, 1990). Similar cracks have been observed in cores taken from marginal slopes of Silurian reefs in the Michigan Basin (Wold and Grammer, 2018; Trout et al., 2018). These cracks bear a striking resemblance to the neptunian dikes found in Pipe Creek Jr. quarry. A block diagram of the Tongue of the Ocean alongside a picture of a neptunian dike at Pipe Creek Jr. is illustrated in Figure 29.

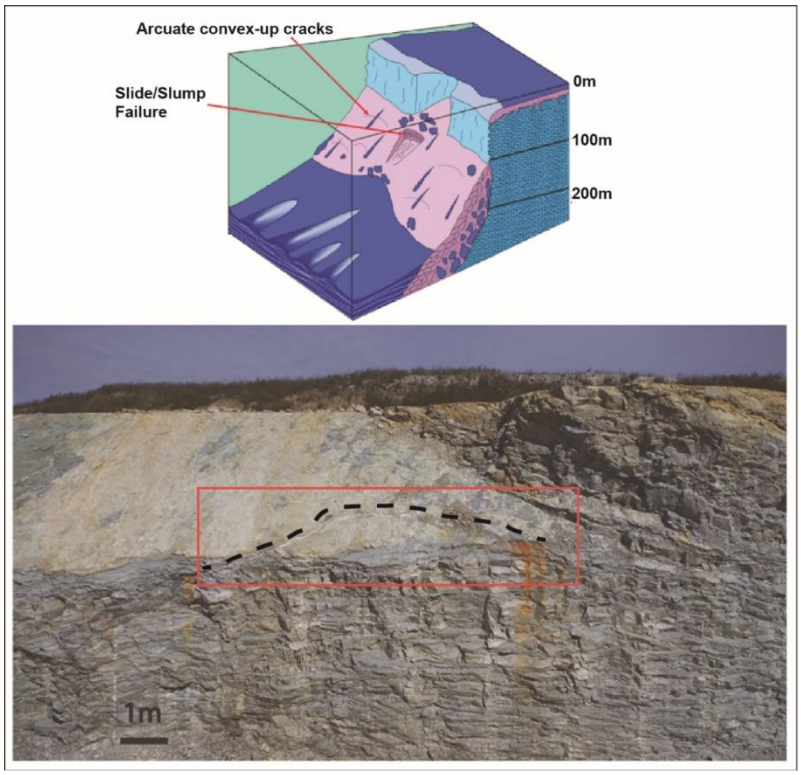

Figure 29: Figure comparing TOTO and Pipe Creek Jr. slopes. Top: Block diagram of the TOTO slopes, showing arcuate, convex-up cracks on the surface of the slopes (Grammer et al., 1993a). Bottom: Image of the surface of the slopes in the Southern section of the quarry, with an arcuate, convex-up crack infilled with white cement outlined in red with dashed line above it tracing the path.

Lehmann and Simo (2000) proposed that syndepositional marine cement might have been a factor in maintaining the slope angles in the quarry. Grammer et al. (1993a) noted an increased amount of syndepositional marine cement on the windward slopes of the Tongue of the Ocean. Grammer et al. (1993b, 1999) also demonstrated the rapid (8-10mm/100yr) growth rates of these cements, indicating the rapid cementation of those slopes within 10s to 100s of years. This allowed the slopes to retain high angles of declivity (up to 45°). Void filling botryoidal cements are present in the Tongue of the Ocean (Grammer et al. 1993b; Grammer et al., 1999), in cores taken from Silurian reef margins in the Michigan Basin (Trout et al., 2018), and in samples from the Pipe Creek Jr. Quarry. The similarities between the Tongue of the Ocean slopes, the slopes of Silurian reefs in the Michigan Basin, and the beds exposed in the Pipe Creek Jr. quarry, along with recent work on the Pipe Creek Jr. complex showing the initial stabilization of the slopes by certain microbial communities (Santiago Torres, 2019), strengthen the claim that the slopes exposed in the quarry cemented rapidly and are at depositional angles.

There has been discussion about whether Pipe Creek Quarry beds were marginal slopes of an aggradational reef or were part of a series of low-angle clinothems on a shelf (Sunderman and Matthews, 1975; Shaver and Sunderman, 1982; Shaver et al., 1983; DeVaney et al., 1986; Lehmann, 1978; Lehmann and Simo, 1989; Frank, 1993; Simo and Lehmann, 2000, etc.). The complex. However, none of these earlier studies had access to the all three sections of the quarry, and therefore did not have the ability to see the reversal of dip direction between the western and eastern sections. Given the intracratonic, platform setting of this area during the late Silurian (Lehmann and Simo, 1989; Spengler and Read, 2010), there is little evidence to suggest a structural explanation of this reversal. Other evidence which points toward a true reef core are the reef talus blocks observed both in this study and others (e.g. Simo and Lehmann, 2000). The most likely explanation is a reef core between the sections of the quarry, indicating the presence of a flat-topped carbonate platform which was truncated during the Tippecanoe-Kaskaskia lowstand (Simo and Lehmann, 2000).

Figure 30 shows a possible progression of the growth of the Pipe Creek Jr. reef complex. Growth was likely initiated as a low relief, bryozoan-crinoid mud mound on the sea floor, much like the Belle River Mills reef (Ritter, 2008; Ritter and Grammer, 2018) and Ray Reef (Wold, 2008; Wold and Grammer, 2018), both of which are Silurian-aged reefs in the Michigan Basin. As the mud mound grew up into shallower water, reef building organisms (stromatoporoids and tabulate corals) started to colonize the mud mound and aggrade. This aggradation caused a carbonate platform to start forming, with steeper slopes on the windward side and gentler slopes on the leeward side. Given the 3rd order sea level cycles which are observable on the Wabash platform during this time (Spengler and Read, 2010), it is likely that there were multiple episodes of reef growth and subaerial exposure of the reef crest and platform. The tops of these presumed 3rd-order sequences are represented by dashed black lines. Finally, latest Silurian and Early Devonian erosion during the Tippecanoe-Kaskaskia lowstand truncated the reef core and the slope beds, leaving only the slope beds exposed in the quarry (Simo and Lehmann, 2000).

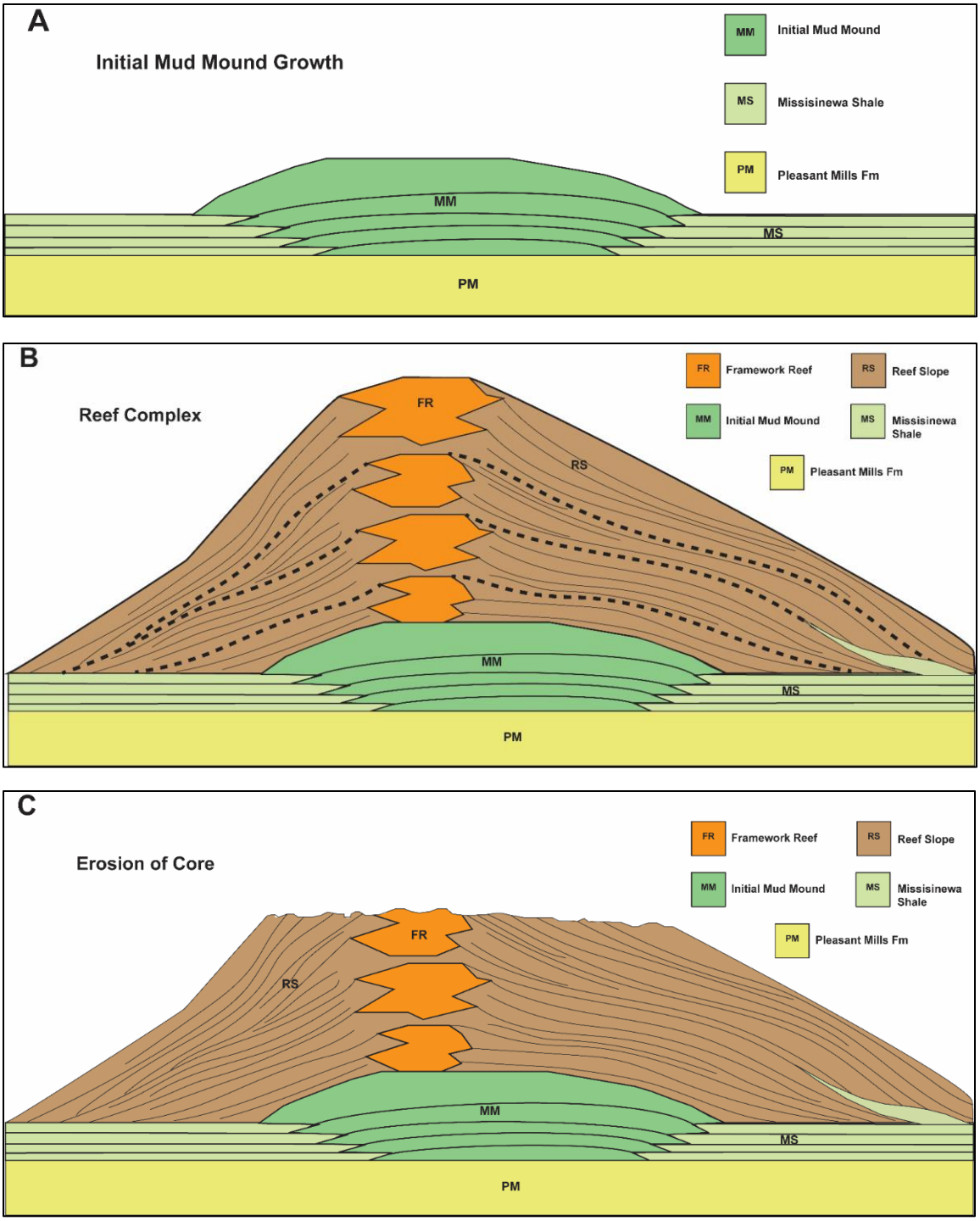

Figure 30: Potential progression of the Pipe Creek Jr. reef complex: A) Low relief crinoid/bryozoan mud mound on the sea floor, B) Carbonate platform displaying multiple sequences (Sequence boundaries represented by dashed black lines) of growth with steeper slopes on windward side and gentler slopes on the leeward side, and C) Erosion of the core of the platform causing only the slopes to be exposed in the quarry.

Windward/Leeward Orientation:

In order to make a determination of a windward/leeward orientation of the Pipe Creek Jr. Reef Complex, several characteristics of windward and leeward margins of carbonate platforms were used as lines of evidence, along with previous determinations of paleowind directions during and around the time of deposition. These characteristics are outlined in Table 7.

Table 7: Table outlining each line of evidence used for determining a windward/leeward orientation for the Pipe Creek Jr. Reef complex. Question marks are used where limitations in either sampling or in-depth observation made it difficult to make a more definitive statement.

Line of Evidence	Present at Pipe Creek	Selected Sources
Steeper slopes on the windward side.	?	Wold and Grammer, 2018; Collins et al., 2006
Higher faunal density and diversity on windward side.	Yes	James and Borque, 1992; Trout et al., 2018
Higher percentage of grainier, more skeletal rich sediments.	?	Grammer et al., 1993a; Wold and Grammer, 2018
More abundant syndepositional marine cement on windward side.	Yes	Klovan, 1974; Grammer et al., 1993a; Gischler, 1995; Trout et al., 2018; Wold and Grammer, 2018, etc.
Low domal to laminar, non-enveloped stromatoporoids on the windward side.	Yes	Klovan, 1974; James and Borque, 1992; Gischler, 1995; Trout et al., 2018

The first line of evidence is steeper slopes along windward margins of a platform. This characteristic of reefs is well documented, including Ray reef in the Michigan Basin, the Tengiz buildup (mostly Carboniferous) in Kazakhstan (Wold and Grammer, 2018; Collins et al., 2006), and Miocene-aged reefs from Malampaya in the Phillipines (Neuhaus et al., 2004). There is some evidence for this in the quarry, with 40-45° slopes in the western and southern sections of the quarry, as well as Neptunian dikes which are related to slope failure in the southern section of the quarry. The eastern section has slopes ranging from 2-35° on the same quarry face and no observable slope beds dipping steeper than 40°. Previous workers have noted more steeply dipping beds (>40°) in the eastern section, but those exposures have been removed by ongoing quarrying. It may also be that the slopes in the eastern section are more distal and therefore the slopes might appear gentler. The eastern section of the quarry is lower in elevation than the

western section (Jon Havens, IMI), personal communication), and so it is possible that the beds exposed in the eastern section had higher dip angles further up dip but have been truncated.

The second line of evidence is that reefs often have higher faunal density and diversity on the windward side of platforms. Ecological succession is typically expressed as increases of species diversity as well as biomass and structural complexity (James and Borque, 1992). Therefore, in higher energy settings, such as along the windward side of a reef or in shallower water, there is an increase in diversity and faunal size in higher energy settings like the windward side of a reef (Trout, 2012; Trout et al., 2018). In this study, faunal density was approximated by the percentage of grains/allochems in the samples from each section of the quarry. The sections with the highest percentage of grains are the western (38%) and southern (44%) sections of the quarry, while the eastern section is lower (29%). Faunal diversity is highest in the western section of the quarry, as it has 5 dominant faunal types in the samples (crinoids, stromatoporoids, tabulate corals, rugose corals, and bryozoans), while the Southern section has 4 dominant faunal types (crinoids, stromatoporoids, tabulate corals, and rugose corals). The eastern section samples are dominated by crinoid grains. Caution should be used when basing claims on this alone, as there were more samples taken from the western and southern sections of the quarry.

The next line of evidence is a higher percentage of packstone-grainstone with larger allochems on the windward side. Previous research on windward carbonate slopes has shown they are dominantly composed of skeletal grainstones with angular or elongate grains which contributes to the steeper foresets, while the leeward foresets have a higher percentage of muddier wackestone and packstone, which are swept from the top of the carbonate platform (Wold and Grammer, 2018; Grammer et al., 1993a). From analysis of the percent cover of each facies on the southern wall in the western section, results indicate that the PS-GS facies represent 51% of the wall, WS-PS represent 12%, and Br 21%, while 16% is indistinguishable. Observations of high-resolution photos from the quarry faces from the eastern section suggests that there is a higher percentage of darker sediment, indicating a higher percentage of the muddier sediments in the eastern section of the quarry. The overall visual estimation results showed the western and southern sections had a higher percentage of grains and lower percentage of mud than the eastern section. Comparison of the percent cover of fauna >3 mm in size showed 25% cover in the western and southern sections, with only 15% cover in the sample from the eastern section.

Windward slopes contain more abundant syndepositional marine cement in the form of isopachous, radiaxial fibrous, and void filling botryoid cements (Klovan, 1974; Grammer et al., 1993a; Gischler, 1995; Trout et al., 2018; Wold and Grammer, 2018, etc.). While the total amount of cement is similar in all sections of the quarry, Radiaxial Fibrous cement was the dominant type of cement in the western section, and void filling botryoids were only found in samples from the western and southern sections of the quarry. The eastern section of the quarry is dominated by blocky calcite cement, and the southern section contains syntaxial overgrowth and blocky calcite cement that is co-dominant.

The last line of evidence is based on the morphotypes of stromatoporoids. There has been some debate on which morphotypes are representative of lower energy/leeward environments and which are representative of higher energy/windward conditions. James and Borque (1992)

showed that the mounded/high domal, enveloped stromatoporoids and columnar stromatoporoids are lower energy morphotypes, and these are only found in the eastern section of the quarry. Low domal to laminar, non-enveloped stromatoporoids, as well as massive colonies of tabulate corals have been shown to occur mostly on the windward side and on the crests of reefs (Klovan, 1974; James and Borque, 1992; Trout et al., 2018). These morphotypes and large colonies are only in samples from the western and southern sections of the quarry. Gischler (1995) found that some of the high domal and mounded stromatoporoids are on the windward side in a higher energy environment in his study of the Devonian Iberg reef, suggesting that this line of evidence is not definitive.

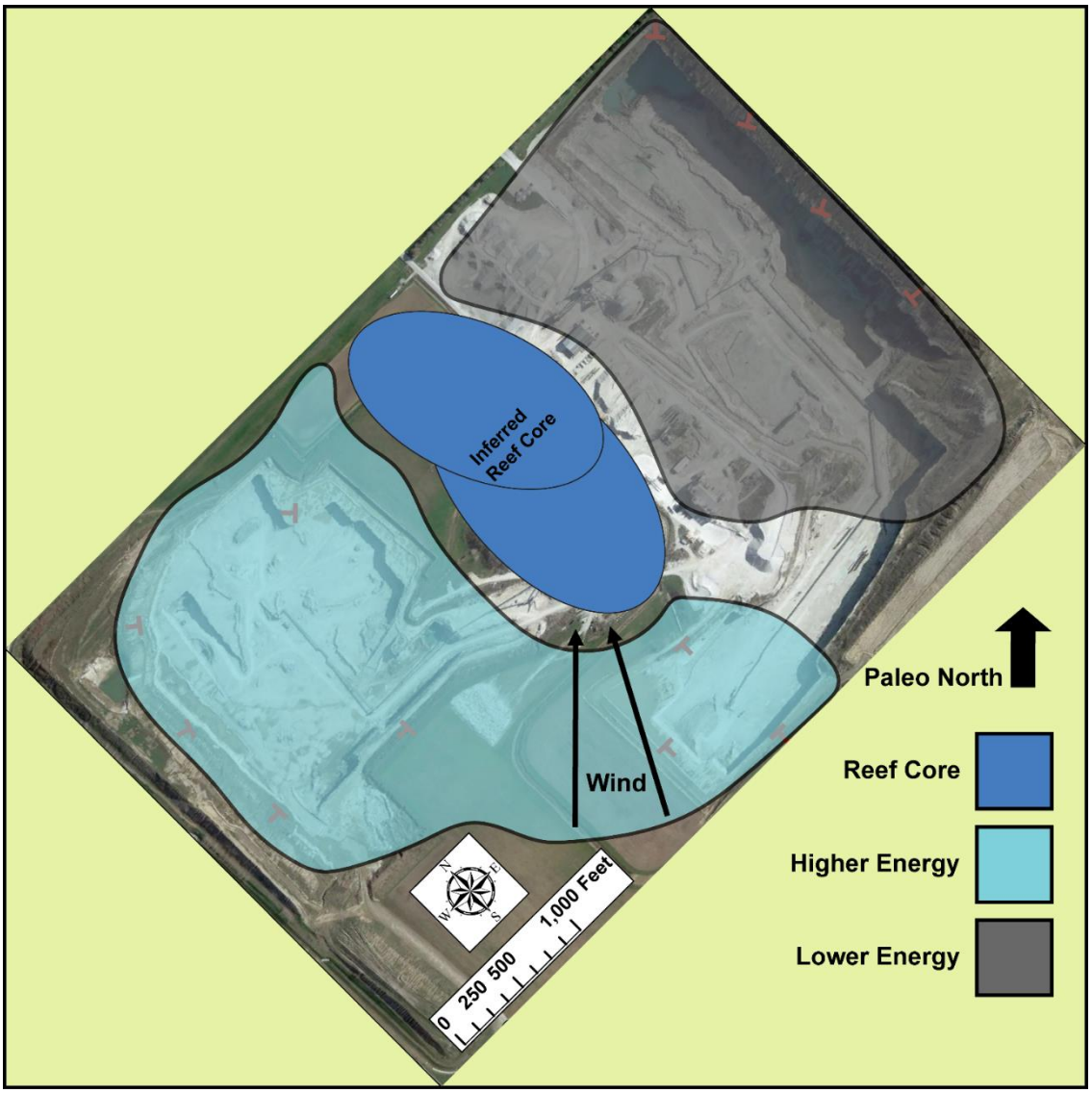

Figure 31: Facies mosaic overlain on a satellite image which has been rotated 45° counterclockwise to match Late Silurian orientation. Light blue overlay represents the windward and more energetic side of the reef complex, while the grey area represents the lower energy, leeward side of the reef complex. Base image from Google Earth.

Combining all these lines of evidence points toward a southerly to southeasterly paleowind direction, which matches with the interpretation of Ray reef (Trout et al., 2018; Wold and Grammer, 2018) and with the estimations of Silurian trade winds from the paleoclimatic modeling of Spengler and Read (2010). Figure 31 is a facies diagram overlain on an aerial view of the quarry, which has been rotated 45° counterclockwise to match the Late Silurian orientation. With a southerly to southeasterly paleo-wind direction, there would be a higher percentage of coarser grained, poorly sorted sediments with more abundant syndepositional marine cement on the more energetic windward slopes, as shown by the overlain light blue area. Conversely on the lower energy, leeward margin, there would be a higher percentage of muddier sediment with somewhat less abundant syndepositional marine cement, as shown by the overlain grey area.

Reservoir Implications:

It is abundantly clear that there is significant lateral (mostly at the meter scale) and vertical (at centimeter to meter scale) heterogeneity of facies. These rapid facies changes would present a unique set of challenges when targeting reefs and reef slopes as reservoirs. Heterogeneities exist at multiple scales in carbonate reservoirs, from a regional or seismic scale (e.g. Permian Capitan Reefs in West Texas) (Kerans and Tinker, 2000), to a reservoir scale (e.g. Ray Reef) (Wold and Grammer, 2018; Trout et al., 2018), and down to a bed by bed, cm scale like the slope beds in the quarry. Much of this heterogeneity is not resolvable by seismic methods, emphasizing the importance of outcrop and core-based study in understanding carbonate rocks as reservoirs.

It has been observed that moving laterally in the foresets comes with rapid changes in facies, but it also comes with rapid chronostratigraphic changes. Moving from a proximal to distal location in the foresets, the primary cross-strata become progressively younger. Sequence stratigraphic studies on Silurian Reefs in the Michigan Basin (Ritter, 2008; Ritter and Grammer, 2018; Wold, 2008; Wold and Grammer, 2018, etc.) demonstrate that understanding the chronostratigraphy of these reefs can lead to enhanced predictability of reservoir intervals. In the case of these Michigan Basin reefs, the best reservoir intervals are associated with the tops of the third order sequences, and it has been posited that exposure horizons in the core and crest of the reef which defined the tops of those sequences are expressed as marine hardgrounds in the slope strata. This led to the ability to map those sequence boundaries into the slopes. This means that understanding the chronostratigraphy, depositional sequence, and geometry of the slope beds is essential to target reservoir intervals in the slope beds.

For example, if one of the older, more proximal sequences had better reservoir quality, a distal well might not even intersect those strata because of the high dip, and in order to target the thickest reservoir interval an even more proximal well would have to be drilled (Figure 32). This example only considers the third order sequences, but it was clear from the aforementioned studies in the Michigan Basin there were higher order frequencies and cycles of sea level change controlling the deposition and distribution of reservoir intervals, and the cyclical nature of the Brachiopod Beds in this study seem to suggest that claim is also valid for the Pipe Creek Jr. slope beds. There is yet more evidence for this when breaking up the individual decimeter scale grain flow beds into meter-scale lobes and lenses. It is likely there are marine hardgrounds separating

these lobes, which may have been caused by these higher order frequencies and cycles of sea level change. These hardgrounds have been observed in samples from this study (many with borings on the surface) and in samples from previous studies of the Pipe Creek Jr. reef (e.g. Lehmann and Simo, 1989). With this knowledge, it becomes clear that understanding only the broader scale sequence stratigraphy does not capture the full story of the deposition of these and other similar foreset strata, and higher resolution sequence stratigraphy is usually necessary to accurately describe and characterize these slope beds as potential reservoirs.

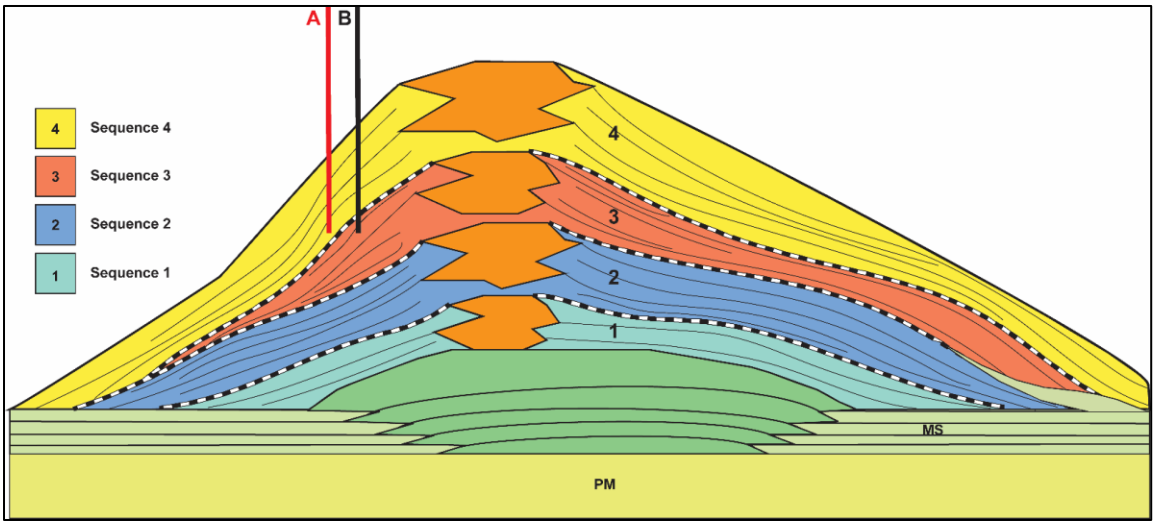

Figure 32: Cross-sectional diagram showing heterogeneity in facies and chronostratigraphy, with the potential for a well drilled to the same depth but slightly more distal or proximal location might result in an intersection of not only different beds, but beds from a different depositional sequence. Diagram is not to scale, but the principle is applicable at multiple scales.

In order to understand carbonate slope strata as reservoirs for hydrocarbons, it is useful to look at other carbonate slopes which have already produced oil and gas, especially to show the effect of paleowind direction on reservoir quality. A reservoir analog which works well for this is the Carboniferous Tengiz buildup in the northern Caspian region of Kazakhstan. The Tengiz Buildup is a flat-topped, isolated carbonate platform with steep marginal slope strata which locally dip 45° (Collins et al., 2006). The platform has an aerial extent of about 90 km^2, which is significantly larger than the estimated 1.5 km^2 aerial extent of the Pipe Creek Jr. reef complex. Despite this size differential, the marginal slopes of the Tengiz buildup show many similarities to the slope facies exposed at Pipe Creek Jr. The marginal slopes of the Tengiz buildup can be divided into an accretionary margin on the NE side of the platform and an allocthonous margin on the SW side of the platform (Collins et al., 2006). The marginal slopes, especially the accretionary margin, contain zones of porosity and permeability due to the primary sediment fabric and interpreted depositional mechanism which show that the marginal slopes contain reservoir intervals which contribute to the overall reservoir volume of the Tengiz field (Collins et al., 2006). The accretionary margin is assumed to be the windward margin because the framework reef builders form a rim on the platform margin and the coarse-grained carbonates which form the slopes are dipping to a greater degree than the allochthonous margin. The lower slope of the accretionary margin is mostly made up of resedimented algal boundstone from the upper slope and skeletal grains from the platform margin deposited by grain flows. This lower

slope portion has the best developed zones of porosity and reaches 18-20% in some areas (Collins et al., 2006). Analysis of the Tengiz buildup shows that wind-driven processes as well as sediment fabric and composition affect the distribution of reservoir intervals within marginal slopes.

Another useful analog is Ray reef, which produced oil and gas and is currently being used for natural gas storage (Wold and Grammer, 2018). Figure 33 shows a cross-sectional view of Ray reef and geo-statistical models of facies, porosity, and permeability (Wold and Grammer, 2018). The porosity and permeability data was obtained from 16 cores with whole core analyses. The data was converted to digital log curves and imported into Petrel, Schlumberger's modeling software. This cross-sectional view also shows the typical asymmetry of these types of isolated, flat topped carbonate platforms as the framework reef can build up higher on the windward side of the platform.

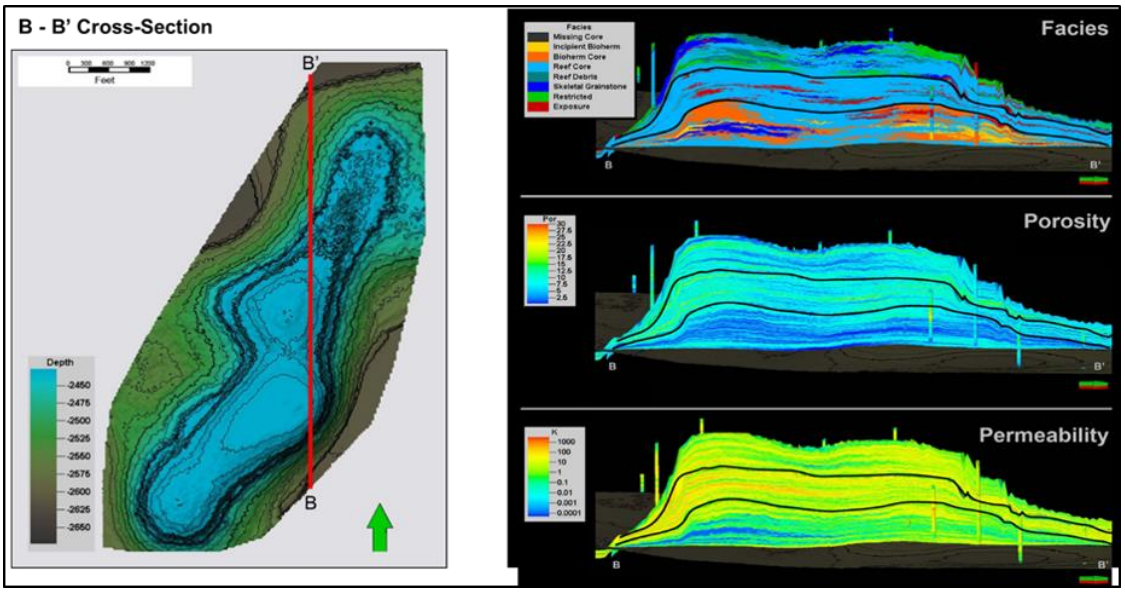

Figure 33: Cross-sectional view of Ray Reef, with geo-statistical models of facies, porosity, and permeability from top to bottom, respectively. In the structure map on the left, steeper slopes can be found on the SE side of the reef complex. Aggradation on the windward side of the reef, which is typical, can be observed in the cross-sectional views on the right. These cross-sections reveal heterogeneity of facies both laterally and vertically. Areas of higher porosity and permeability exist at the tops of the 3rd Order sequences (Solid black lines) as well as in the windward slopes. Source: Wold and Grammer, 2018

Silurian reefs in the southern reef trend in the Michigan Basin, like Ray reef, average about 15-20% primary production when exploited for hydrocarbons (Grammer et al., 2009). This is due to the complex internal heterogeneity of facies and porosity types within the reef cores and flanks. Finding a correlation between reservoir quality porosity and permeability and facies types has historically been difficult in carbonate reservoirs (Grammer et al., 2004). However, a sequence stratigraphic framework with detailed facies analysis, like the above Wold and Grammer (2018) example, has been shown to enhance correlations between reservoir porosity and permeability and facies types in carbonate reservoirs, as well as increase predictability of

reservoir intervals because of the consistency of facies stacking patterns (Grammer et al., 2009). In the case of Ray Reef, areas of reservoir quality porosity and permeability were found to be associated with the 3rd and 4th order sequence boundaries, which were represented by exposure intervals along which karstification and associated alteration enhanced the porosity and permeability (Wold and Grammer, 2018). Detailed facies analysis and modeling done on the reef flanks points towards another interval of high reservoir quality on the windward slope of Ray Reef (Wold and Grammer, 2018), showing the potential for paleo wind-driven currents to influence the reservoir quality within a reef reservoir.

Detailed and more precise measurements of porosity and permeability were not possible for this study, nor was the detailed facies and sequence stratigraphic analysis from the above examples. Future work could involve a series of cores behind the quarry walls and/or shallow seismic, which might give the detail necessary to work out a sequence stratigraphic framework for the slope beds in the quarry. Combining these analyses with measurements of porosity and permeability would likely lead to a more complete characterization of the Pipe Creek Jr. slope strata as potential reservoirs.

CHAPTER IV

Conclusions

Depositional Processes:

The Pipe Creek Jr. quarry has approximately 4.8 km of vertical exposures of limestones from the Wabash Formation. The slope beds exposed in the quarry are decimeter-scale, lenticular beds which are grouped together into meter-scale lobes or lenses. The coarse, angular, skeletal fragments which make up the individual lenticular beds are consistent with sediments deposited by a grain flow process. This same process is proposed to be the main depositional process for slope sediments at the Tongue of the Ocean of the Bahamas and Silurian reefs in the Michigan Basin.

The slope strata exposed at Pipe Creek Jr. show many other similarities to the Tongue of the Ocean and other Silurian reefs in the Michigan Basin. Similarities include beds dipping at 40 to 45°, presence of void-filling botryoidal cements, and variation of fauna, facies, and abundance of early syndepositional marine cements consistent with a windward/leeward orientation. These similarities as well as other work on the angles of repose for carbonate slopes show that these slopes are likely dipping at depositional angles and were not tilted or enhanced significantly post deposition.

The overall structure of the reef system can be observed by looking at the dip direction of the beds in the quarry, which show a general reversal when moving from the western to eastern sections and seem to point to a common center when moving around the quarry. The presence of talus blocks consisting of reefal material and a noted increase in the dip of the beds when moving from the bottom to the top of certain quarry walls gives additional evidence pointing towards the existence of a true, aggradational reef core. The reef likely started out as a low relief mud mound on the sea floor and eventually grew into a carbonate platform with steeper slopes on the windward side and lower declivity slopes on the leeward side.

The three main lithofacies in the quarry are a skeletal packstone to grainstone, skeletal wackestone to packstone, and brachiopod beds. The percentage of packstone to grainstone seems to be higher in the Western and Southern sections of the quarry and lower in the eastern section. The areas with a higher percentage of coarse, angular material has been shown in other reservoirs to have better potential reservoir quality. Although the visual estimation results suggest very similar porosity results for each of the quarry sections, it is likely that the abundance of larger,

cm-scale vugs (which could not be measured in thin sections) in the Western and Southern sections makes those slopes the better reservoir target.

Windward/Leeward Orientation:

A southerly to southeasterly paleowind direction is proposed for the Pipe Creek Jr. reef complex. This conclusion is supported by the western and southern sections having higher slope declivities, a higher percentage of coarse-grained sediment, more diverse and larger fauna, a greater abundance of syndepositional marine cement and void filling botryoidal cements, and massive colonies of tabulate corals and low domal/laminar non-enveloped stromatoporoids. The eastern section of the quarry had overall lower slope declivities, less abundant syndepositional marine cement (radiaxial fibrous and isopachous), muddier sediments, and the high domal, enveloped and columnar stromatoporoids associated by some with lower energy settings. The S to SE wind direction is consistent with interpretations from previous studies of Silurian reefs in the Michigan Basin and regional, paleoclimactic studies of the Silurian Wabash platform.

REFERENCES

Baccelle, L., and Bosellini, A., 1965, Diagrammi per la stima visiva della composizione percentuale nelle rocche sedimentarie: Annali dell'Universita di Ferrara (Nuova Serie), Sezione 9, Scienze geologiche e paleontologiche, v. 1, p. 59-62.

Bathurst, R. G. C., 1980, Stromatactis-origin related to submarine-cemented crests in Paleozoic mud mounds: Geology, v. 8, p. 131-134

Collins, J. F., Kenter J. A. M., Harris, P. M., Kuanysheva G., Fischer, D. J., and Steffen, K. L., 2006, Facies and reservoir-quality variations in the late Visean to Bashkirian outer platform, rim, and flank of the Tengiz buildup, Precaspian Basin, Kazakhstan, *in* P. M. Harris and L. J. Weber, eds., Giant hydrocarbon reservoirs of the world: From rocks to reservoir characterization and modeling: AAPG Memoir 88/SEPM Special Publication, p. 55-95.

Devaney, K. A., Wilkinson, B. H., and Voo, R. V. D., 1986, Deposition and compaction of carbonate clinothems: The Silurian Pipe Creek Junior complex of east-central Indiana: Geological Society of America Bulletin, v. 97, no. 11, p. 1367.

Frank, T. D., Wilkinson, B. H., and Lohmann, K. C., 1993, Origin of submarine pisoliths and the sedimentology of midwestern Silurian reefs: Journal of Sedimentary Petrology, v. 63, p. 1070–1077.

Gischler, E., 1995, Current and wind induced facies patterns in a Devonian atoll: Iberg Reef, Harz Mts., Germany: Palaios, v. 10, p. 180-189.

Gradstein, F. M., Ogg, J. G., Smith, A. G., Agterberg, F. P., and others, 2004, A geologic time scale 2004: Cambridge, U.K., Cambridge University Press, 384 p.

Grammer, G. M., Crescini, C., McNeill, D., Taylor, L., 1999, Quantifying Rates of syndepositional marine cementation in deeper platform environments – New insight into a fundamental process: Journal of Sedimentary Research, v. 69, p. 202-207.

Grammer, G. M., Barnes, D. A., Harrison, W. B., Sandomierski, A. E., and Mannes, R. G., 2009, Practical synergies for increasing domestic oil production and geological sequestration of anthropogenic CO2: An example from the Michigan Basin, *in* Grobe, M., et al., eds. Carbon dioxide sequestration in geological media – State of the Science, AAPG Studies in Geology 59, p. 689-706.

Grammer, G. M., Harris, P. M., and Eberli, G. P., 2004, Integration of modern and outcrop analogs for reservoir modeling-Overview and examples from the Bahamas, *in* G. M. Grammer, P. M. Harris, and G. P. Eberli, eds., Integration of outcrop and modern analogs in reservoir modeling: AAPG Memoir 80, p. 1 – 22.

Grammer, G. M., Ginsburg, R., and Harris, P. M., 1993a, Timing of Deposition, Diagenesis, and Failure of Steep Carbonate Slopes in Response to a High-Amplitude/High-Frequency Fluctuation in Sea Level, Tongue of the Ocean, Bahamas, *in* R.Loucks, J. F. Sarg, eds., Carbonate Sequence Stratigraphy: Recent Developments and Applications, AAPG Memoir 57, p. 107-131.

Grammer, G. M., Ginsburg, R., Swart, P., McNeill, D., Jull, A., and Prezbindowski, D., 1993b, Rapid Growth Rates of Syndepositional Marine Aragonite Cements in Steep Marginal Slope Deposits, Bahamas and Belize: Journal of Sedimentary Petrology, v. 63, p. 983-989.

Gray, H. H., Ault, C. H., and Keller, S. J., 1987, Bedrock geologic map of Indiana: Indiana Geological Survey Miscellaneous Map 48, scale 1:500,000.

Haq, B. U., and Schutter, S. R., 2008, A chronology of Paleozoic sea-level changes, Science, v. 322, p. 64-68.

Hasenmueller, W. A., Hasenmueller, N. R., and Daniels, M. S., 2013, Indiana Geologic Names Information System: Indiana Geological Survey website, <http://igs.indiana.edu/IGNIS/Search.cfm>.

James, N. P. and P. A. Bourque, 1992, Reefs and Mounds, in R.G. Walker and N. P. James eds., Facies models. Response to Sea Level Change: Geological Association of Canada, p. 323-347.

Johnson, M. E., 2010, Tracking Silurian eustasy: Alignment of empirical evidence or pursuit of deductive reasoning: Palaeogeography, Palaeoclimatology, Palaeoecology, v. 296, p. 276-284.

Kenter, J. A., 1990, Carbonate platform flanks: slope angle and sediment fabric. Sedimentology, v. 37, no. 5, p. 777-794

Klovan, J. E., 1974, Development of Western Canadian Devonian reefs and comparison with Holocene analogues, American Association of Petroleum Geologists Bulletin, v. 58, p. 787-799.

Lehmann, P. J., 1978, Deposition, porosity evolution and diagenesis of the Pipe Creek Jr. Reef (Silurian), Grant County, Indiana: Master's Thesis, University of Wisconsin–Madison, Madison, Wisconsin, 234 p.

McGovney, J. E., 1988, Thornton reef, Silurian, Northeastern Illinois. *in* Geldsetzer, H. H. J., James, N. P., and Tebbutt, G. E., eds., Reefs, Canada and Adjacent Areas: Canadian Society of Petroleum Geologists Memoir 13, p. 330-338.

Playton, T. E., Johnson, X., and Kerans, C., 2010, Carbonate Slopes. *in* N. P. James & R. W. Dalrymple eds., Facies models: 4. Newfoundland: Geological Association of Canada, p. 449-476.

Ritter, A., 2008, Evaluating the Controls on Reservoir Heterogeneity of Silurian Pinnacle Reefs, Michigan Basin: Master's Thesis, Western Michigan University, Kalamazoo, Michigan, 247 p.

Ritter, A., and G. M. Grammer, 2018, Utilizing sequence stratigraphy to develop a depositional model for Silurian (Niagaran) reefs in the Michigan Basin, *in* G.M. Grammer, W.B. Harrison and D.A. Barnes, eds., Paleozoic stratigraphy and resources of the Michigan Basin: GSA Special Paper 531, p. 81-104.

Ross, C. A., and Ross, J. R. P., 1996, Silurian sea-level fluctuations, *in* B. J. Witzke, G. A. Ludvigson, and J. Day, eds., Paleozoic Sequence Stratigraphy: Views from the North American Craton, v. 306: Boulder, Geological Society of America, p. 187-192.

Santiago Torres, A., 2019, Significance of microbial binding in the formation and stabilization of carbonate forereef slope deposits, Master's Thesis, Oklahoma State University, Stillwater, Oklahoma, 76 p.

Schlager, W., and Camber, O., 1986, Submarine slope angles, drowning unconformities, and self-erosion of limestone escarpments: Geology, v. 14, p. 762-765.

Shaver, R. H., 1977, Silurian Reef Geometry--New Dimensions to Explore SEPM Presidential Address, Washington, D.C., June 13, 1977: SEPM Journal of Sedimentary Research, v. 47, no. 4, p. 1409-1424

Shaver, R. H., Ault, C. H., Burger, A. M., Carr, D. D., and others, 1986, Compendium of Paleozoic rock-unit stratigraphy in Indiana—a revision: Indiana Geological Survey Bulletin 59, 203 p.

Shaver, R. H., and Sunderman, J. A., 1982, Silurian reefs at Delphi and Pipe Creek Jr. Quarry, Indiana, with emphasis on the question of deep vs. shallow water: Field Trip 5, North-Central Section, Geological Society of America, West Lafayette, Ind., Purdue University, 39 p.

Shaver, R. H., Sunderman, J. A., Mikulic, D. G., Kluessendorf, J., McGovney, J. E. E., and Pray, L. C., 1983, Silurian reef and interreef strata as responses to cyclical succession of environments, southern Great Lakes area (Field Trip 12), *in* Shaver, R. H., and Sunderman, J. A., eds., Field trips in midwestern geology: Geological Society of America, Indiana Geological Survey and Indiana University Department of Geology, p. 141–196.

Shelley, S., Grammer, G. M., and Pranter, M. J., 2019, Outcrop-based reservoir characterization and modeling of an Upper Mississippian mixed carbonate-siliciclastic ramp, Northeastern Oklahoma, *in* Grammer, G.M., J. Gregg, J. Puckette, P. Jaiswal, M. Pranter, S. Mazzullo, and R. Goldstein, eds., Mississippian Reservoirs of the Mid-Continent, U.S.A., American Association of Petroleum Geologists Memoir 122.

Simo, J., and Lehmann, P. J., 2000, Diagenetic history of Pipe Creek Jr. reef, Silurian, North-Central Indiana, U.S.A., Journal of Sedimentary Research, v. 70, no. 4, p. 937-951.

Spengler, A. E., and Read, J. F., 2010, Sequence development on a sediment-starved, low accommodation epeiric carbonate ramp: Silurian Wabash Platform, USA mid-continent during icehouse to greenhouse transition, Sedimentary Geology, v. 224, p. 84-115.

Suchomel, D. M., 1975, Paleoecology and petrology of Pipe Creek Jr. Reef (Niagaran-Cayugan), Grant County, Indiana: Master's Thesis, Indiana University, Bloomington, Indiana, 38 p.

Sunderman, J. A., and Mathews, G. W., eds., 1975, Silurian reef and interreef environments: Field Trip Guidebook, Great Lakes Section, Society of Economic Paleontologists and Mineralogists, Fort Wayne, Ind., 94 p.

Thompson, T. A, Sowder, K. H., and Johnson, M. R., 2016, Generalized stratigraphic column of Indiana bedrock: Indiana Geological Survey Poster 6.

Trout, J. L., 2012, Faunal distribution and relative abundance in a Silurian (Wenlock) pinnacle reef complex – Ray Reef, Macomb county, Michigan: Master's Thesis, Western Michigan University, Kalamazoo, Michigan, 300 p.

Trout, J. L., Grammer, G. M., and Harrison, W. B., 2018, Windward vs. leeward variability of faunal distribution in a Silurian (Wenlockian) pinnacle reef complex-Ray Reef, Macomb County, Michigan, *in* G.M. Grammer, W.B. Harrison and D.A. Barnes, eds., Paleozoic stratigraphy and resources of the Michigan Basin: GSA Special Paper 531, p. 131-156.

Wold, J. L., 2008, Sequence stratigraphy and 3-D reservoir characterization of a Silurian (Niagaran) reef – Ray Gas Storage Field, Macomb County, Michigan: Master's Thesis, Western Michigan University, Kalamazoo, Michigan, 294 p.

Wold, J. L. and Grammer, G. M., 2018, Rock based 3-D reservoir characterization of a Silurian (Niagaran) Reef – Ray Gas Storage Field, Macomb County, Michigan, *in* G.M. Grammer, W.B. Harrison and D.A. Barnes, eds., Paleozoic stratigraphy and resources of the Michigan Basin: GSA Special Paper 531, p. 105-130.

APPENDICES

List of Abbreviations			
Allochems	**Cement Types**	**Pore Types**	**Other**
CR = Crinoids	BLC = Blocky Calcite	WP = Intragranular	STY = Stylolite
STR = Stromatoporoids	RF = Radiaxial Fibrous	BP = Intergranular	PPL = Plane Polarized Light
BR = Brachiopods	IP = Isopachous	BC = Intercrystalline	XPL = Cross Polarized Light
TC = Tabulate Corals	SO = Syntaxial Overgrowth	MO = Moldic	
RC = Rugose Corals	VLD = Vug Lining Dolomite	VUG = Vuggy	
BRY = Bryozoa		GF = Growth Framework	
TR = Trilobite			
OST = Ostracod			
GP = Gastropod			

West Quarry Thin Sections:

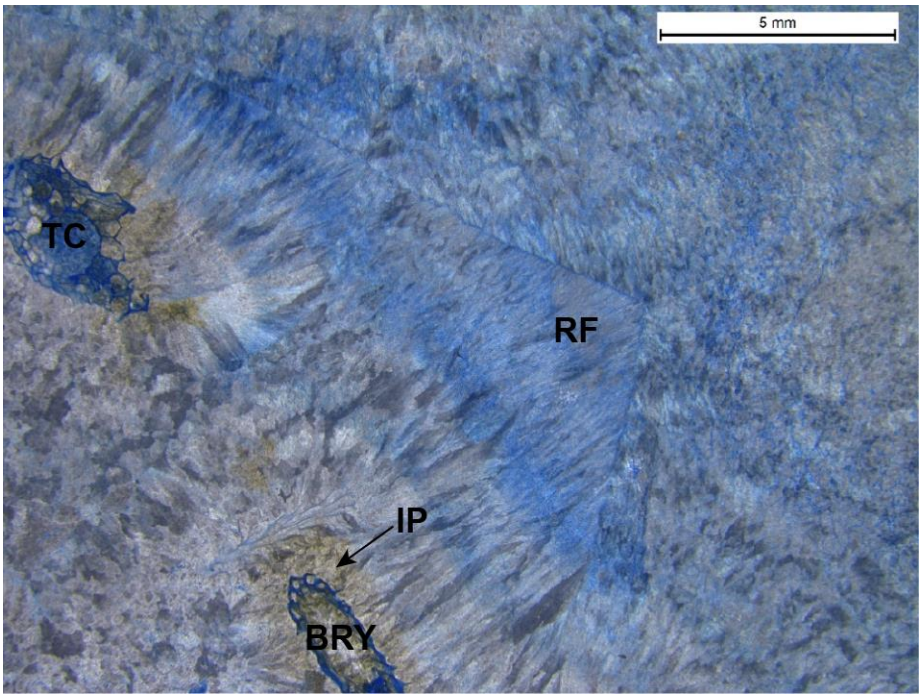

Sample PC-05: Photomicrograph showing mostly radiaxial fibrous cement and isopachous cement growing on tabulate corals and bryozoa. Scale: 5mm, XPL.

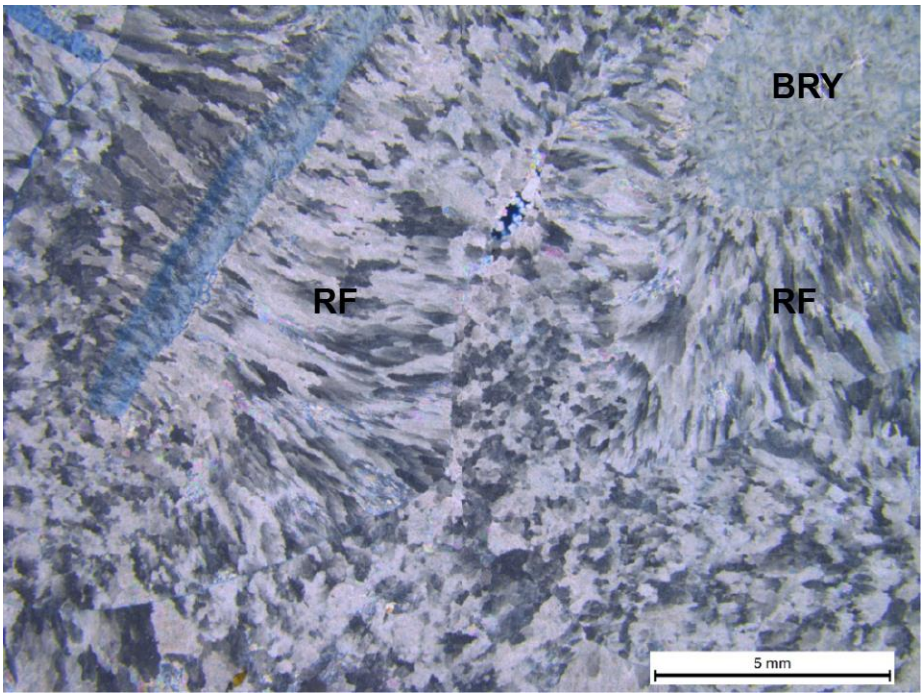

Sample PC-08: Photomicrograph showing radiaxial fibrous cement growing on bryozoa. Scale: 5mm, XPL.

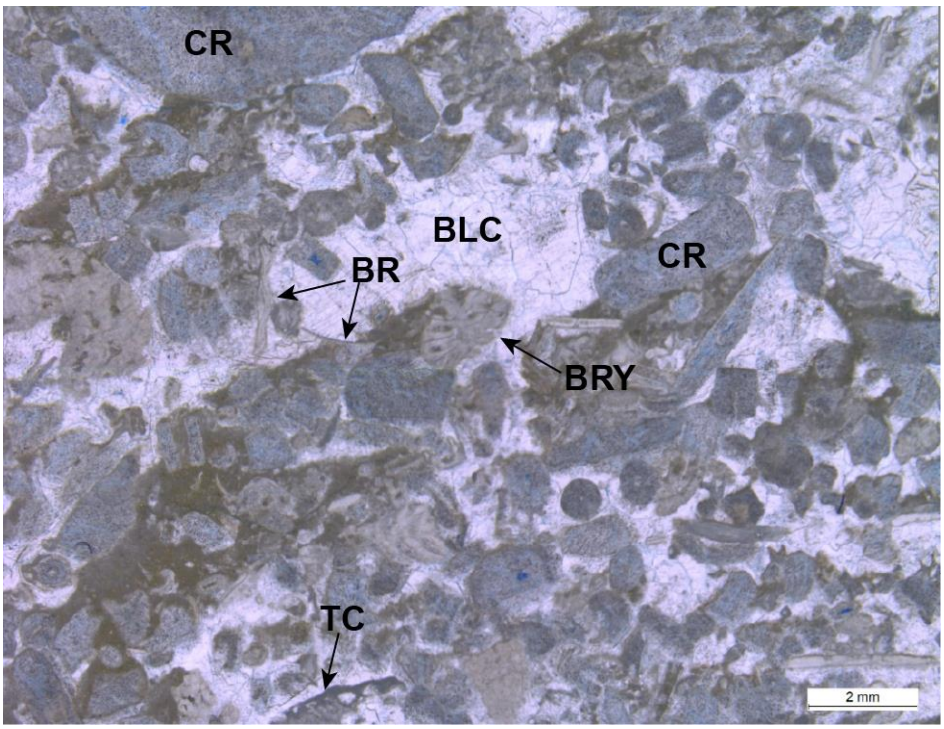

Sample 10a_01: Dominantly crinoidal packstone-grainstone. Other allochems include brachiopod and bryozoan fragments and tabulate corals. Cement is dominantly blocky calcite with very little porosity. Scale: 2mm, PPL.

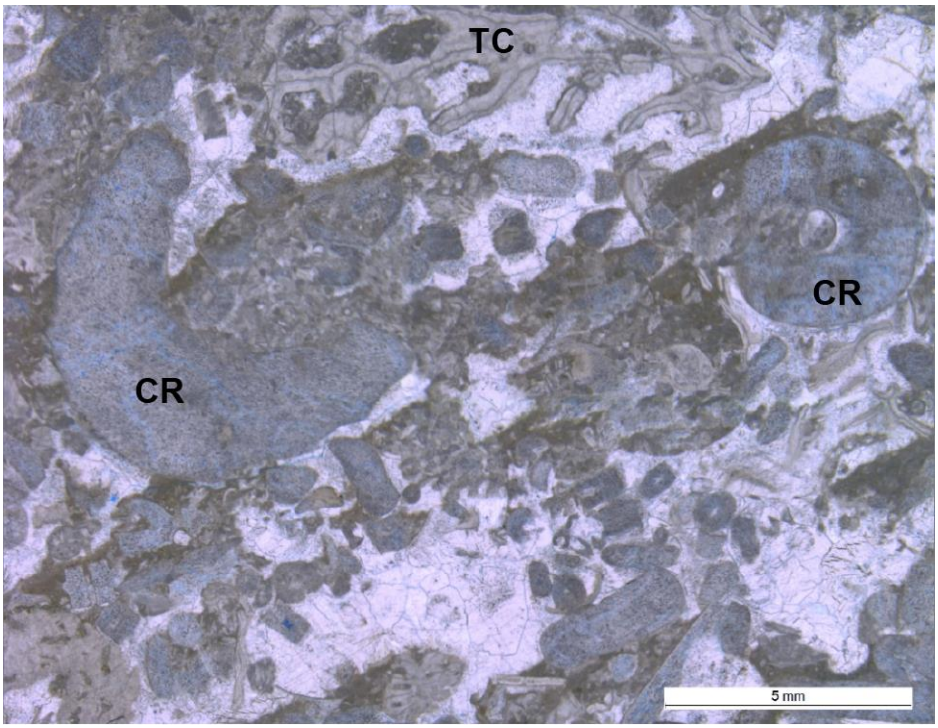

Sample 10a_02: Photomicrograph showing a wider view of sample 10a. Note large crinoidal fragments and tabulate coral at the top of the image. Scale: 5mm, PPL.

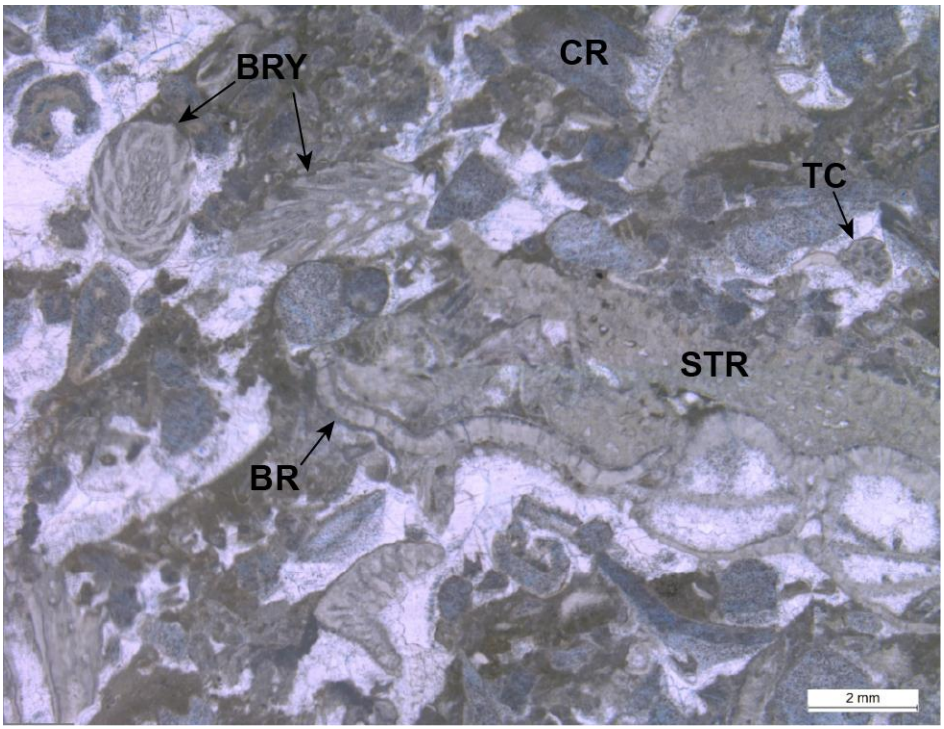

Sample 10a_03: Photomicrograph showing diverse fauna including crinoids, tabulate corals, bryozoa, stromatoporoids, and brachiopod fragments. Scale: 2mm, PPL.

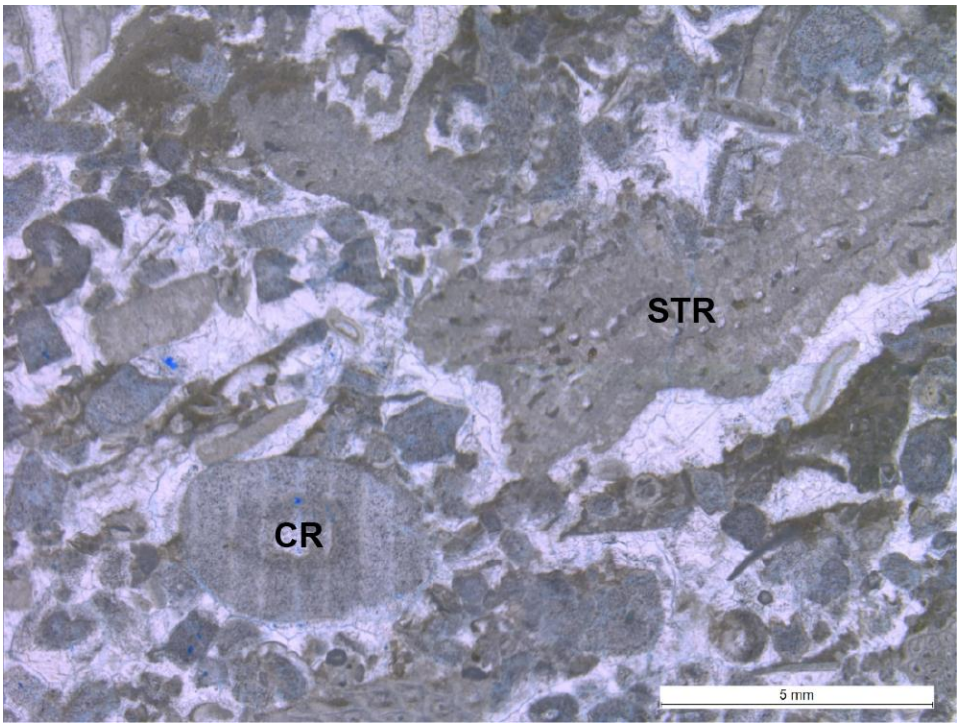

Sample 10a_04: Photomicrograph with large crinoid fragments and a large stromatoporoid fragment. Scale: 5mm, PPL.

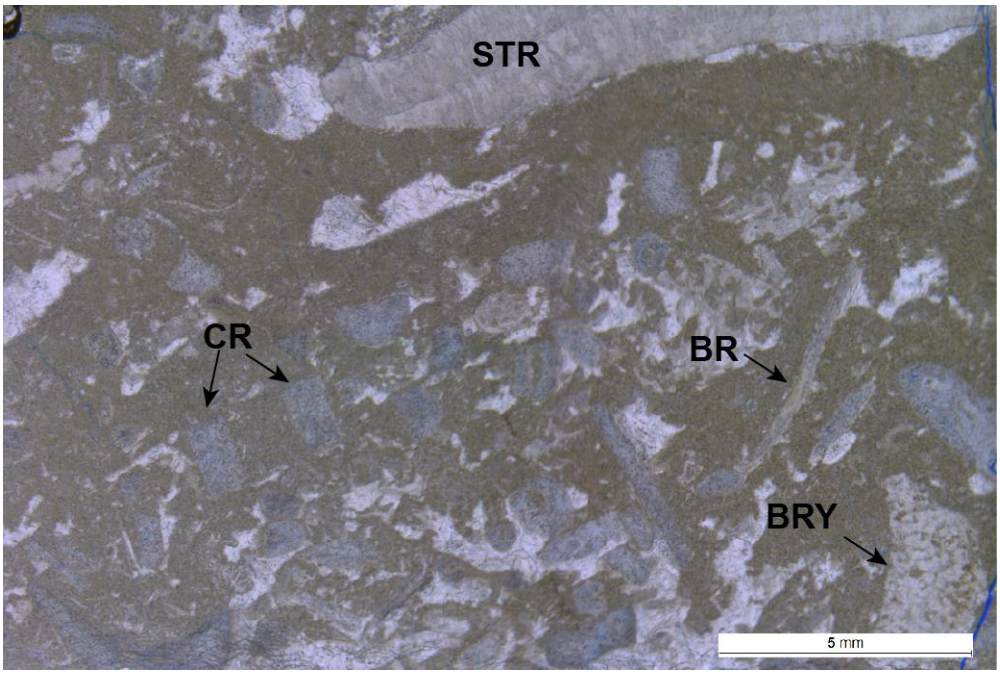

Sample 10b_01: Skeletal wackestone to packstone containing crinoidal debris, and stromatoporoid, brachiopod, and possible bryozoa fragments. Cement is blocky calcite, and there is very little porosity. Scale: 5mm, PPL.

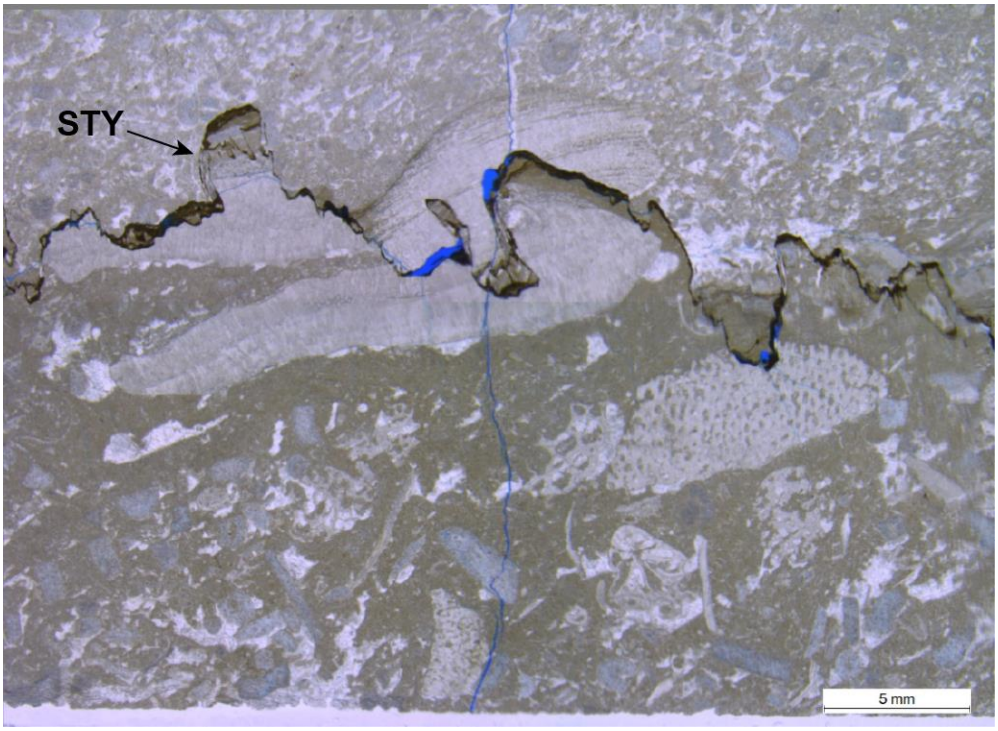

Sample 10b_02: Wider view showing the contact between bed 10b and 10c. Note the sutured seam stylolite separating the two beds. Fracture is not mineralized and is therefore likely induced. Scale: 5mm, PPL.

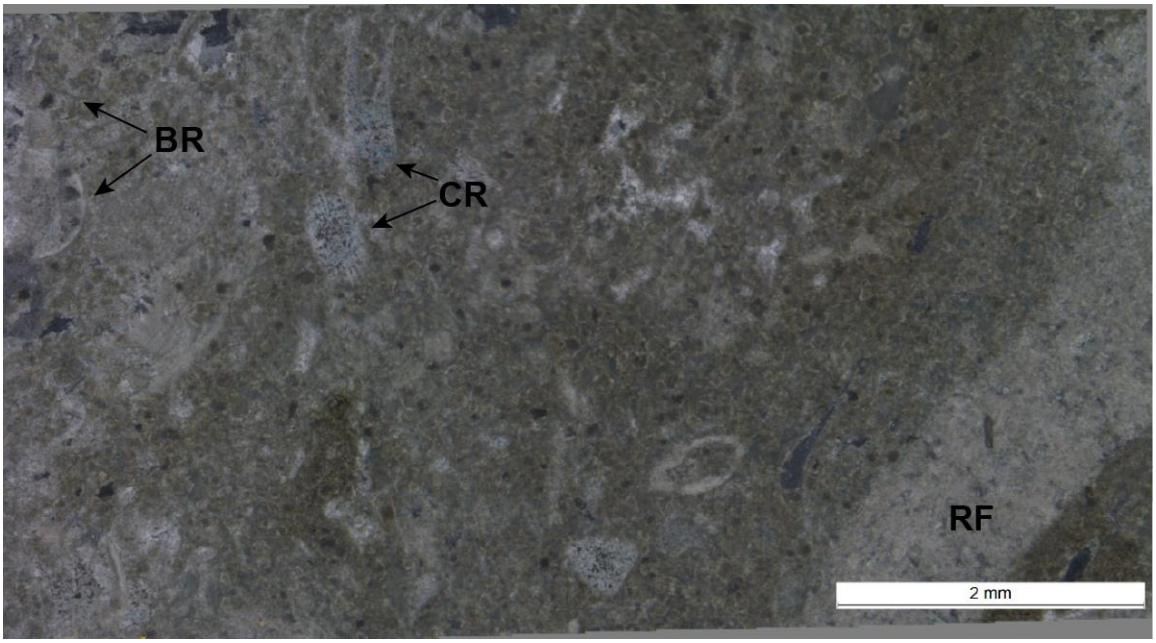

Sample 10c_02: Skeletal grainstone with crionoids and brachiopods as the dominant skeletal components. Cement is radiaxial fibrous cement. Little to no porosity. Scale: 2mm, XPL.

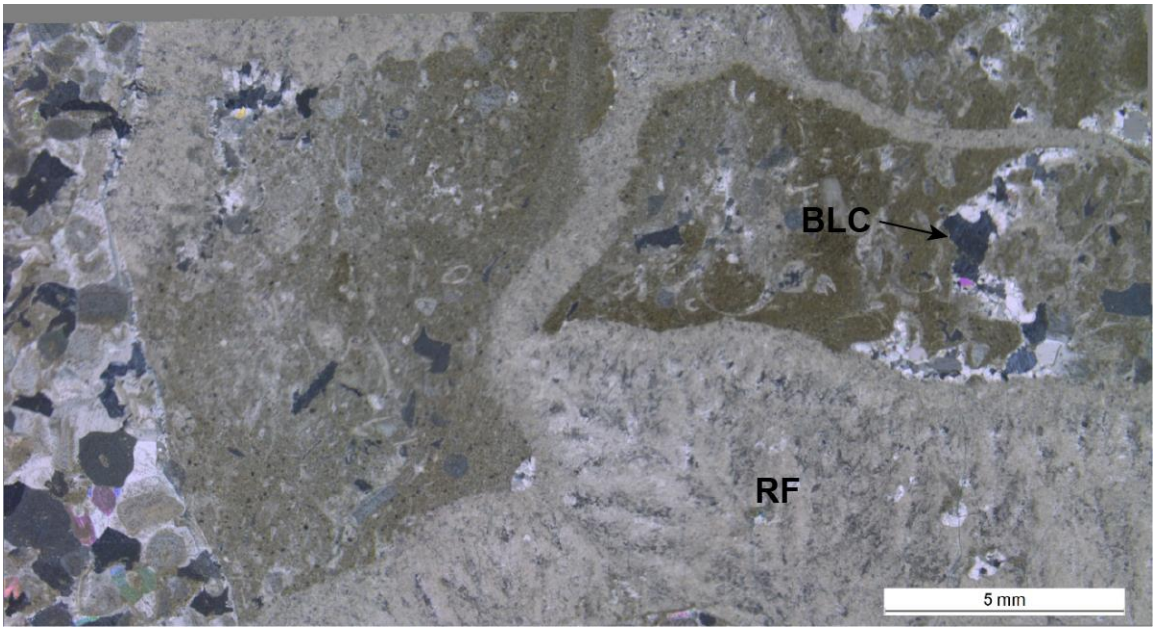

Sample 10c_03: Wider field of view showing the large amounts of radiaxial fibrous cement. There is a small amount of blocky calcite cement present. Scale: 5mm, XPL.

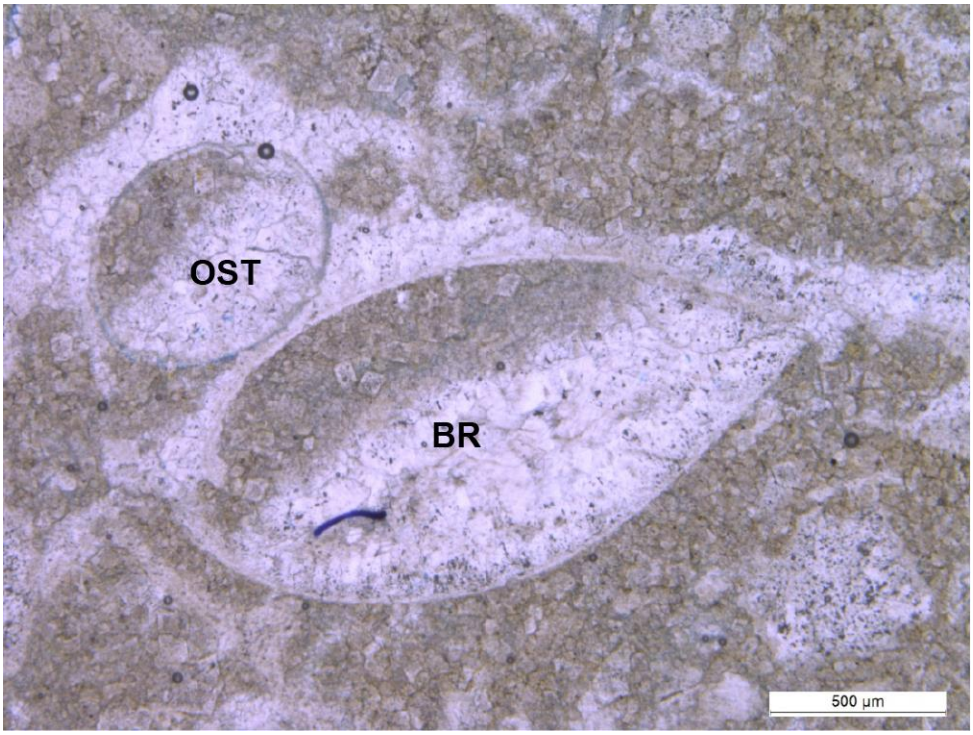

Sample 10d_01: Skeletal wackestone to packstone. Note the geopetal structure inside the brachiopod and possible ostracod. Also note the mud/matrix has been dolomitized. Cement is blocky calcite. Scale: 500µm, PPL

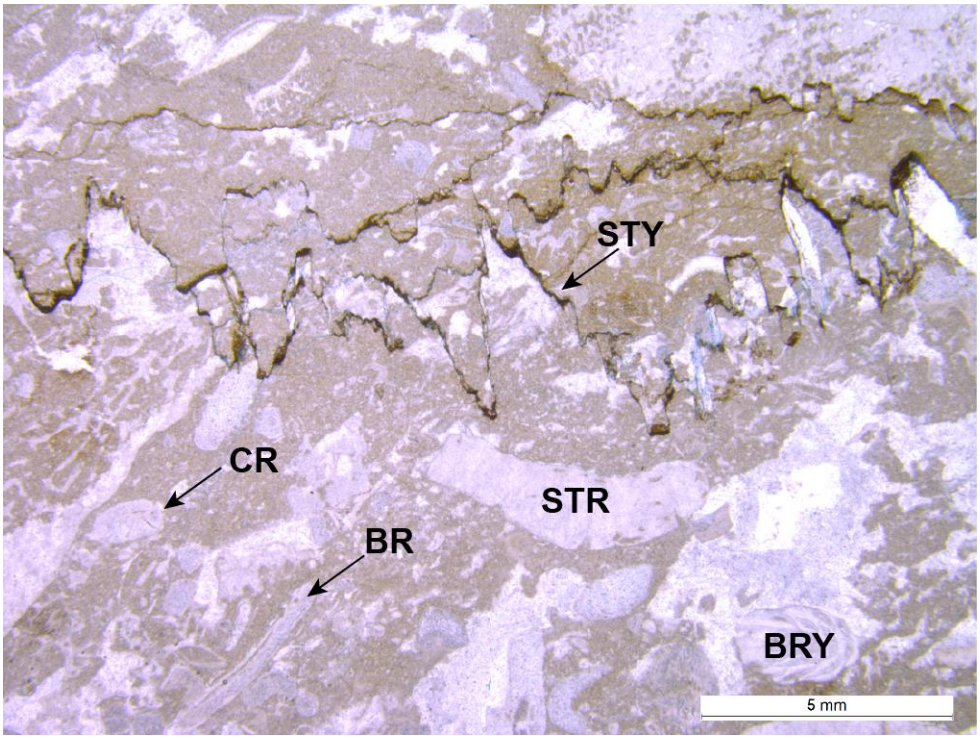

Sample 10d_02: Wider field of view showing diverse fauna, including crinoids, stromatoporoids, bryozoa, and brachiopods. Also note the sutured seam stylolites. Scale: 5mm, PPL.

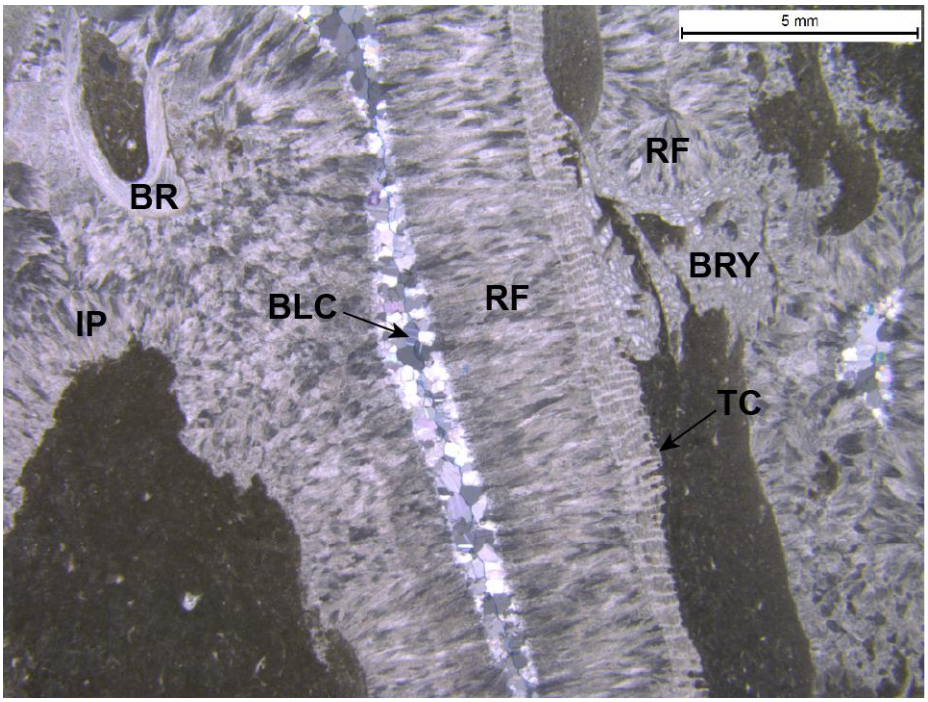

Sample PCo1_A_01: Skeletal packstone to grainstone containing abundant radiaxial fibrous cement. Skeletal components include bryozoa, brachiopods, and tabulate coral. Limited blocky calcite cement is present as well. Scale: 5mm, XPL.

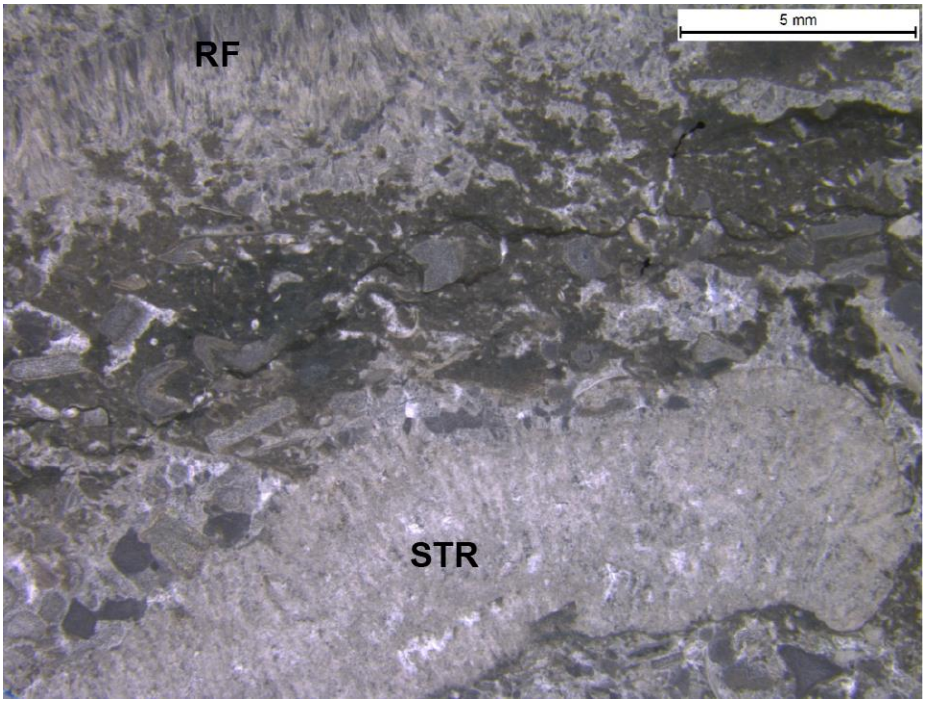

Sample PCo1_A_02: Photomicrograph showing a large stromatoporoid fragment along with abundant radiaxial fibrous cement and slight amounts of blocky calcite cement. Scale: 5mm, XPL.

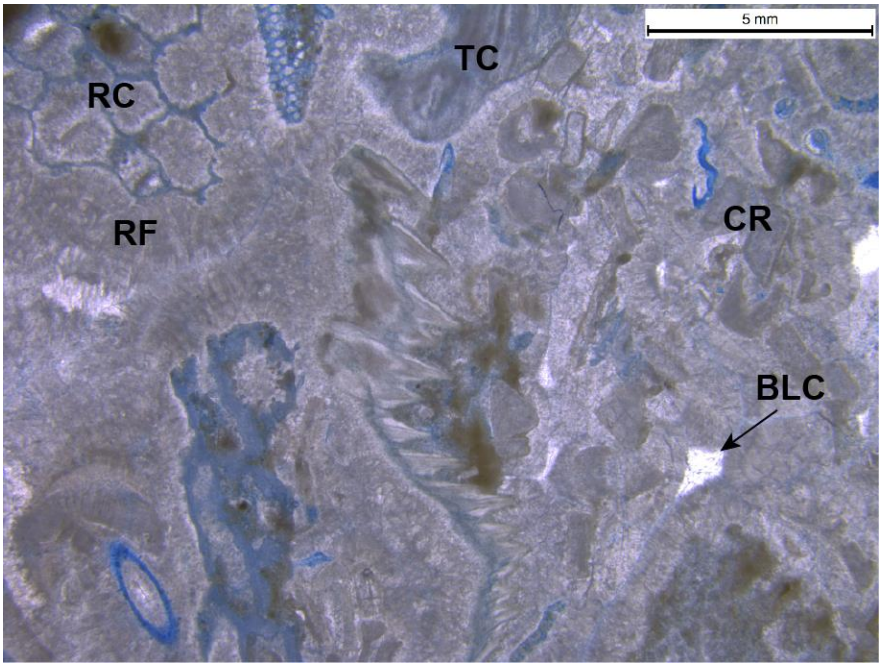

Sample PCo1_B_01: Skeletal Grainstone containing tabulate coral, rugose coral, crinoids, and brachiopods. Cement is dominantly radiaxial fibrous or isopachous with minor blocky calcite. Scale: 5mm, PPL

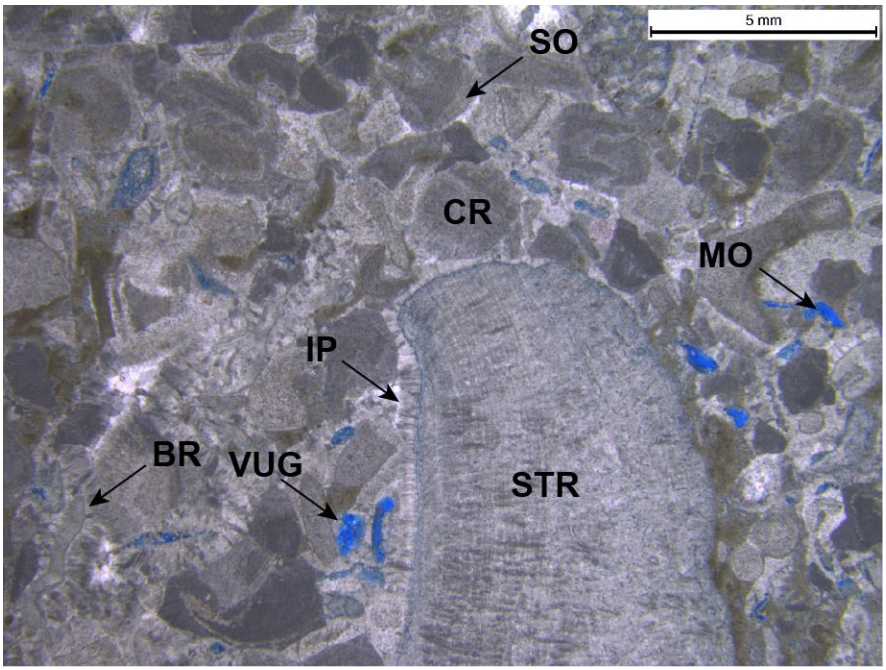

Sample PCo1_C_01: Dominantly crinoidal grainstone with large stromatoporoid fragment and brachiopod fragments. Cement is dominantly isopachous or syntaxial overgrowth with minor blocky calcite. Moldic and vuggy pores are present. Scale: 5mm, XPL.

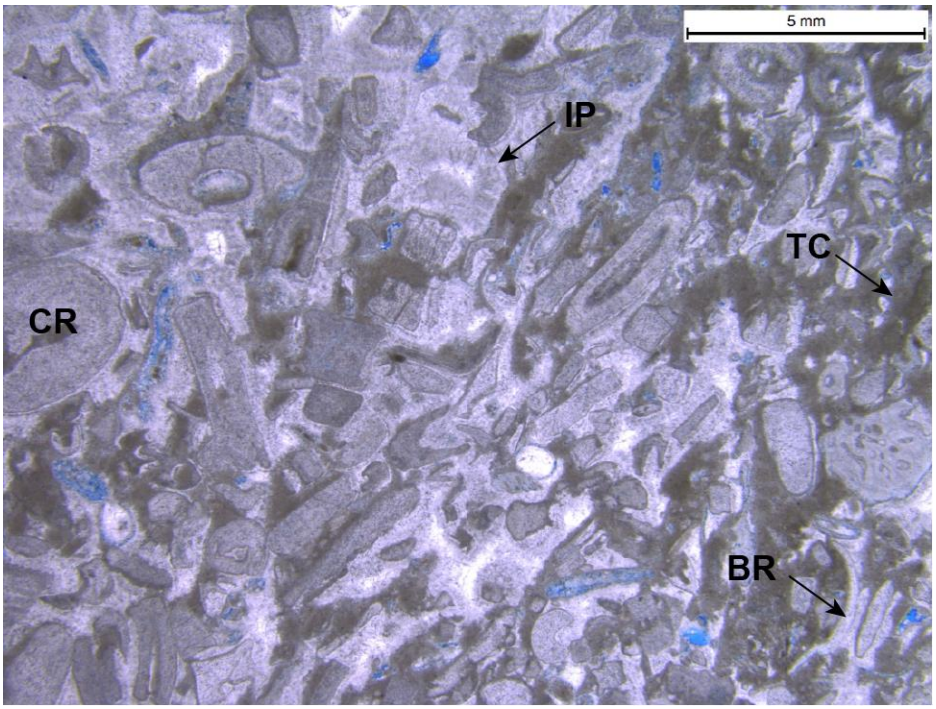

Sample PCo1_D_01: Dominantly crinoidal packstone, with minor tabulate coral and brachiopod fragments. Cement is dominantly isopachous and syntaxial overgrowth, with minor blocky calcite. Scale: 5mm, PPL

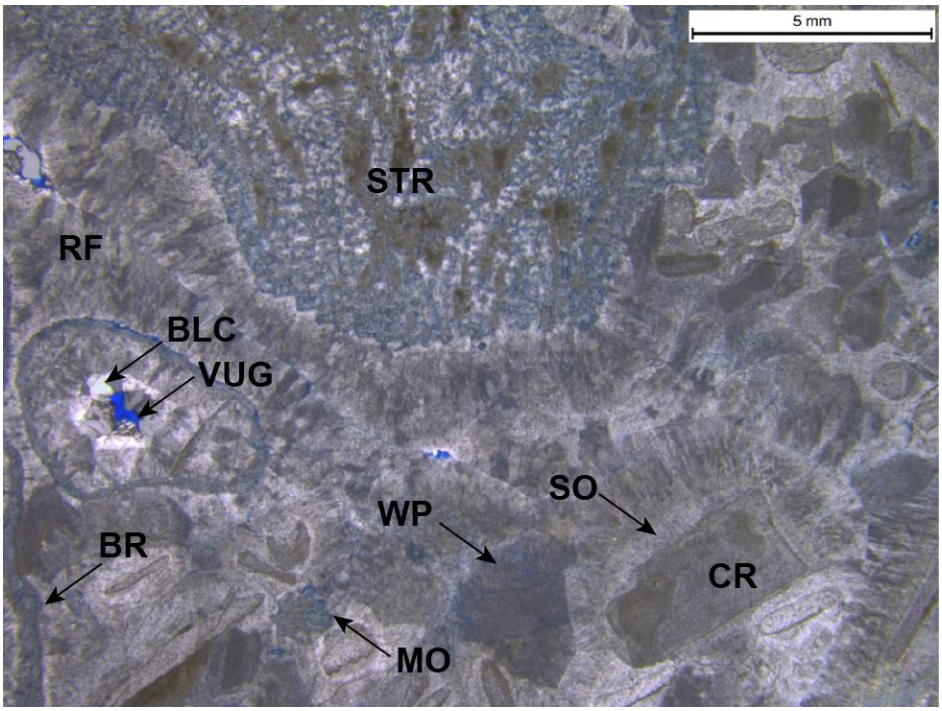

Sample PCo1_E_01: Skeletal grainstone with large stromatoporoid as well as crinoidal debris and brachiopod fragments. Radiaxial fibrous/isopachous cements dominate, with syntaxial overgrowth and blocky calcite cements present as well. Intragranular, moldic, and vuggy pores present. Scale: 5mm, XPL.

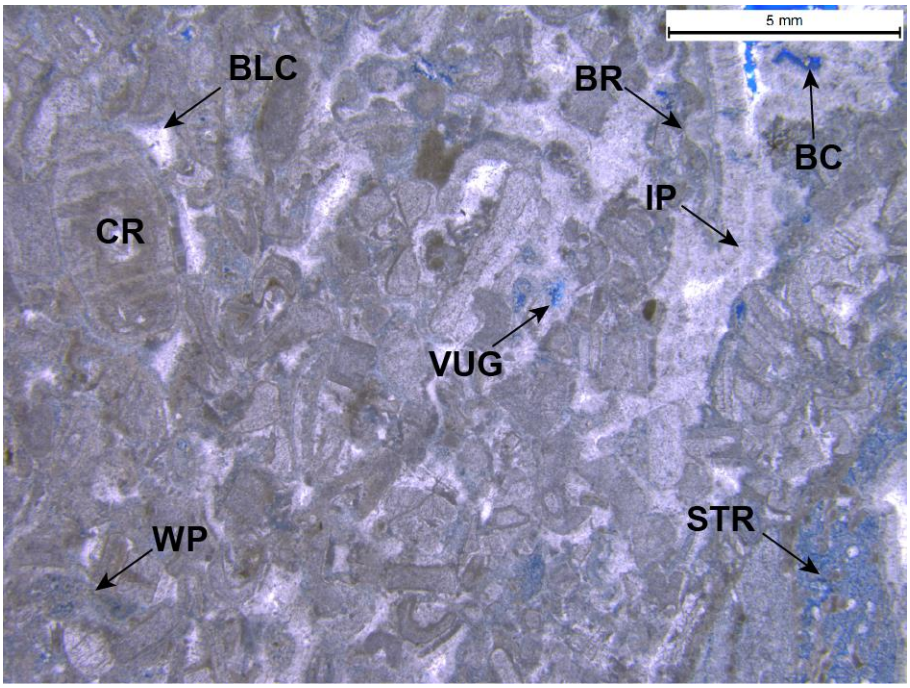

Sample PCo1_F_01: Skeletal grainstone containing crinoids, brachiopods, and possible stromatoporoid fragments. Cement is dominantly radiaxial fibrous or isopachous, but also contains blocky calcite and syntaxial overgrowth cements. Intragranular, vuggy, and intercrystalline pores present. Scale: 5mm, PPL.

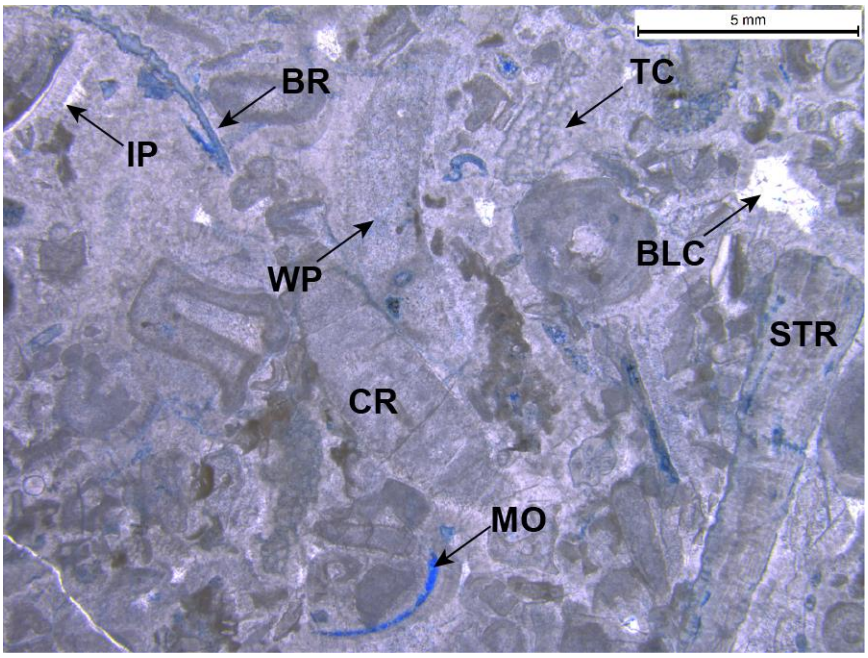

Sample PCo1_G_01: Skeletal grainstone containing crinoids, stromatoporoids, tabulate corals, and brachiopods. Cement is dominantly radiaxial fibrous/isopachous, with minor blocky calcite and syntaxial overgrowth cement. Moldic and intragranular pores present. Scale: 5mm, PPL.

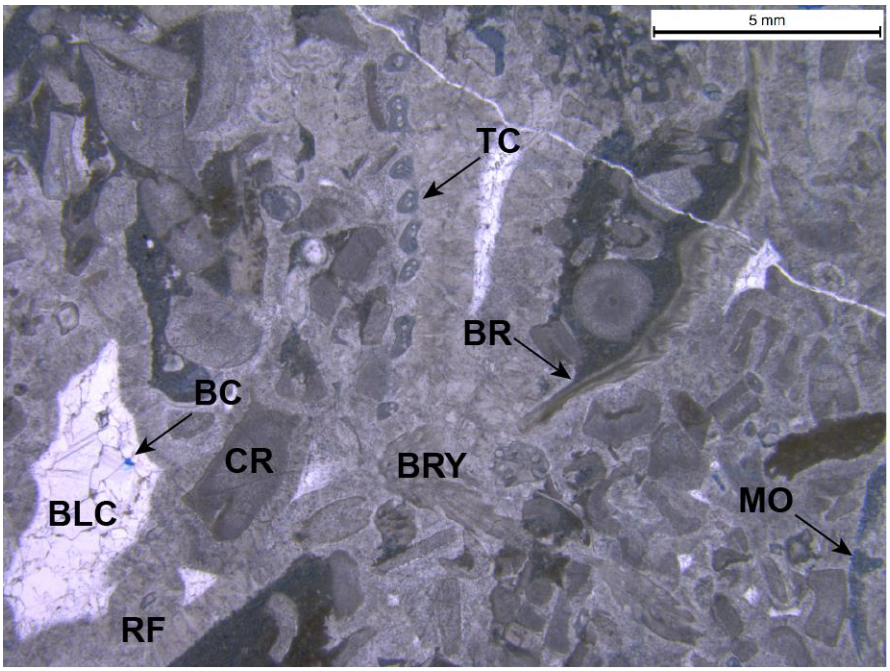

Sample PCo1_H_01: Skeletal packstone containing crinoids, tabulate corals, brachiopods, and bryozoa. Cement is dominantly radiaxial fibrous/isopachous, with minor blocky calcite and syntaxial overgrowth cement. Moldic and Intercrystalline pores are present. Scale: 5mm, XPL.

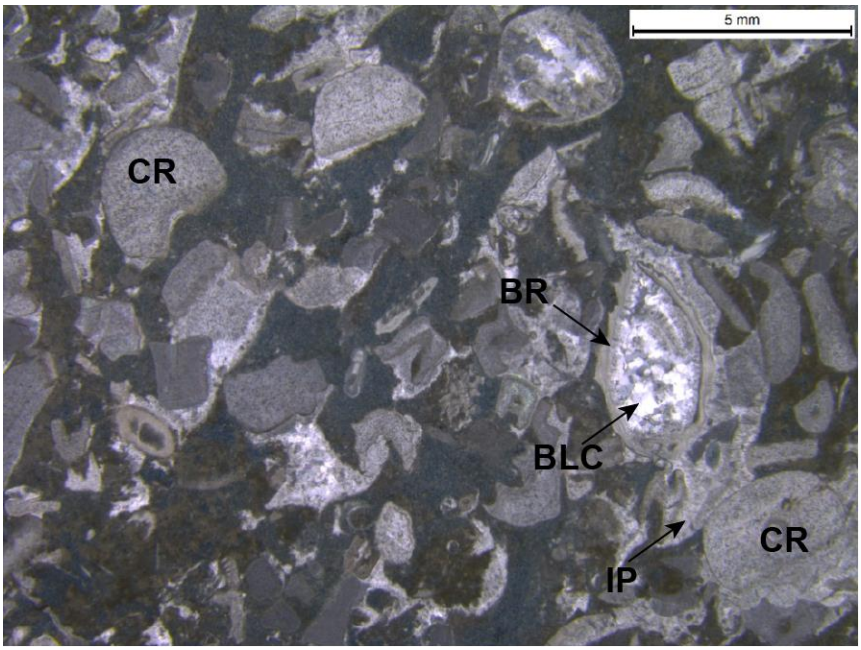

Sample PCo1_H_04: Skeletal Packstone containing crinoids and brachiopods. Cement is dominantly blocky calcite, with some radiaxial fibrous/isopachous and syntaxial overgrowth cement. Little to no porosity is present. Scale: 5mm, XPL.

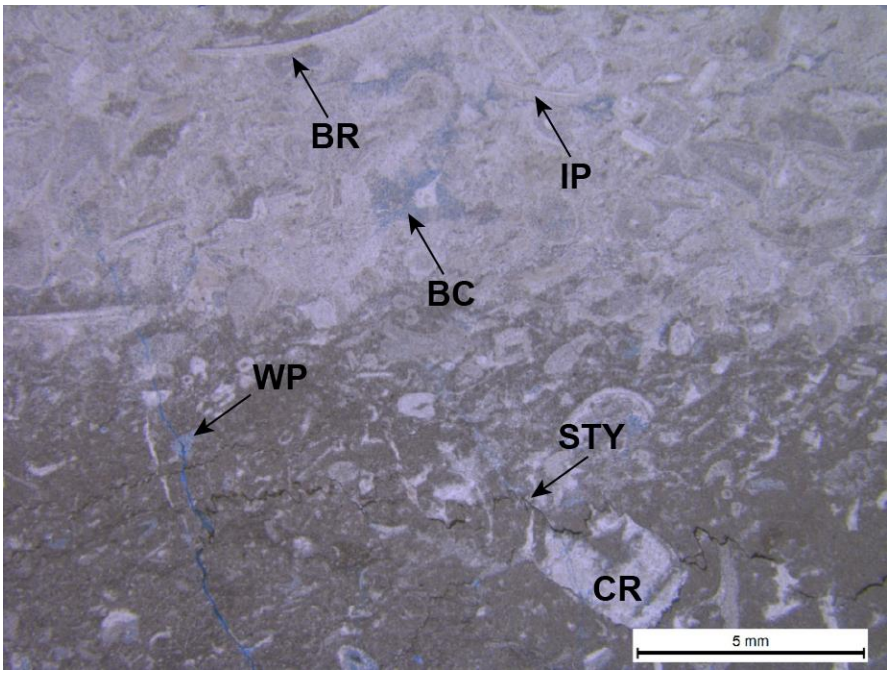

Sample WQB13_01: The bottom half of the sample is a skeletal packstone and the top half of the sample is a skeletal grainstone. Both contain crinoids and brachiopods. The packstone contains dominantly blocky calcite cement with some vug lining dolomite. The grainstone contains dominantly radiaxial fibrous/isopachous cement with some blocky calcite cement. Note the stylolite in the packstone. Intercrystalline, moldic, and intragranular pores are present. Scale: 5mm, PPL.

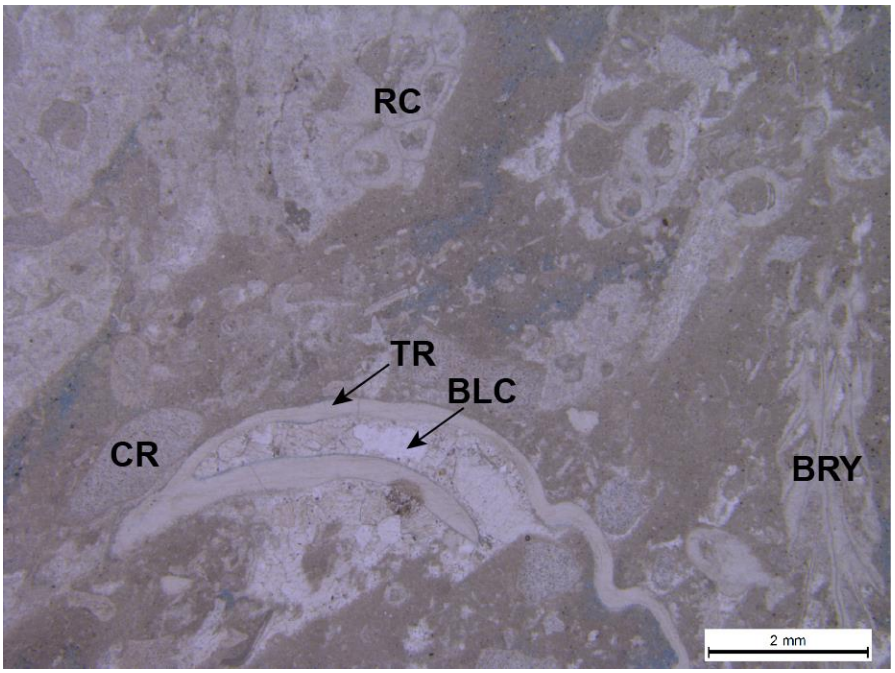

Sample WQB15_bot_01: Skeletal packstone containing rugose corals, tabulate corals, crinoids, and a trilobite fragment. Cement is dominantly radiaxial fibrous/isopachous with some blocky calcite and vug lining dolomite. Scale: 2mm, PPL.

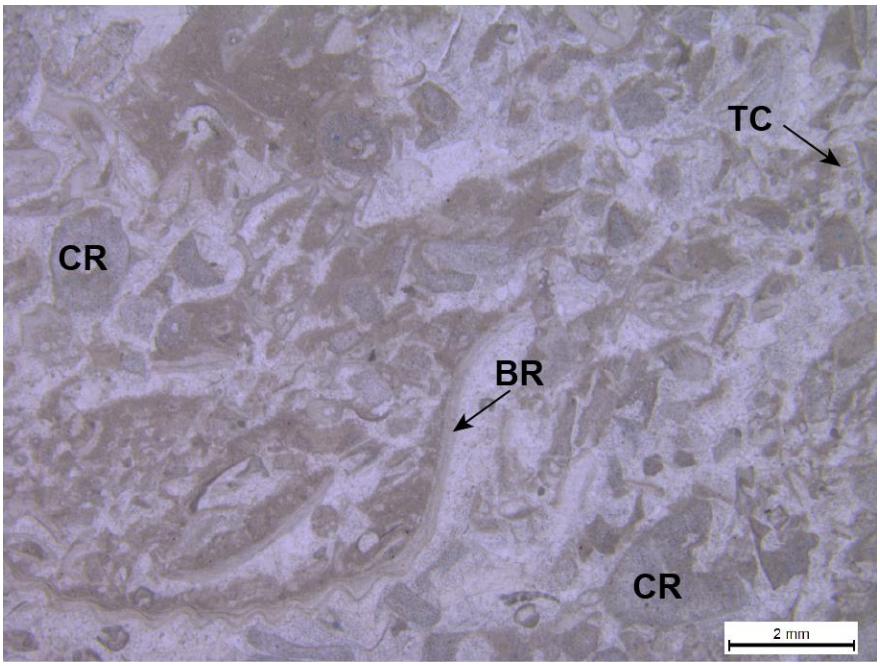

Sample WQB15_top_01: Skeletal packstone containing crinoids, tabulate corals, brachiopods, and possible ostracods. The cement is dominantly radiaxial fibrous/isopachous with some blocky calcite cement. Multiple geopetal structures at different angles. Scale: 2mm, PPL.

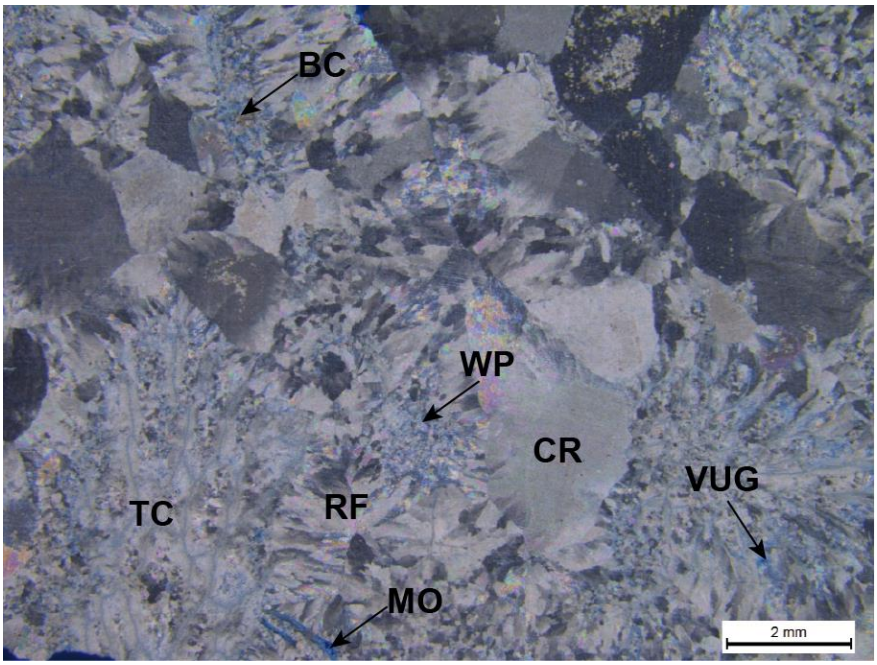

Sample WQB18_02: Skeletal grainstone containing tabulate corals and crinoids. Cement is dominantly radiaxial fibrous/isopachous with minor blocky calcite cement. Intragranular, intercrystalline, vuggy, and moldic pores are present. Scale: 2mm, XPL.

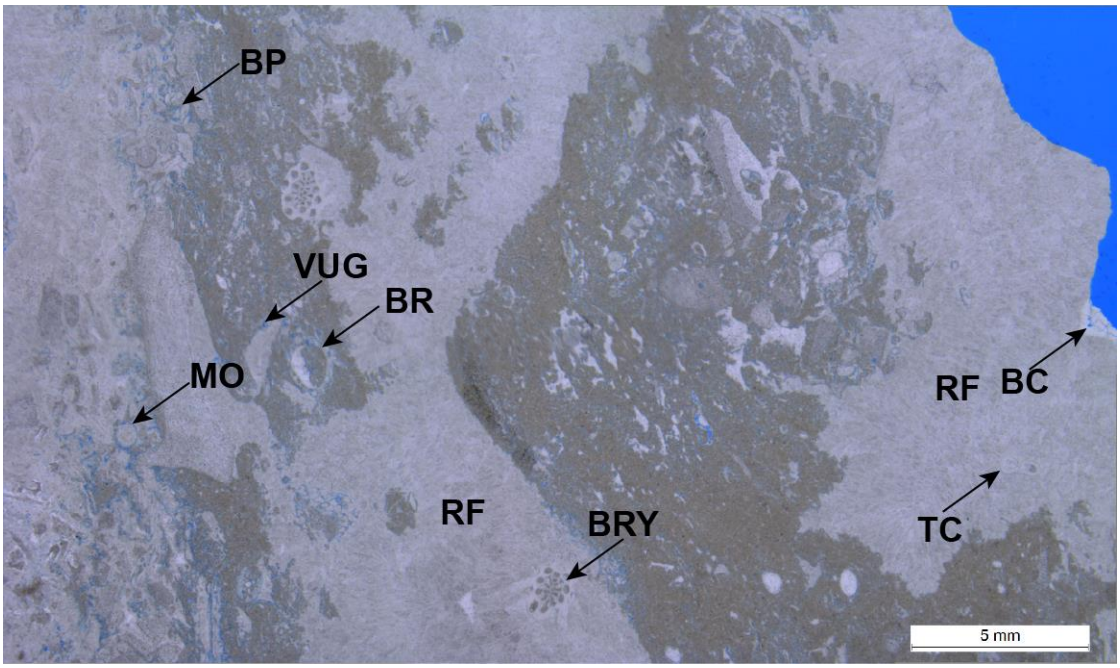

Sample WQB19_01: Skeletal packstone containing crinoids, brachiopods, tabulate corals, and bryozoa. Cement is dominantly radiaxial fibrous/isopachous, with minor blocky calcite and vug lining dolomite cement. Intergranular, vuggy, moldic, and intercrystalline pores are present. Scale: 5mm, PPL.

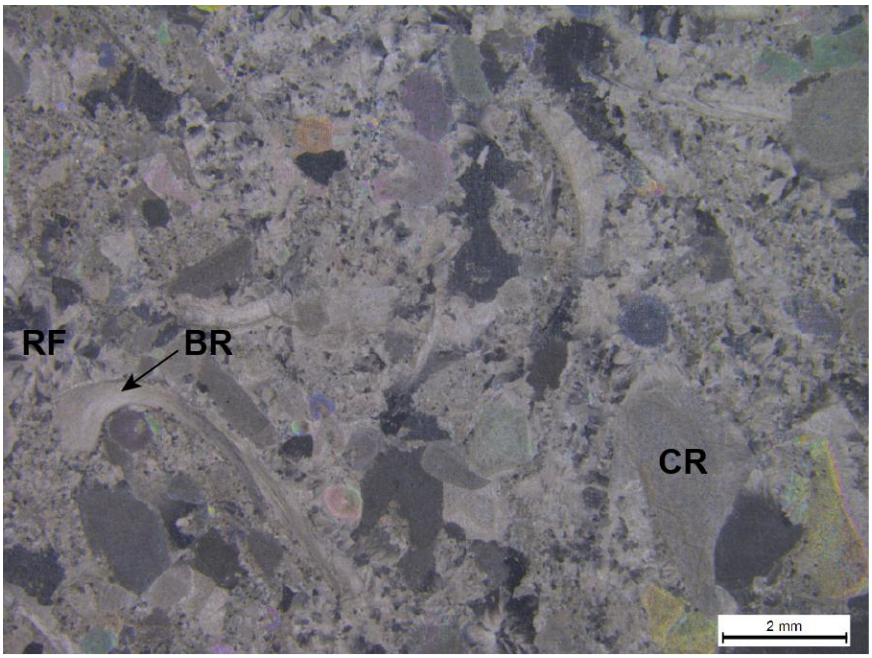

Sample WQB21_01: Skeletal grainstone containing crinoids, brachiopods, tabulate corals, and rugose corals. Cement is dominantly radiaxial fibrous/isopachous with some syntaxial overgrowth cement. Scale: 2mm, XPL.

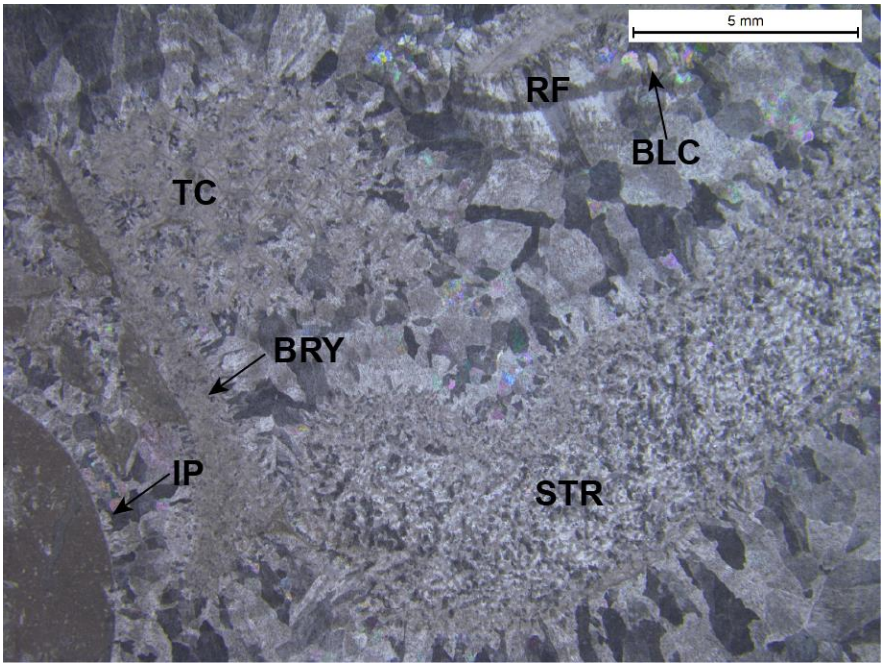

Sample WQB16_01: Skeletal grainstone containing bryozoa, tabulate corals, stromatoporoids, and crinoids. Cement is dominantly radiaxial fibrous/isopachous with some blocky calcite cement. Little to no porosity. Scale: 5mm, XPL

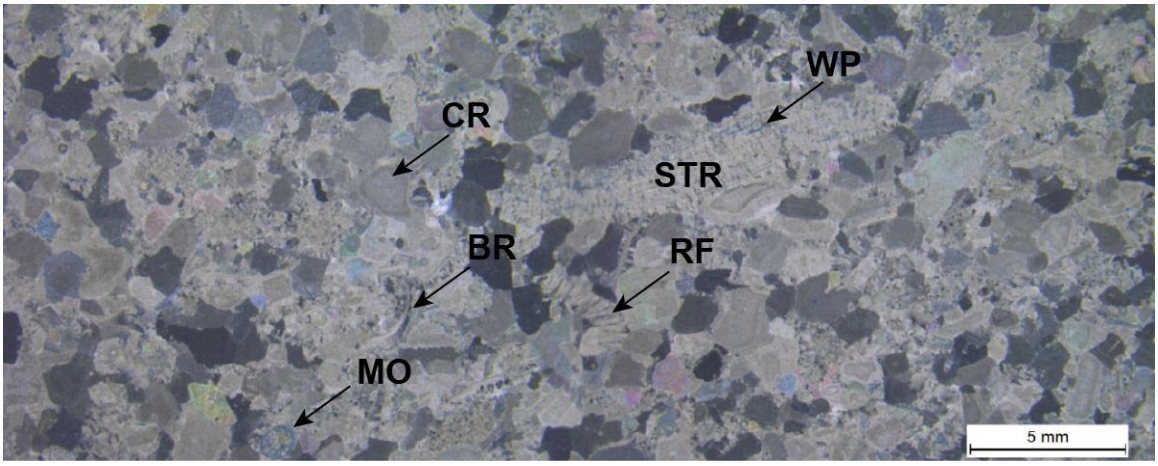

Sample WQUB2_01: Skeletal grainstone containing crinoids, stromatoporoids, and brachiopods. Cement is dominantly radiaxial fibrous/isopachous and syntaxial overgrowth, with minor blocky calcite cement. Intragranular and moldic pores are present. Scale: 5mm, XPL.

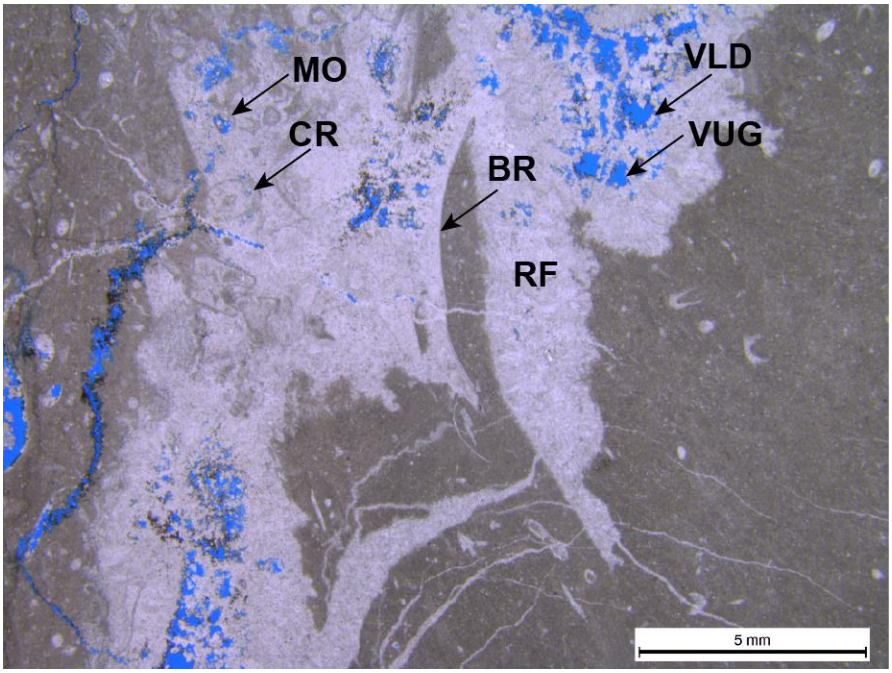

Sample WQUB3_01: Skeletal wackestone to packstone containing crinoid/crinoid molds and brachiopods. Cement is dominantly radiaxial fibrous and vug lining dolomite with minor blocky calcite cement. Vuggy and moldic pores are present. Scale: 5mm, PPL.

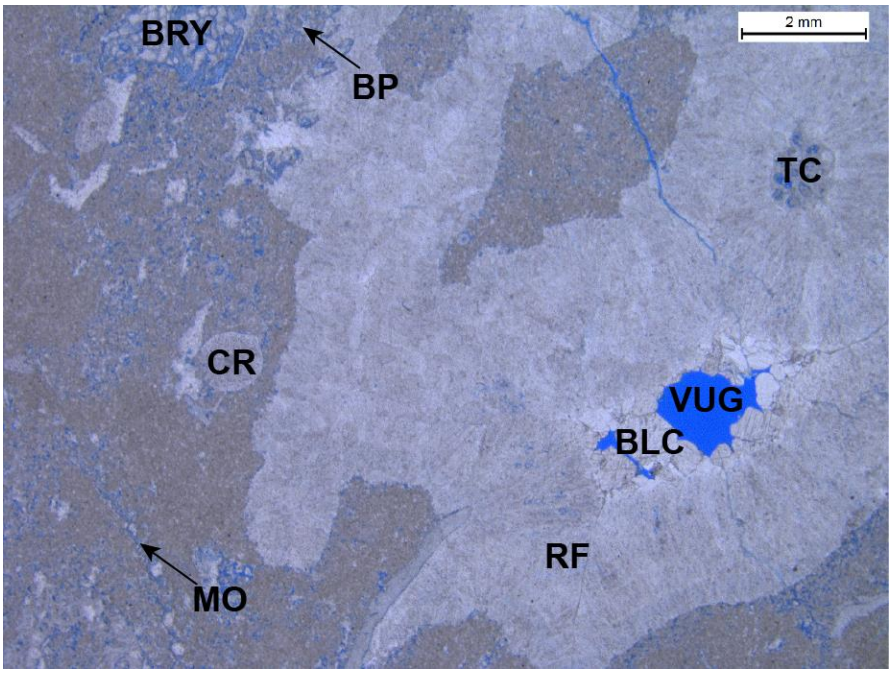

Sample WQUB4_01: Skeletal packstone containing tabulate corals, crinoids, and bryozoa. Cement is dominantly radiaxial fibrous, with some blocky calcite and vug lining dolomite cement. Intergranular, vuggy, and moldic pores are present. Scale: 2mm, PPL.

South Quarry Thin Sections:

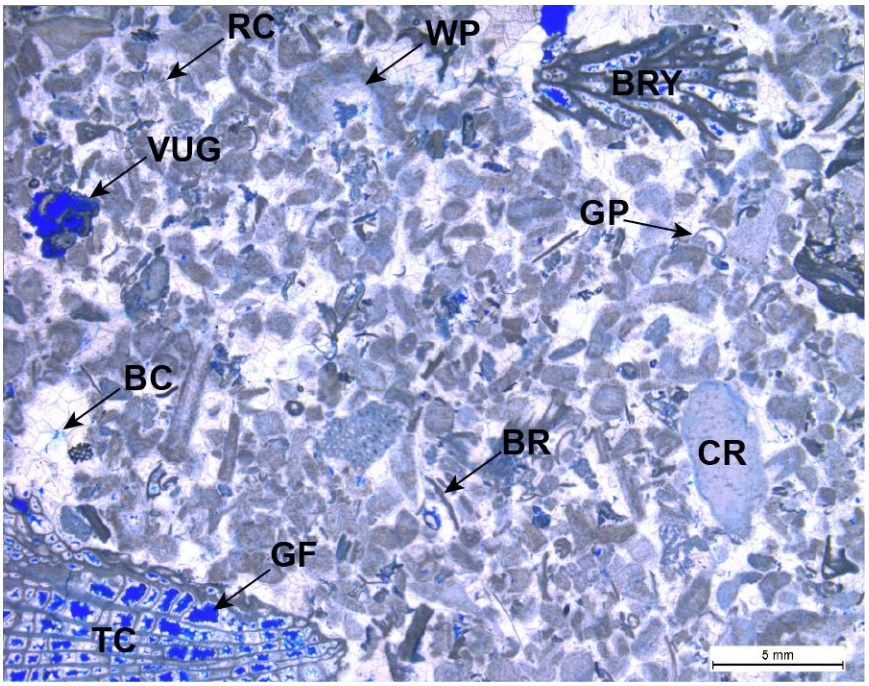

Sample PC4_02: Grainstone to local rudstone containing crinoids, tabulate corals, rugose corals, gastropods, brachiopods, and bryozoa. Cement is dominantly blocky calcite and multiple types of pores are present, including framework, intragranular, vuggy, and intercrystalline porosity. Scale: 5mm, PPL

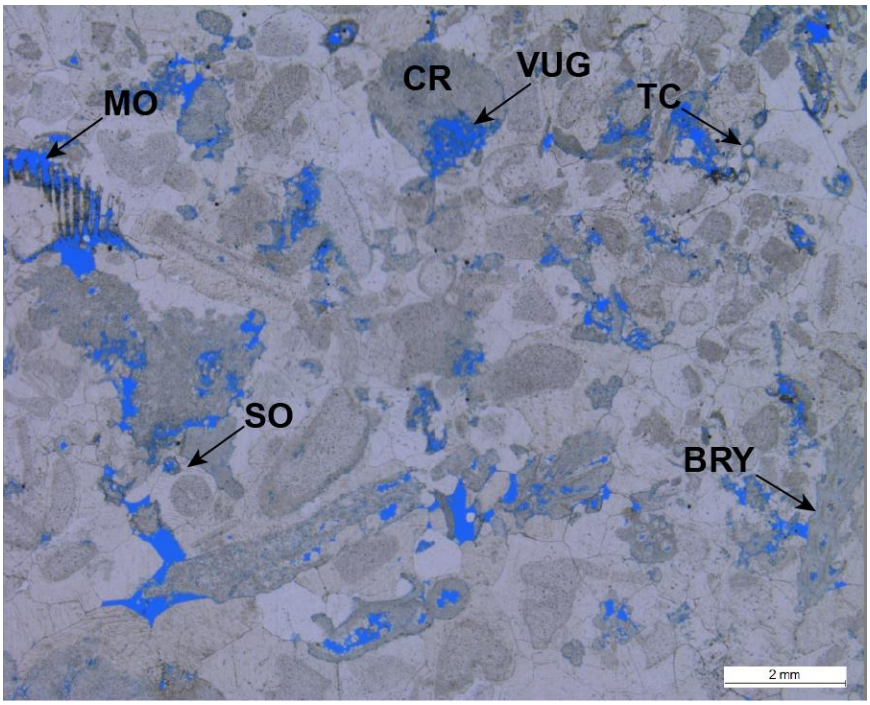

Sample PC6_02: Dominantly crinoidal grainstone with minor tabulate corals and bryozoa. Cement is dominantly syntaxial overgrowth and pores are dominantly vuggy and moldic. Scale: 2mm, PPL.

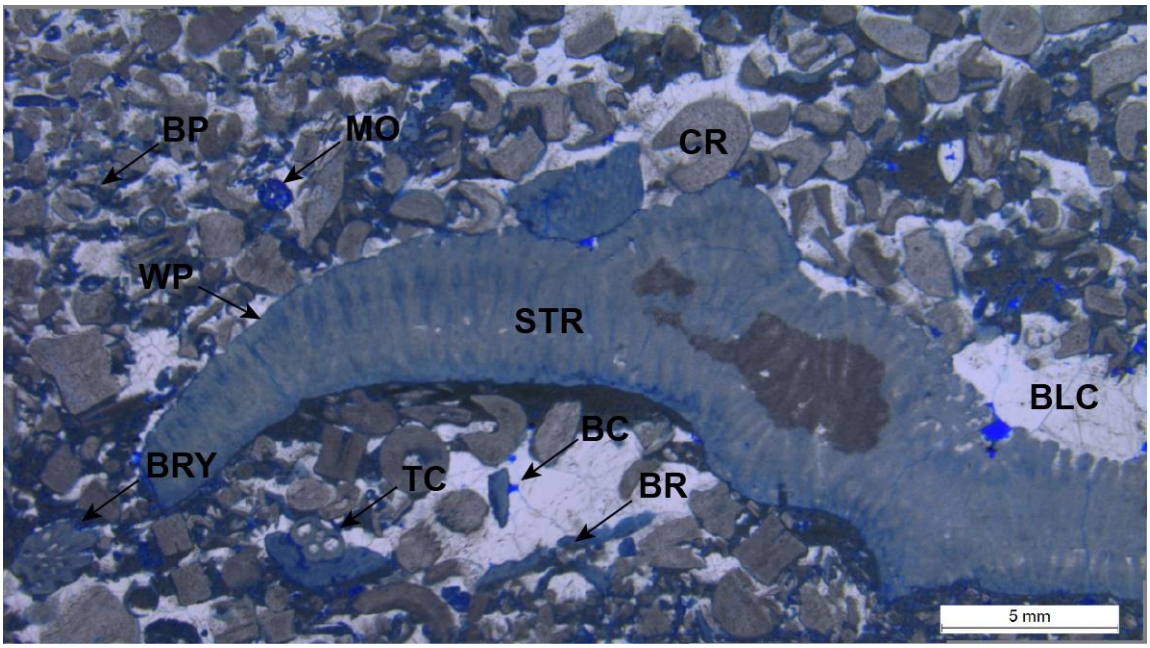

Sample PC9_02: Dominantly crinoidal grainstone with large stromatoporoid fragment and minor brachiopod, bryozoa, and tabulate coral fragments. Porosity is estimated at 15% and includes intergranular, intragranular, moldic, intercrystalline, and framework porosity. Cement is dominantly blocky calcite. Scale: 5mm, PPL.

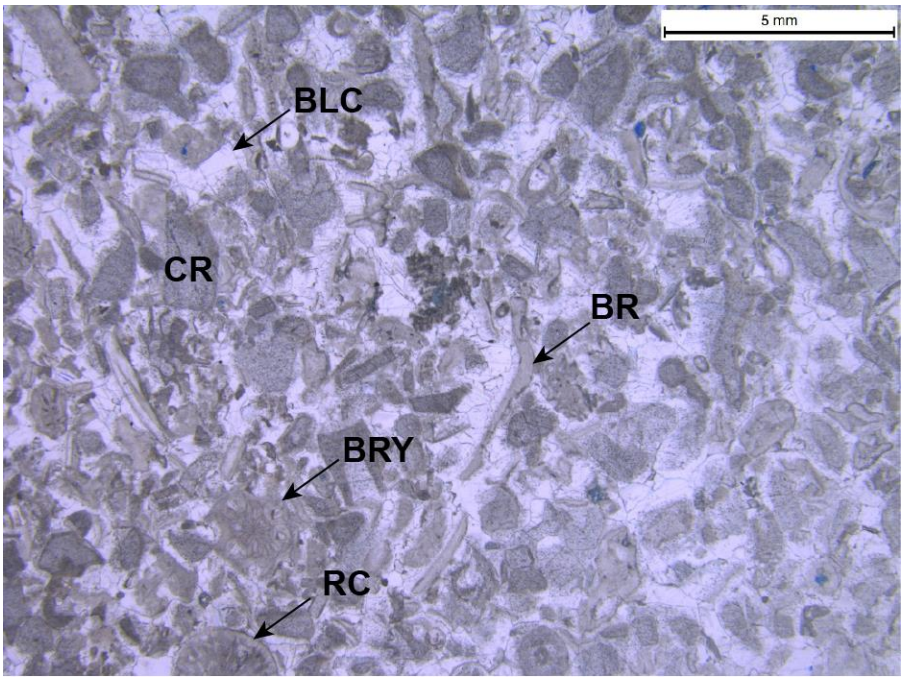

Sample PCo2_A_01: Dominantly crinoidal grainstone with brachiopods, rugose corals and bryozoa. Cement is dominantly blocky calcite, with minor syntaxial overgrowth and fibrous cements. Scale: 5mm, PPL.

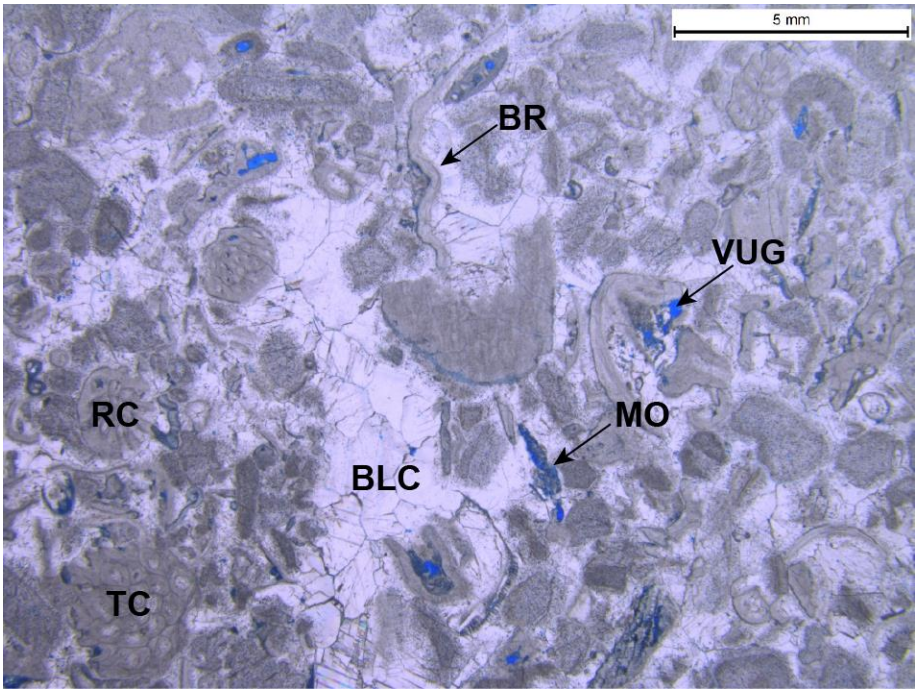

Sample PCo2_B_01: Dominantly crinoidal grainstone with tabulate corals, rugose corals, and brachiopods. Cement dominantly blocky calcite and syntaxial overgrowth, with minor fibrous cement. Pores are mostly vuggy and moldic. Scale: 5mm, PPL.

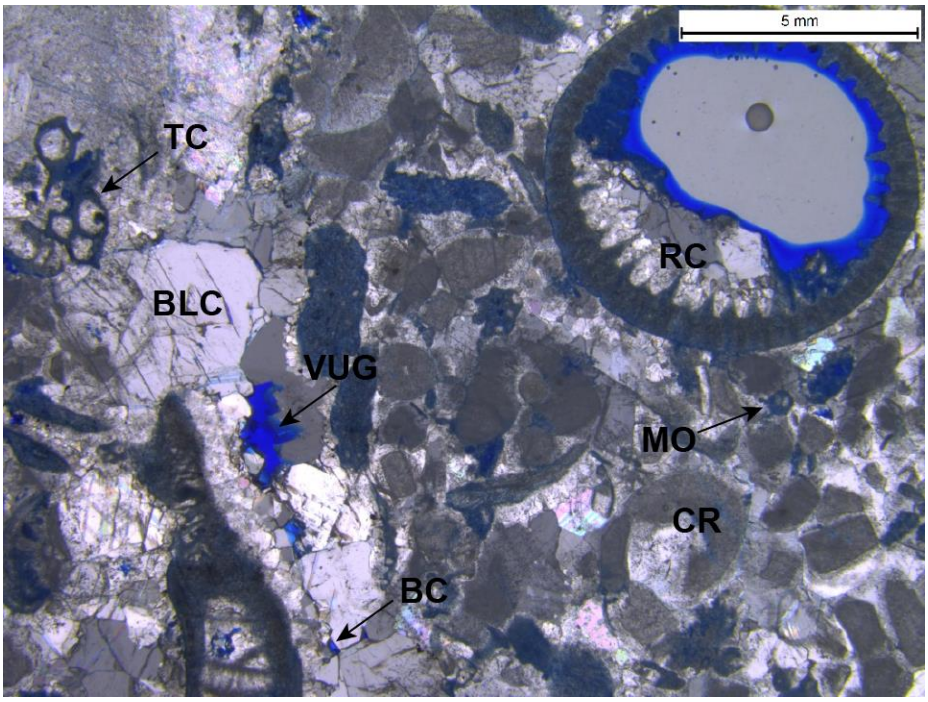

Sample PCo2_C_01: Dominantly crinoidal grainstone with large rugose coral fragment and minor tabulate coral fragments. Cement is dominantly blocky calcite and syntaxial overgrowth. Pores are moldic, intercrystalline, and vuggy. Scale: 5mm, XPL.

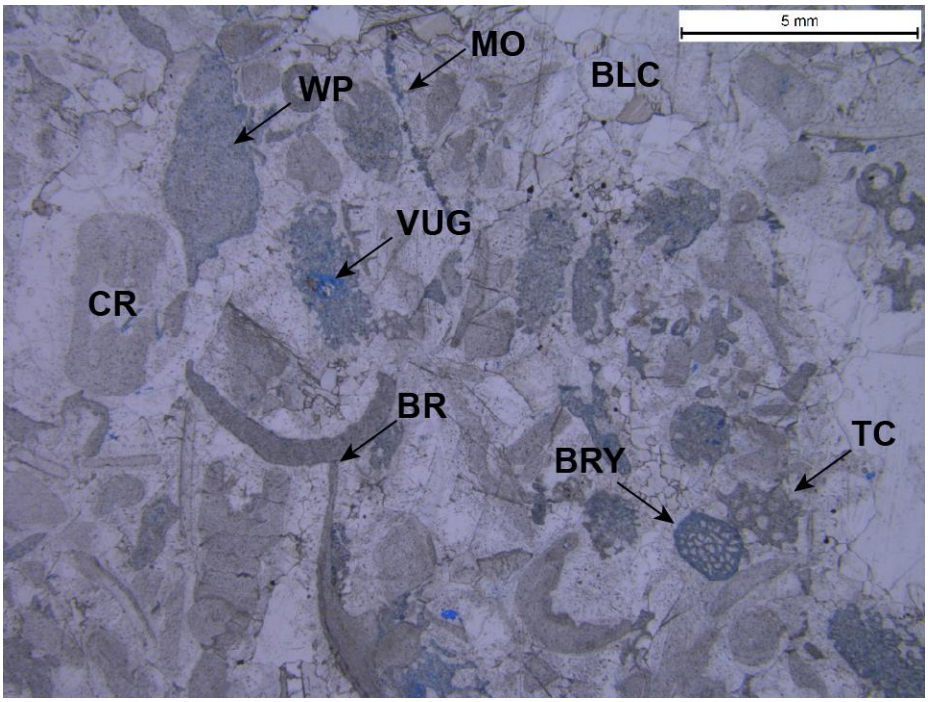

Sample PCo2_D1_01: Dominantly crinoidal grainstone, with brachiopods, tabulate corals, and bryozoa. Cement is dominantly blocky calcite and syntaxial overgrowth, with mine fibrous cements. Pores include intragranular, vuggy, and moldic. Scale:5mm, PPL.

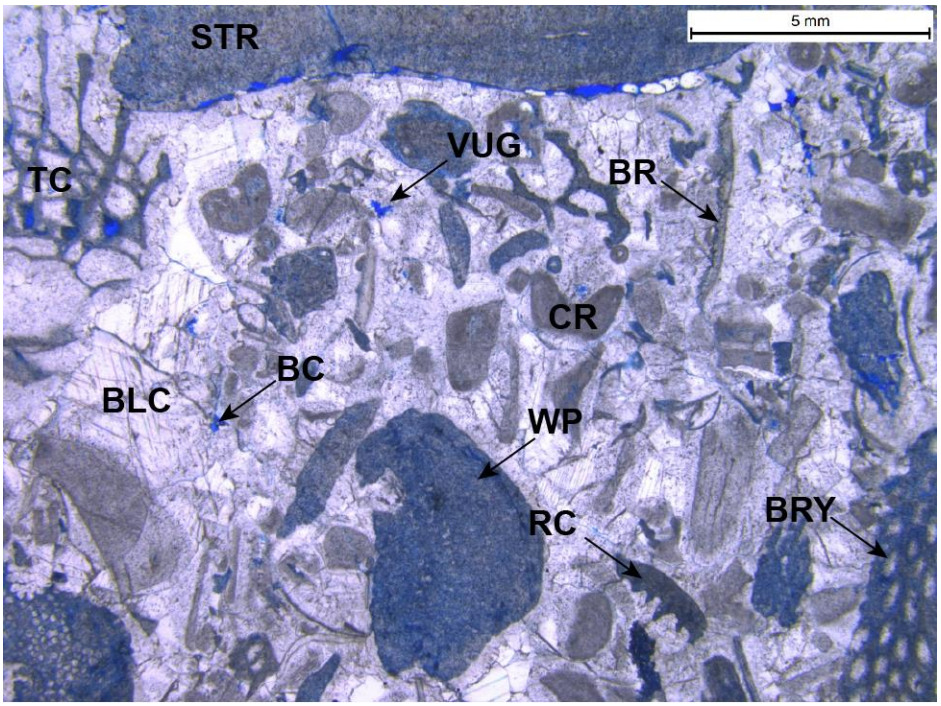

Sample PCo2_D2_01: Grainstone to rudstone with stromatoporoids, crinoids, tabulate and rugose corals, brachiopods, and bryozoa. Cement is dominantly blocky calcite and syntaxial overgrowth, with minor fibrous cements. Pore types include intragranular, vuggy, and intercrystalline. Scale: 5mm, PPL.

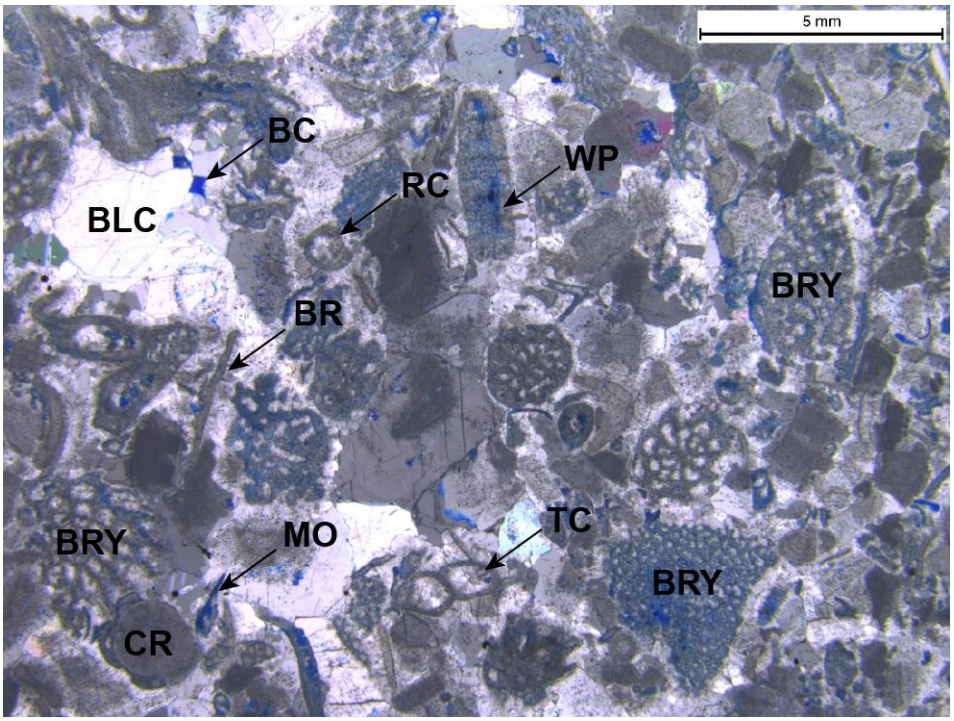

Sample PCo2_E_01: Grainstone with tabulate and rugose corals, crinoids, brachiopods, and bryozoa. Cement is dominantly blocky calcite and syntaxial overgrowth, with minor fibrous cements. Pore types include intragranular, intercrystalline, and moldic. Scale: 5mm, XPL.

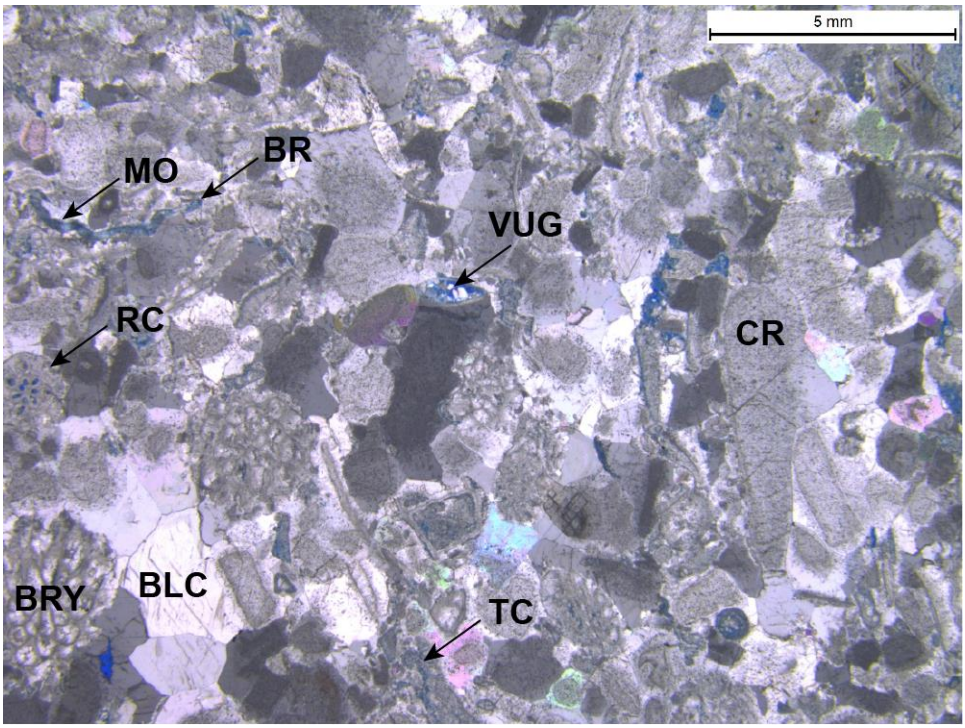

Sample PCo2_F_02: Grainstone with tabulate and rugose corals, crinoids, brachiopods, and bryozoa. Cement is dominantly blocky calcite and syntaxial overgrowth, with minor fibrous cements. Pore types include moldic and vuggy. Scale: 5mm, XPL.

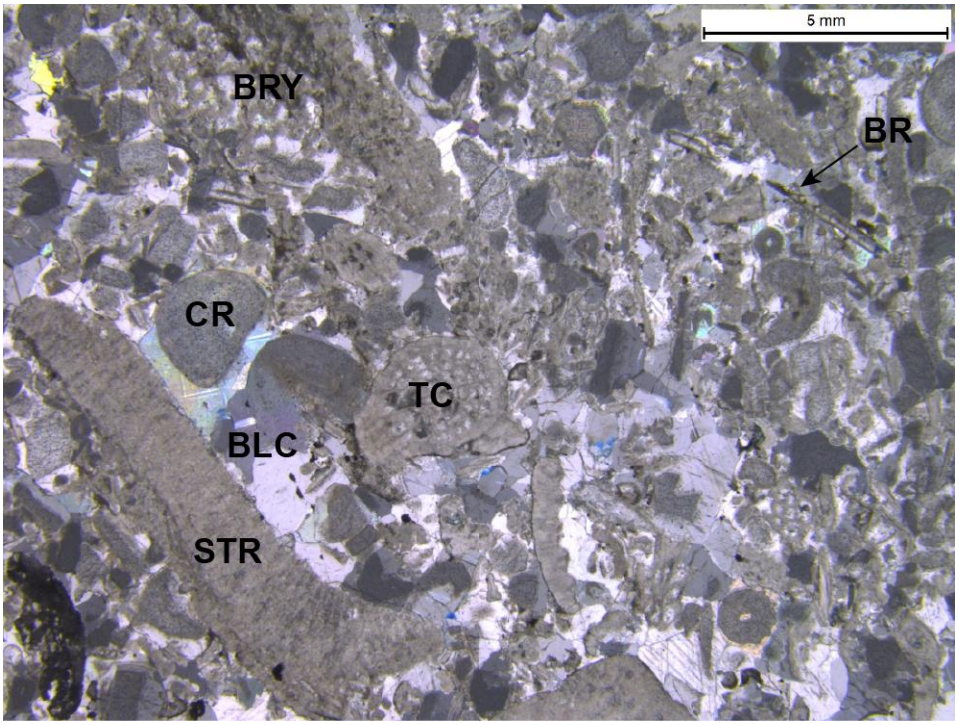

Sample PCo2_G_02: Dominantly crinoidal grainstone to rudstone, with stromatoporoids, tabulate corals, brachiopods and bryozoa. Cement is dominantly blocky calcite and syntaxial overgrowth. Little to no porosity is present. Scale: 5mm, XPL.

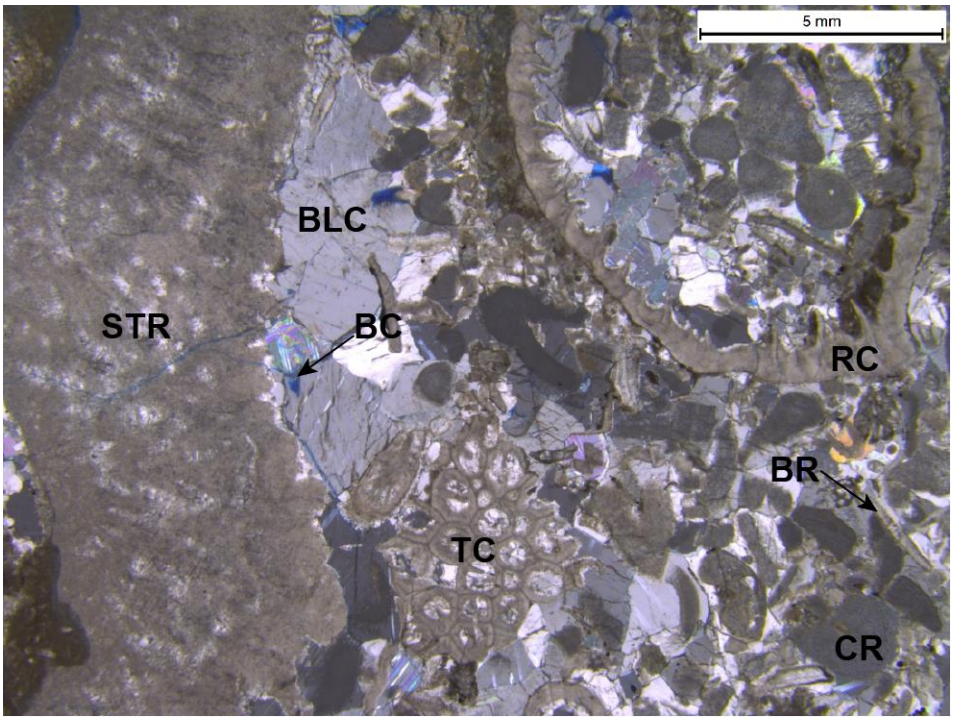

Sample PCo2_H_02: Grainstone to rudstone with stromatoporoids, tabulate and rugose corals, crinoids, and brachiopods. Cement is dominantly blocky calcite and syntaxial overgrowth. Pore types include intercrystalline and framework. Scale:5mm, XPL.

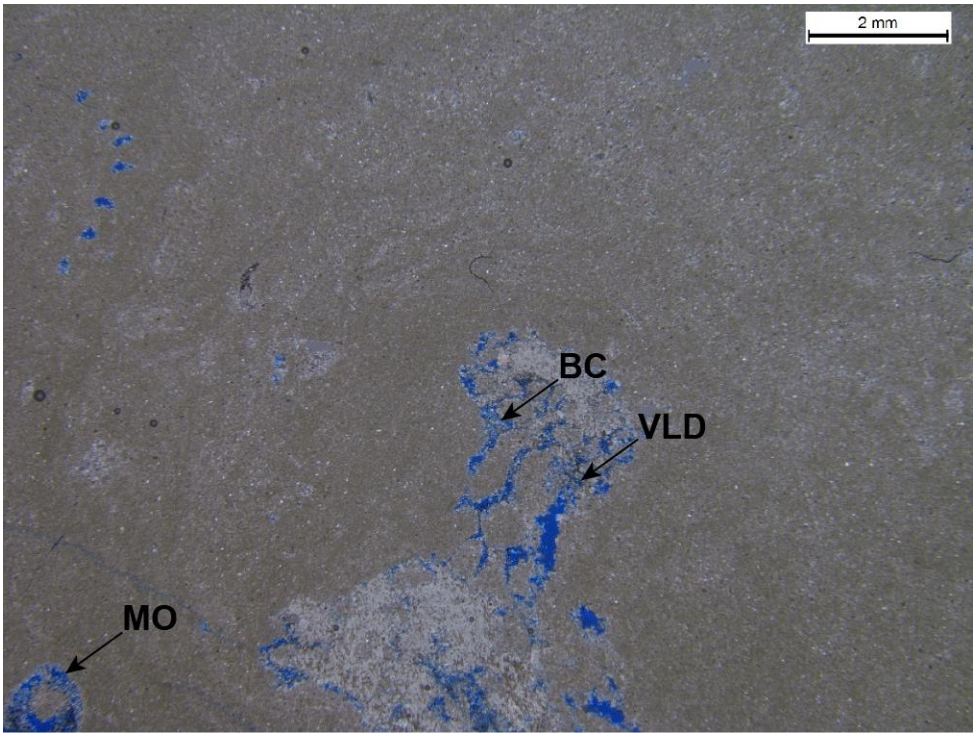

Sample SQ B23_A_Bottom: Wackestone with crinoid and other molds. Cement is dominantly vug lining dolomite with very minor blocky calcite. Pore types include moldic and intercrystalline. Scale: 2mm, PPL.

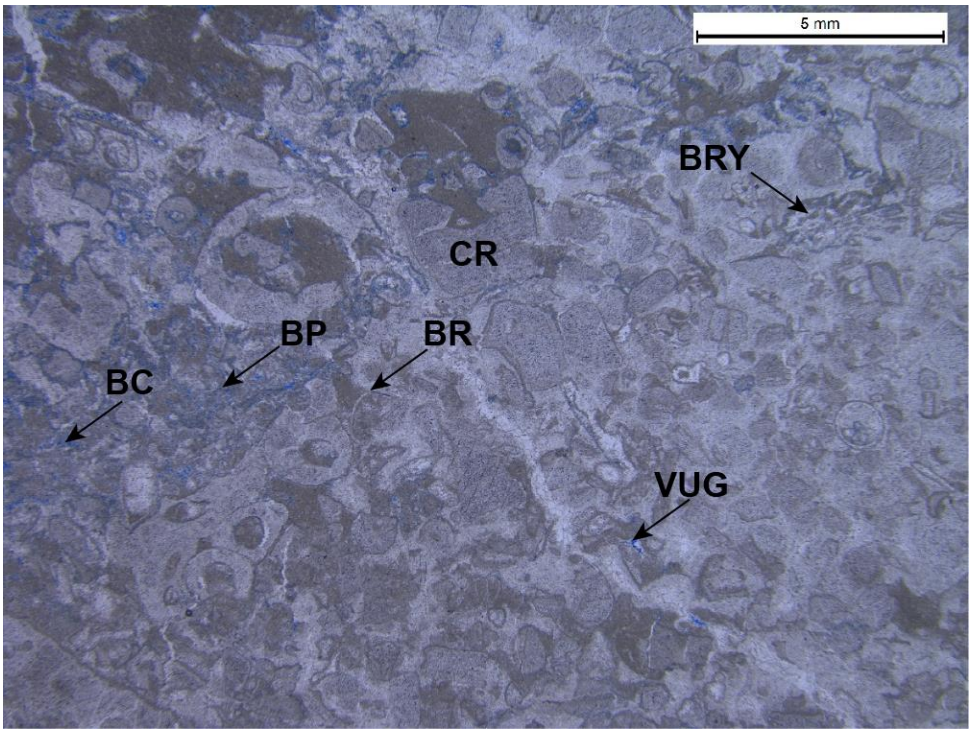

Sample SQ B23_Top: Dominantly crinoidal grainstone (local packstone) with brachiopods and bryozoa. Cement is dominantly syntaxial overgrowth, with minor fibrous and vug lining dolomite cement. Pore types include intergranular, intercrystalline, and vuggy. Scale: 5mm, PPL.

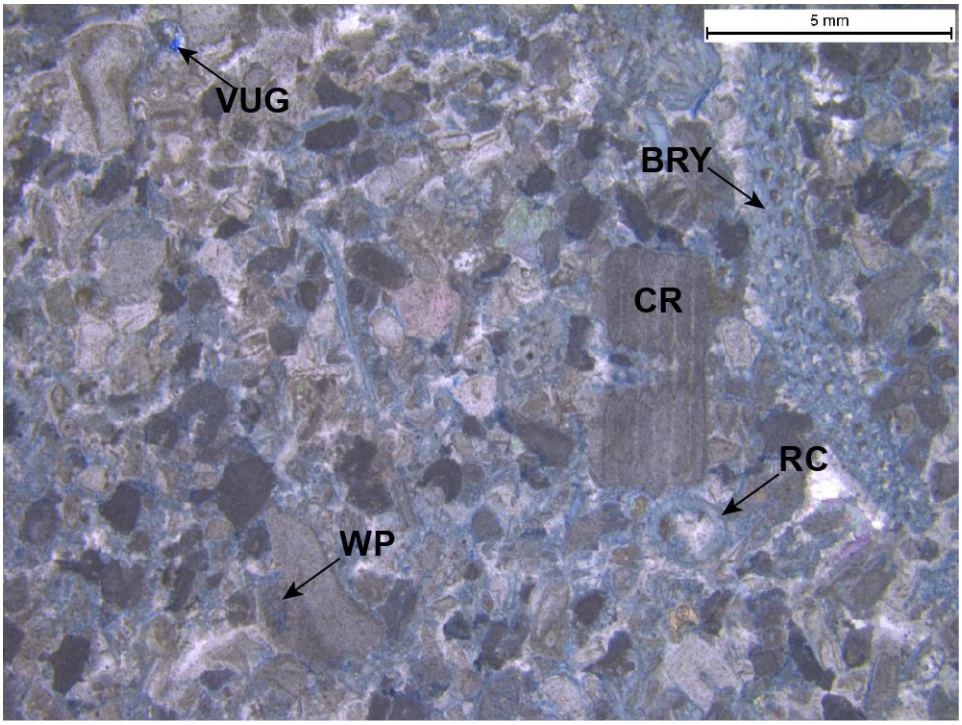

Sample SQ_1_02: Dominantly crinoidal grainstone with bryozoa, tabulate corals, and rugose corals. Cement is dominantly syntaxial overgrowth, with minor blocky calcite and fibrous cements. Pore types include intragranular, intergranular, and vuggy. Scale: 5mm, XPL.

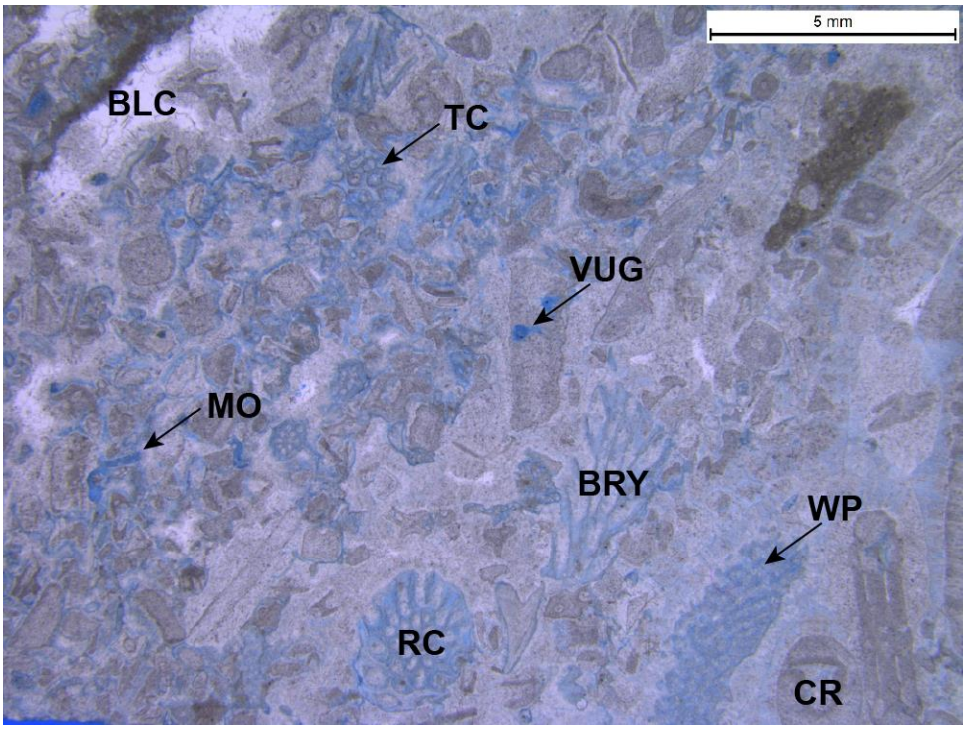

Sample SQ_A_01: Dominantly crinoidal grainstone with tabulate corals, rugose corals, and bryozoa. Cement is dominantly blocky calcite and syntaxial overgrowth, with minor fibrous cements. Pore types include intragranular, moldic, and vuggy. Scale: 5mm, PPL.

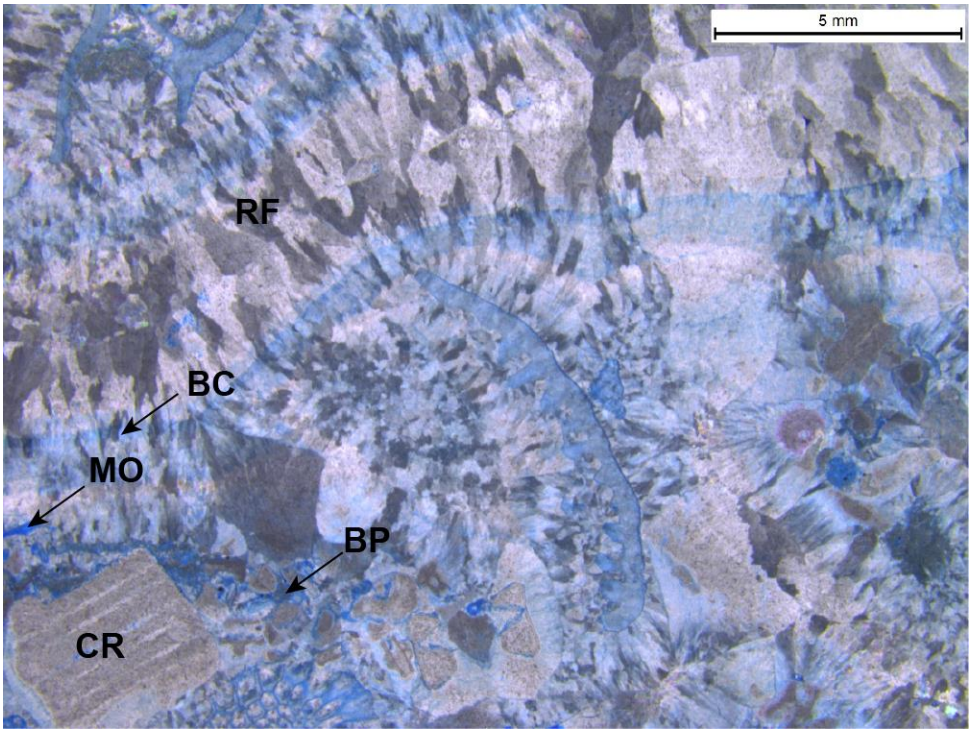

Sample SQ_B_02: Grainstone to rudstone with crinoids and coral fragments. Cement is almost all fibrous, with minor blocky calcite and vug lining dolomite. Pore types include intercrystalline, moldic, and intragranular. Scale: 5mm, XPL.

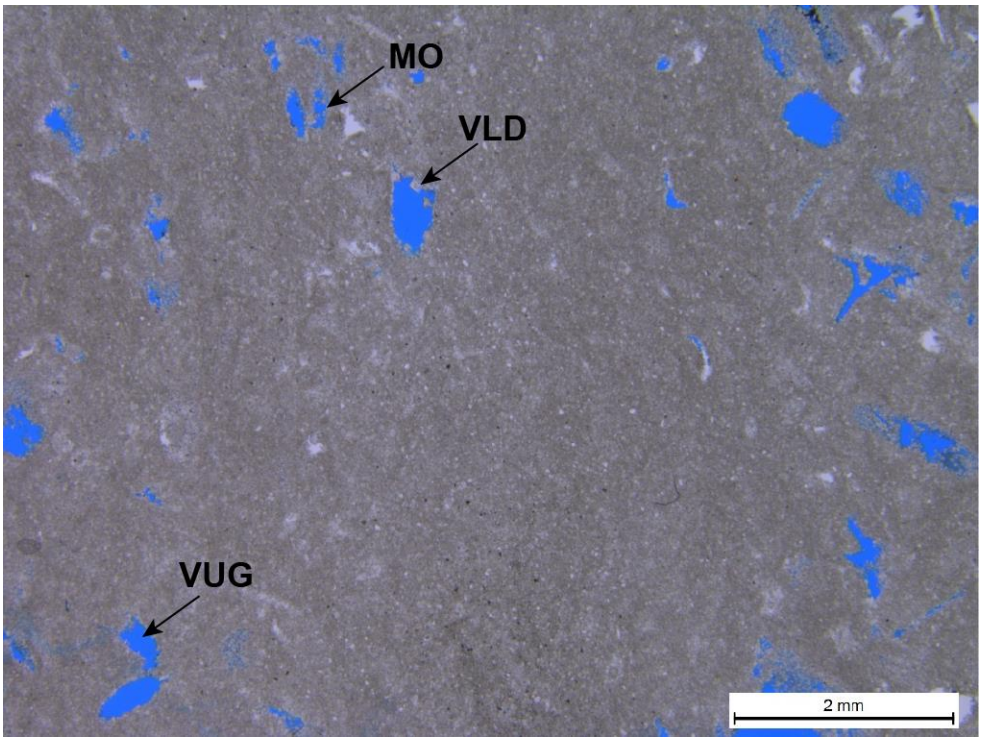

Sample SQB9_01: Wackestone with crinoid and brachiopod molds. Cement is vug lining dolomite, and pore types are moldic and vuggy. Scale: 2mm, PPL.

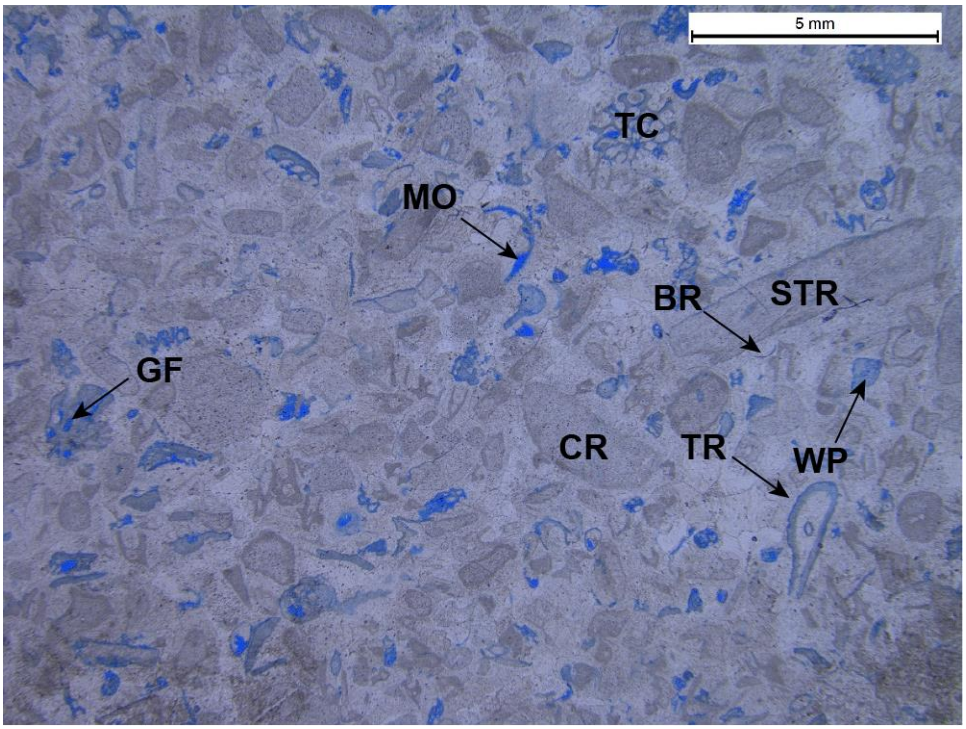

Sample SQUB 2: Dominantly crinoidal grainstone to rudstone with tabulate corals, stromatoporoids, trilobite fragments, and brachiopod fragments. Cement is dominantly syntaxial overgrowth and blocky calcite. Pore types include moldic, intragranular, and framework. Scale: 5mm, PPL.

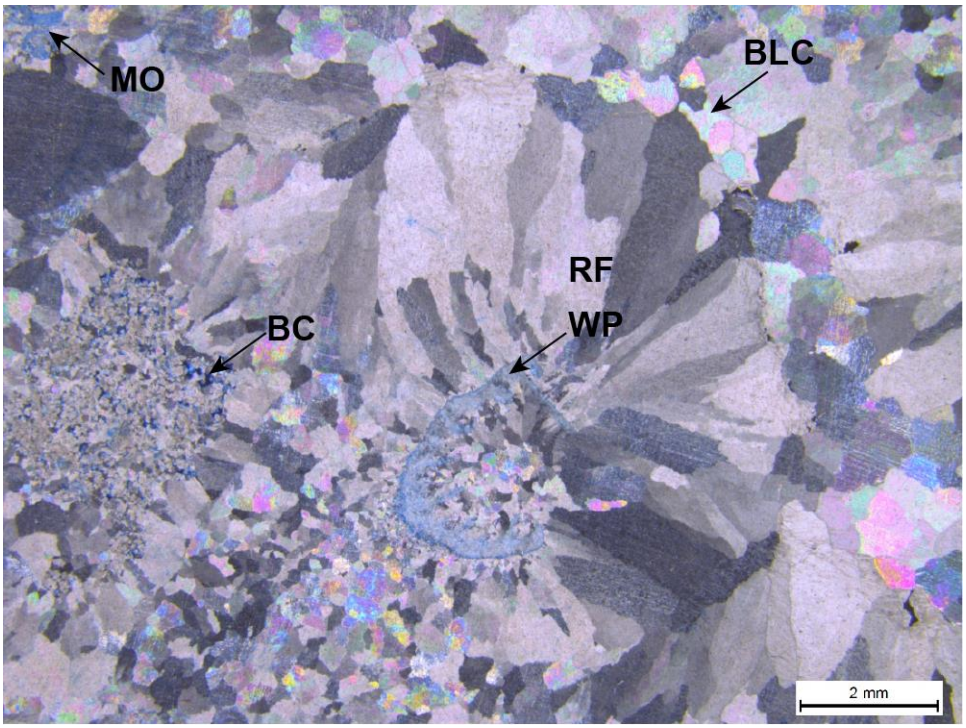

Sample SQUB1_01: Grainstone with fibrous cements surrounding a coral fragment. Pore types include intragranular, intercrystalline, and moldic. Scale: 2mm, XPL.

East Quarry Thin Sections:

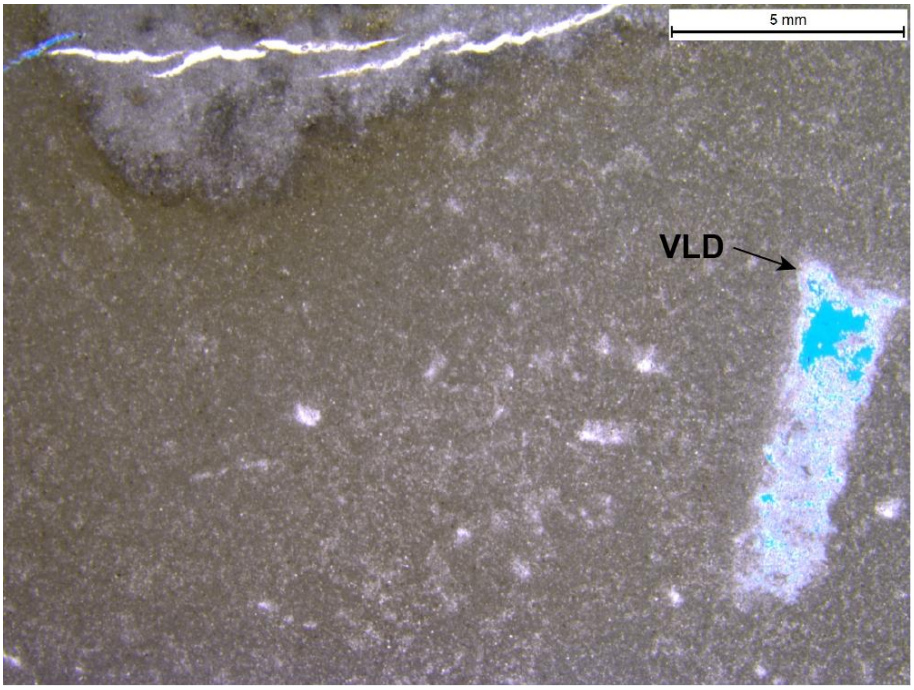

Sample EQ_A_01: Wackestone with crinoid molds. Cement is dominantly vug lining dolomite with minor blocky calcite. Pore types include moldic and vuggy. Scale: 5mm, PPL

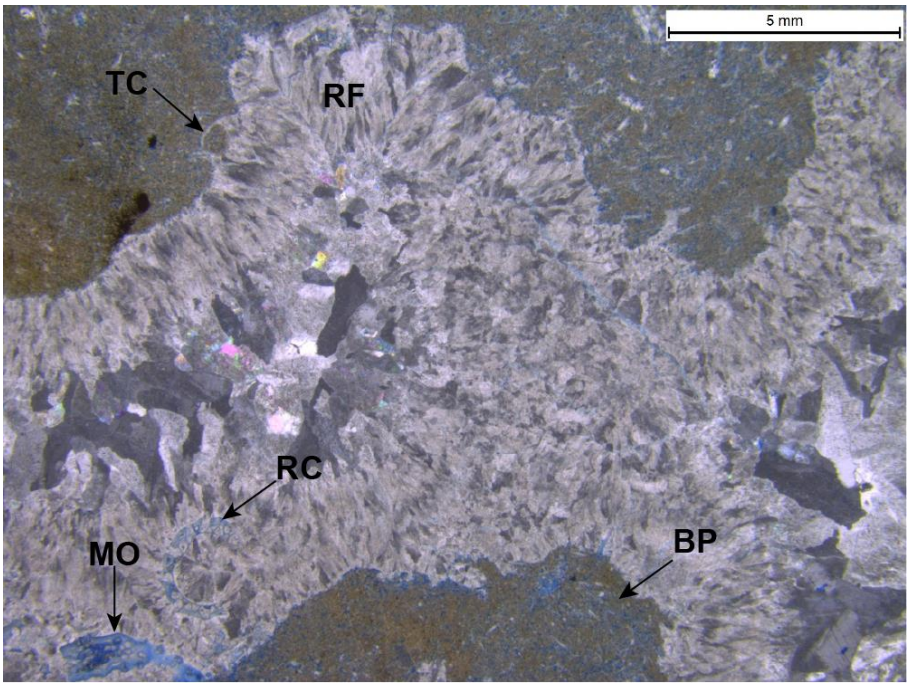

Sample EQ_B1_01: Dominantly crinoidal packstone with tabulate and rugose corals. Cement is dominantly fibrous with minor blocky calcite. Pore types include moldic and intercrystalline. Scale: 5mm, XPL.

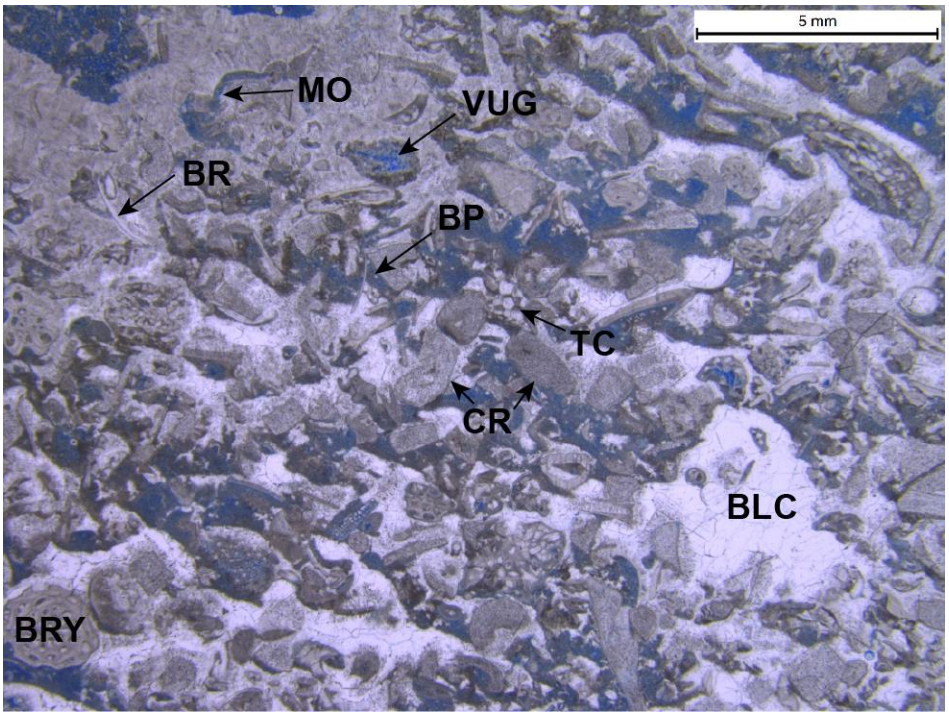

Sample EQ_B2_01: Dominantly crinoidal grainstone with tabulate corals, brachiopods, and bryozoa. Cement is dominantly blocky calcite with minor fibrous cements. Pore types include moldic, intergranular, vuggy, and intragranular. Scale: 5mm, PPL.

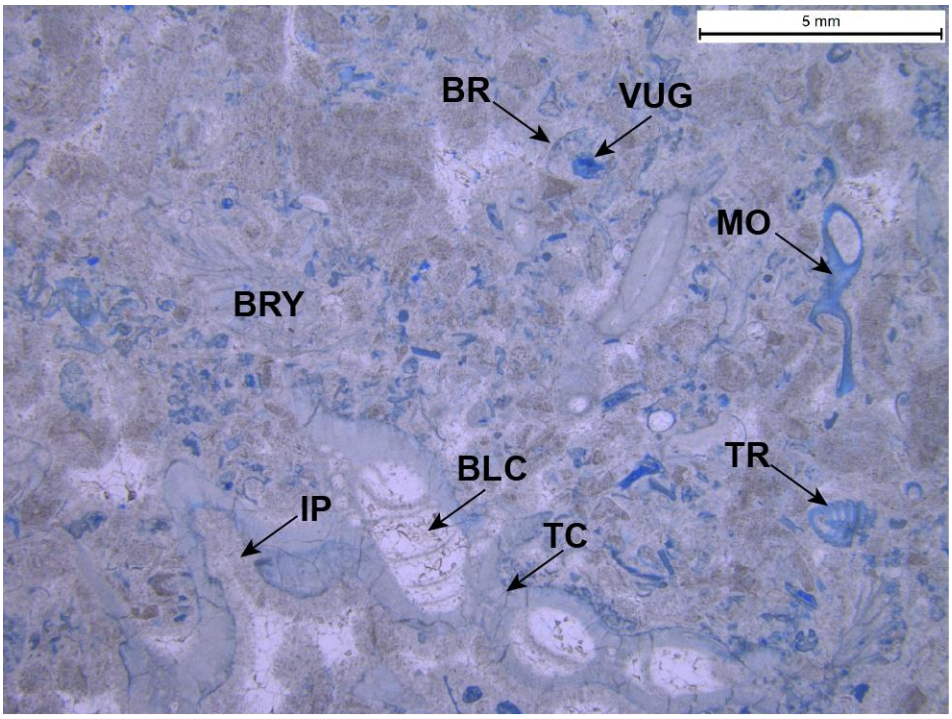

Sample EQ_C_01: Crinoidal grainstone to rudstone with tabulate corals and a trilobite mold. Cement is dominantly blocky calcite with minor fibrous and syntaxial overgrowth cements. Pore types include moldic and vuggy. Scale: 5mm, PPL.

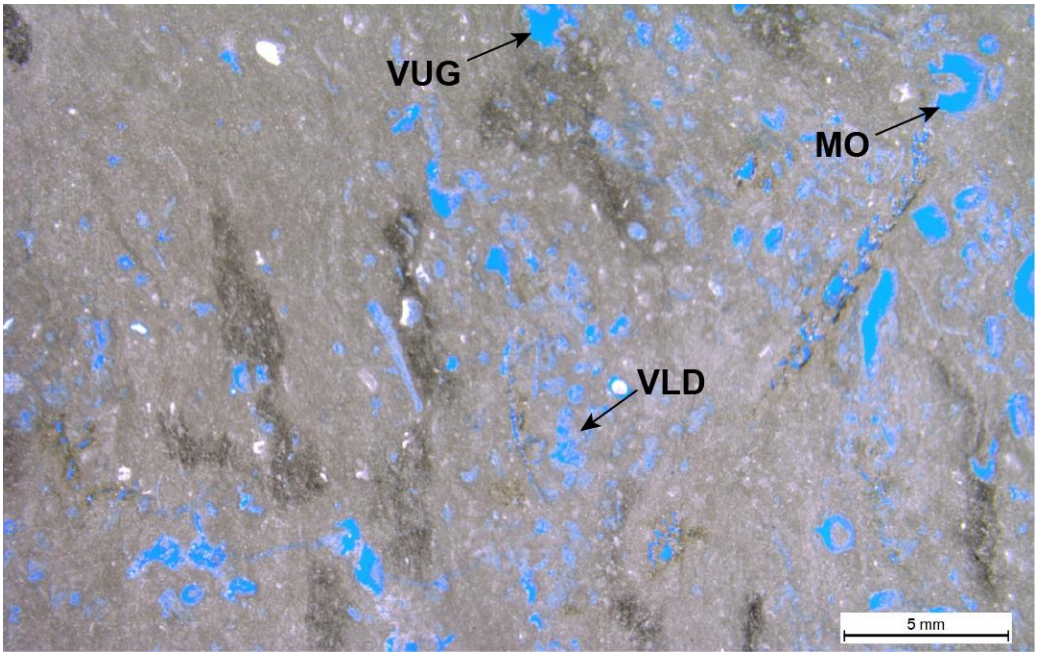

Sample PC3_01: Wackestone with crinoids and crinoid molds. Cement is vug lining dolomite, and pore types include moldic and vuggy. Scale: 5mm, PPL.

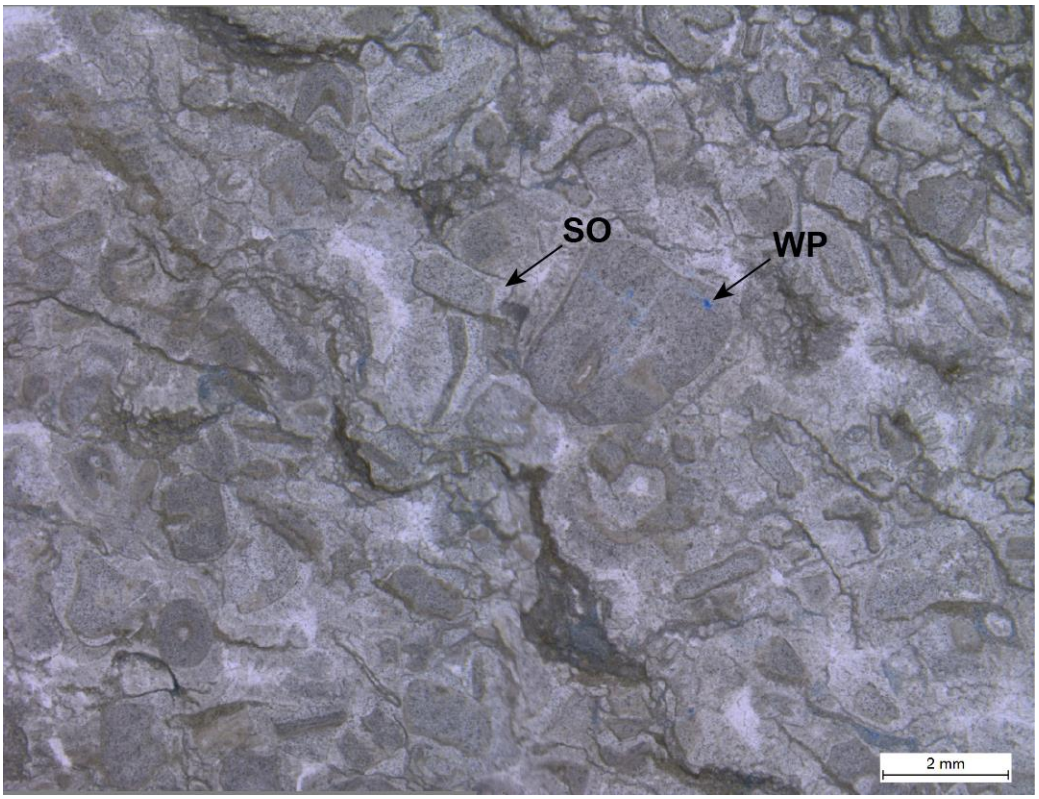

Sample PC 7 GS: Crinoidal grainstone with syntaxial overgrowth cement. Intragranular pores are present. Scale: 2mm, PPL.

VITA

James Wynton Karsten

Candidate for the Degree of

Master of Science

Thesis: DEPOSITION AND DIFFERENTIATION OF WINDWARD AND LEEWARD SLOPES IN A SILURIAN REEF COMPLEX: PIPE CREEK JR. QUARRY, GRANT COUNTY, INDIANA

Major Field: Geology

Biographical:

Education:

Completed the requirements for the Master of Science in Geology at Oklahoma State University, Stillwater, Oklahoma in May, 2020.

Completed the requirements for the Bachelor of Science in Geology at Calvin College, Grand Rapids, Michigan in 2015.

Experience:
Hydrogeology Intern at SES Environmental 2015-2016
Geoscience Intern at Wolverine Gas & Oil, Grand Rapids, MI - Summer 2018
Intern at Seismic Source Company, Ponca City, OK – Summer 2019-Present

Professional Memberships:
American Association of Petroleum Geologists
American Institute of Professional Geologists
Geological Society of America
Society for Sedimentary Geology